Mechanical, Sensor and Control System Design for an Accelerometer Calibrator with One Part Per Million Accuracy

by

BRADLEY NEVINS DAMAZO

B.S.E.,
Walla Walla College,
College Place, Washington
(1986)

Submitted to Department of Mechanical Engineering
in Partial Fulfillment of the
Requirements for the Degree of
Masters of Science in Mechanical Engineering

at the

Massachusetts Institute of Technology

January,15 1988

Signature of Author _____
Department of Mechanical Engineering
January 15, 1988

Certified by _____
Alexander H. Slocum
Assistant Professor of Civil Engineering
Thesis Supervisor

Accepted by _____
Professor Ain A. Sonin
Chairman, Departmental Graduate Committee
Department of Mechanical Engineering

Mechanical, Sensor and Control System Design for an Accelerometer Calibrator with One Part Per Million Accuracy

by

BRADLEY NEVINS DAMAZO

Submitted to Department of Mechanical Engineering
on January 15, 1988 in Partial Fulfillment of the
Requirements for the Degree of
Masters of Science in Mechanical Engineering

ABSTRACT

This thesis presents the design and implementation of a low frequency accelerometer calibrator that will be used to calibrate United States Primary Standard Transducers at the U.S. National Bureau of Standards, Gaithersburg Maryland.

Accelerometers convert a rate of change of velocity into a measurable quantity, typically voltage, and must be calibrated to find their sensitivity as the ratio of volts to acceleration. Calibration of a Primary Standard Transducer must be based on fundamental units of length and time. Currently this is accomplished by mounting the test accelerometer on the moving coil of an electrodynamic exciter and driving it with a sinusoidal signal of known frequency. The amplitude of oscillation is measured using laser interferometry techniques. Knowing the frequency and amplitude of oscillation, the acceleration can be derived and subsequently the sensitivity calculated. The uncertainty in the calibration is ±1.0% in the existing system while it is limited to a 1 7/8 inch double amplitude displacement and 2 to 49 Hz bandwidth.

This thesis presents four designs as the solution to a new, more accurate calibrator. The worst case design has a predicted 10 parts per million accuracy, while the best design has a predicted 1 part per million accuracy, 10,000 times better than the existing calibrator. The worst case design was the least expensive to implement and therefore a prototype of this design was built using the following components: linear air bearing with 20 inch travel, linear brushless DC motor with continuous force output rating of 18 lbf and laser interferometer transducer system with 0.1 microinch resolution and maximum allowable slew rate of 70 in/sec. This design has a 8.5 times increase in double amplitude displacement, a predicted 1,000 times increase in accuracy and 1/2 times decrease in bandwidth in comparison to the existing calibrator. The large double amplitude displacement is required to study the bandwidth characteristics of an accelerometer under a constant peak accelerations, this is not possible with existing calibrators.

Thesis Supervisor: Professor Alexander H. Slocum
Title: George Macomber Assistant Professor of Civil Engineering

To the memory of my father

Acknowledgements

I would like to thank Professor Slocum for his advice and technical support and Donald S. Blomquist of the Automated Production Technology Division, U.S. National Bureau of Standards Gaithersburg, Maryland for his advice and support on this thesis. In addition, I would like to thank Paul Parise of Zygo Corporation for the loan of an Axiom 2/20 laser transducer system that was used in developing this thesis.

Table of Contents

List of Figures

Lists of Tables

Chapter 1
Introduction

1.1 Purpose of Research

The United States Constitution states the federal government shall define and maintain fundamental standards such as length, mass and time. The government agency assigned to set and maintain standards is the U.S. National Bureau of Standards (NBS) located in Gaithersburg, Maryland. In addition to maintaining the above fundamental standards, the NBS maintains the acceleration standard. The transducer used to measure acceleration is an accelerometer. Accelerometers convert a rate of change of velocity into a measurable quantity, typically voltage, and must be calibrated to find their sensitivity as the ratio of volts to acceleration. This research focuses on the continuing improvement of the acceleration standard with the mechanical, sensor and control system design for an accelerometer calibrator with one part per million accuracy, 10,000 times better than the existing capability.

Specifically, this research is aimed at improving accelerometer calibration accuracy in the low frequency range of 1 to 100 Hz. Improving the accuracy is a two step process, 1) decrease the uncertainties within the mechanical calibration hardware which develops the reference acceleration input and 2) decrease the uncertainties in the instrumentation hardware which determines the output quantities of the accelerometer under test conditions. This thesis addresses apportion of the first step by leading to the development of a machine to calibrate accelerometers.

The motion of such calibrator hardware, referred to as a vibration exciter or shaker, must have very low distortion and minimal components of motion in all directions other than axial. In addition, the attainable amplitude must be large enough to produce a transducer signal that can be accurately measured. The attainable amplitude and accuracy of the accelerometer calibration on any vibration exciter is limited by accelerometer size, weight, geometry and vibration sensitivity. This accelerometer calibrator will calibrate servo or force balanced, piezoelectric, piezoresistive and strain gage accelerometer with emphasis on the servo and piezoelectric accelerometers.

1.2 Background

Advances in technology have created complex structures and machines which have equally complex vibration problems, thus the need for accurate measurements of vibrations has become very important. Accelerometers are used to measure vibrations, the output is post processed for its particular application. Several applications are as follows: In high speed machining, the dimensional stability of the work piece is maintained because the heat generated in the cutting operation is localized in the material to be removed; thus spindle speeds can be greater than 10,000 RPM. However, bearing failures are catastrophic at these speeds. Bearing monitors utilize accelerometers to measure vibration levels within the spindle bearings and predict failures before their occurrence.

Another application is predicting machine tool wear [1]. An accelerometer measures the vibration signature of the tool during the

machining operation The signature changes as the tool wears and when a predetermined threshold is reached the tool is considered worn out and replaced. Such a device has applications to unattended machining.

Recently Newport Corporation won the prestigious IR 100 Award from Research and Development Magazine for its new Electronic Vibration Isolation System (EVIS) [2]. EVIS is an anti-vibration platform that electronically achieves an order of magnitude better vibration isolation then conventional pneumatic systems. The same technology has been applied to wafer steppers in the semiconductor industry allowing for throughput increases as high as 12 times [3]. The anti-vibration platforms use highly sensitive accelerometers to measure the onset of vibrational forces, the resultant signals are used to generate out of phase forces which effectively cancel the incoming vibrations.

Modal testing requires the use of accelerometers to determine the dynamic properties (natural frequencies and modal shapes) of a structure. These experimental properties can be correlated with those solve by a finite element analysis [4]. Differences in the properties can be qualified and modifications made to the finite element model to achieve more comparable results. The finite element model can then be used to simulate the response to actual operating environments.

These examples show that accelerometers are a fundamental engineering tool whose accuracy is critical to the performance of many high-tech systems.

1.3 Calibration Methods

Accelerometer Calibration refers to the procedure used to verify the performance characteristics that influence the transducers measurement accuracy [5]. Three methods are use to calibrate accelerometers: laser interferometer absolute calibrations, sinusoidal comparison calibration and random signal FFT comparison calibration.

1.3.1 Absolute Calibration

A typical absolute calibration setup is shown in Figure 1.1 [6]. A sinusoidal function generator applies a signal to a power amplifier that drives the exciter. The test accelerometer is mounted on the exciter. The displacement is measured using a Helium-Neon laser and Michelson interferometer. For every $\lambda/2$ displacement of the retroreflector, a fringe occurs and is detected with a photodiode. The number of fringes are counted per period of the sine wave. The output of the accelerometer is measured with a RMS voltmeter. The accelerometer's sensitivity is the ratio of volts to acceleration. The acceleration is given by

$$A = -\omega^2 X_o \sin(\omega t) = -A_o \sin(\omega t) \qquad (1.1)$$

$$A_o = \omega^2 X_o = (2\pi f)^2 \, n \, \lambda/8 \qquad (1.2)$$

where f is the frequency of excitation, n is the number of fringes per cycle and λ is the wavelength of a Helium-Neon laser.

For the existing NBS low frequency calibration setup the system uncertainties are listed in Table 1.1 [7]. The root mean square error is 0.4%. Due to errors introduced by cable positioning of test accelerometers, the overall accuracy is estimated to be ±1.0%. Accelerometers calibrated using this method are Primary Standard

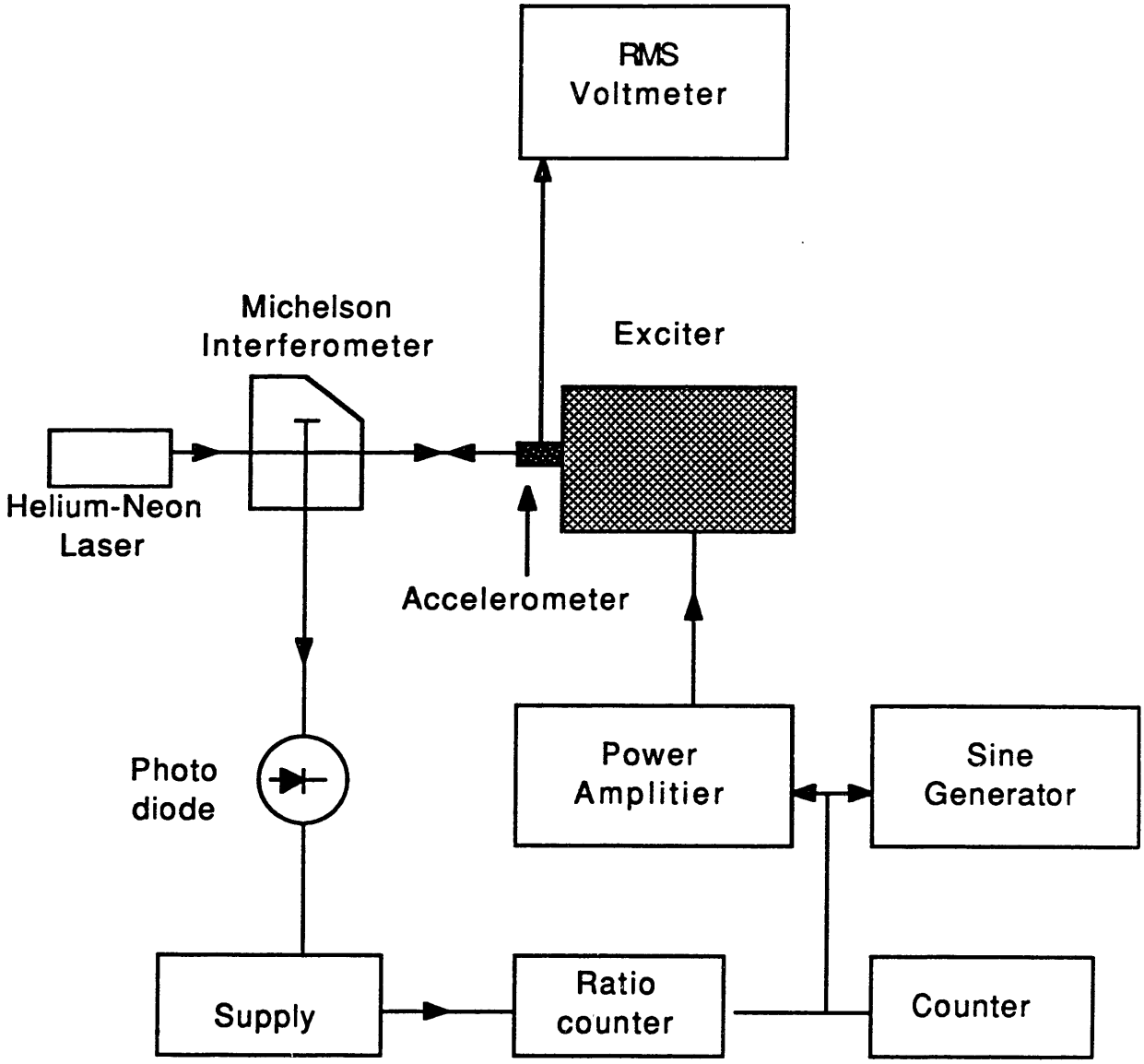

Figure 1.1, Absolute calibration system.

Table 1.1 Estimate of error in the NBS low frequency calibration system

Source of Error	Maximum Estimated Error
Voltage Measurement	0.3%
Cross Coupling	0.1%
Wave length of Laser	0.0%
Signal Frequency	0.0%
Fringe Counts	0.2%
RMS Total	0.4%

Transducers. The cross axis motion and harmonic distortion is estimated as ±1.0% [8].

1.3.2 Sinusoidal Comparison Calibration

A sinusoidal comparison calibration set up is shown in Figure 1.2. A sinusoidal function generator applies a signal to a power amplifier that drives the exciter. The test accelerometer is mounted on the exciter along with a reference accelerometer traceable to a national standard (Transfer Standard Transducer). The output of the two accelerometers are measured with a RMS voltmeter. The test accelerometer's sensitivity is

$$S_{test} = V_{test}/V_{reference}S_{reference} \qquad (1.3)$$

where V_{test} and $V_{reference}$ are the measured output voltages and $S_{reference}$ is the reference accelerometers sensitivity. The same equipment is used at NBS for the absolute and comparison test, therefore the calibration uncertainty is ±1.0%.

1.3.3 Random signal FFT Comparison Calibration

The FFT comparison calibration setup is shown in Figure 1.3. The sensitivity of the test accelerometer is given by

$$S_t(f) = H_f(f)S_r(f) \qquad (1.4)$$

where $H_f(f)$ is the frequency response from the analyzer and S_r is the reference accelerometer's sensitivity. Accuracies of ±1.0% are achievable by the FFT comparison method [5].

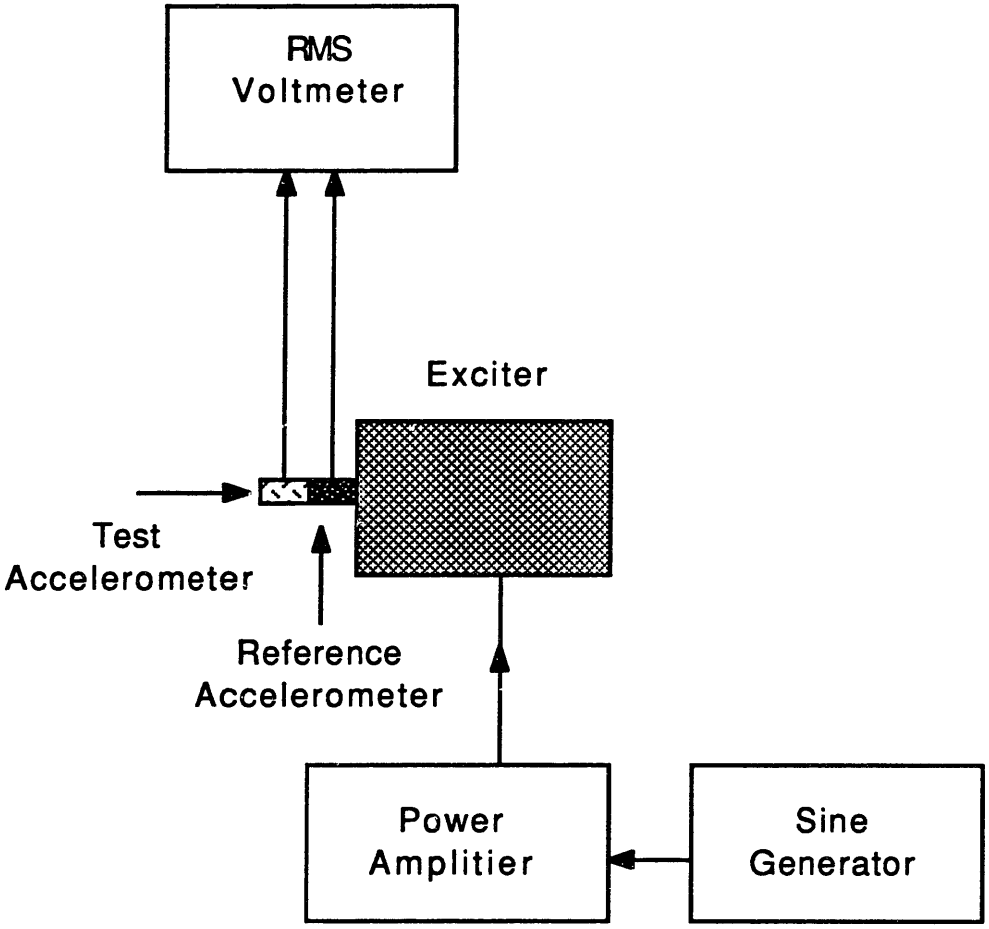

Figure 1.2, Sinusoidal comparison calibration system.

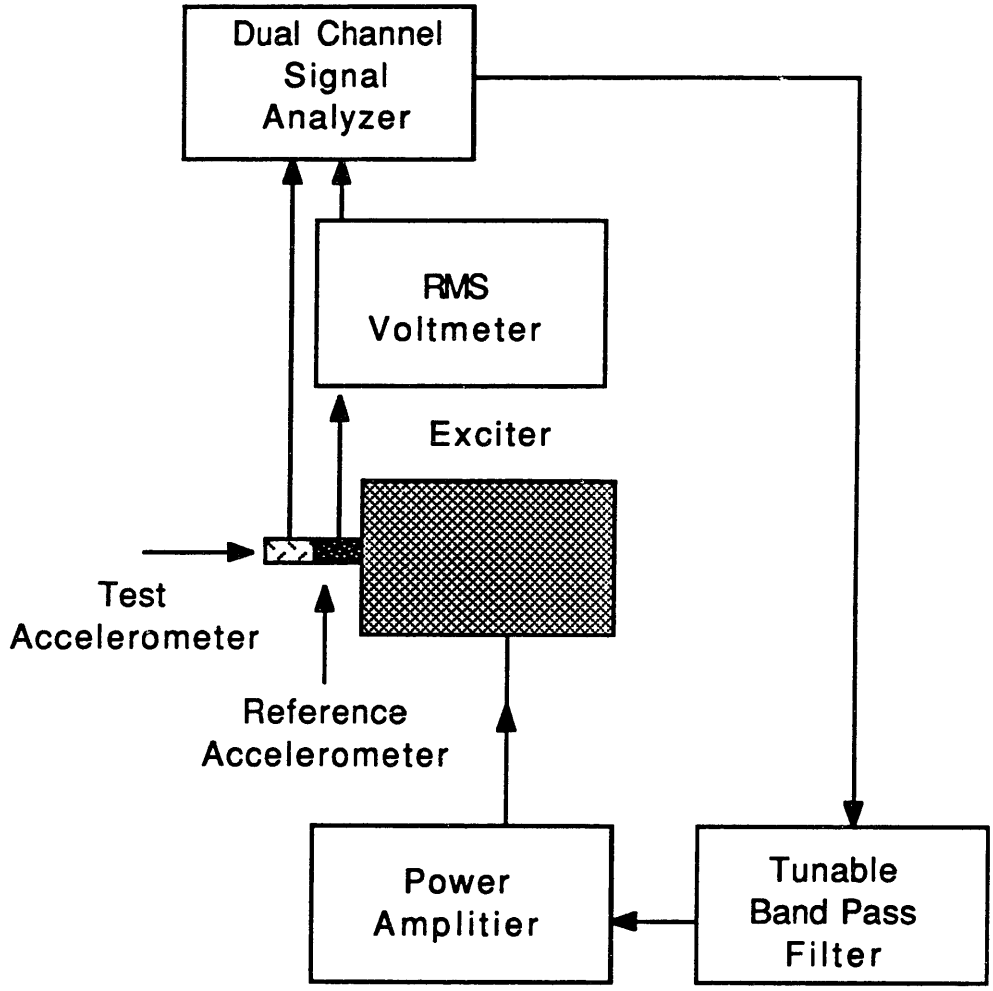

Figure 1.3, Random signal FFT comparison calibration system.

1.4 Existing National Bureau of Standards Calibrator

The U.S. National Bureau of Standards (NBS) offers accelerometer calibration services for industry. The calibrations are preformed on a low-frequency vibration exciter with a frequency range of 2 to 50 Hz [7,8,9,10,11,12,13,14]. The exciter has a maximum double amplitude displacement of 1-7/8 inches and will calibrate accelerometers weighing up to 0.5 lbs. The electrodynamic exciter at 50 Hz develops a maximum acceleration of approximately 1.5 g's. The acceleration is limited by the available magnetic flux from a permanent magnet and by the maximum 2 amp current in the driving coil. On the low end of the frequency range, the acceleration is limited by the maximum double amplitude displacement which is a function of the magnet pole piece thickness.

The NBS vibration exciter uses an air bearing design to reduce cross axis motion to a maximum of 1% over the frequency range. Cross axis motion is motion that is not axially with the accelerometer's sensitive axis. The exciter uses an overhead "rubber band" suspension system for vertical support of the moving element as shown in Figure 1.4. To prevent the moving element from rotating, an anti-rotation air bearing is used as shown in Figure 1.5. This anti-rotation air bearing is a parallel-surface-thrust bearing that requires the overhead suspension system to be rotated to supply a torque which keeps the guide vane against the air bearing surface. Use of this rubber suspension system and misalignments cause harmonic distortions in the exciter motion of 1% in the frequency range of 2 to 49 Hz. Harmonic distortion is the presences of higher order harmonics (e.g. $A\sin\omega_1 t + B\sin\omega_2 t + C\sin\omega_3 t + ..$). At frequencies of 50 Hz the distortions

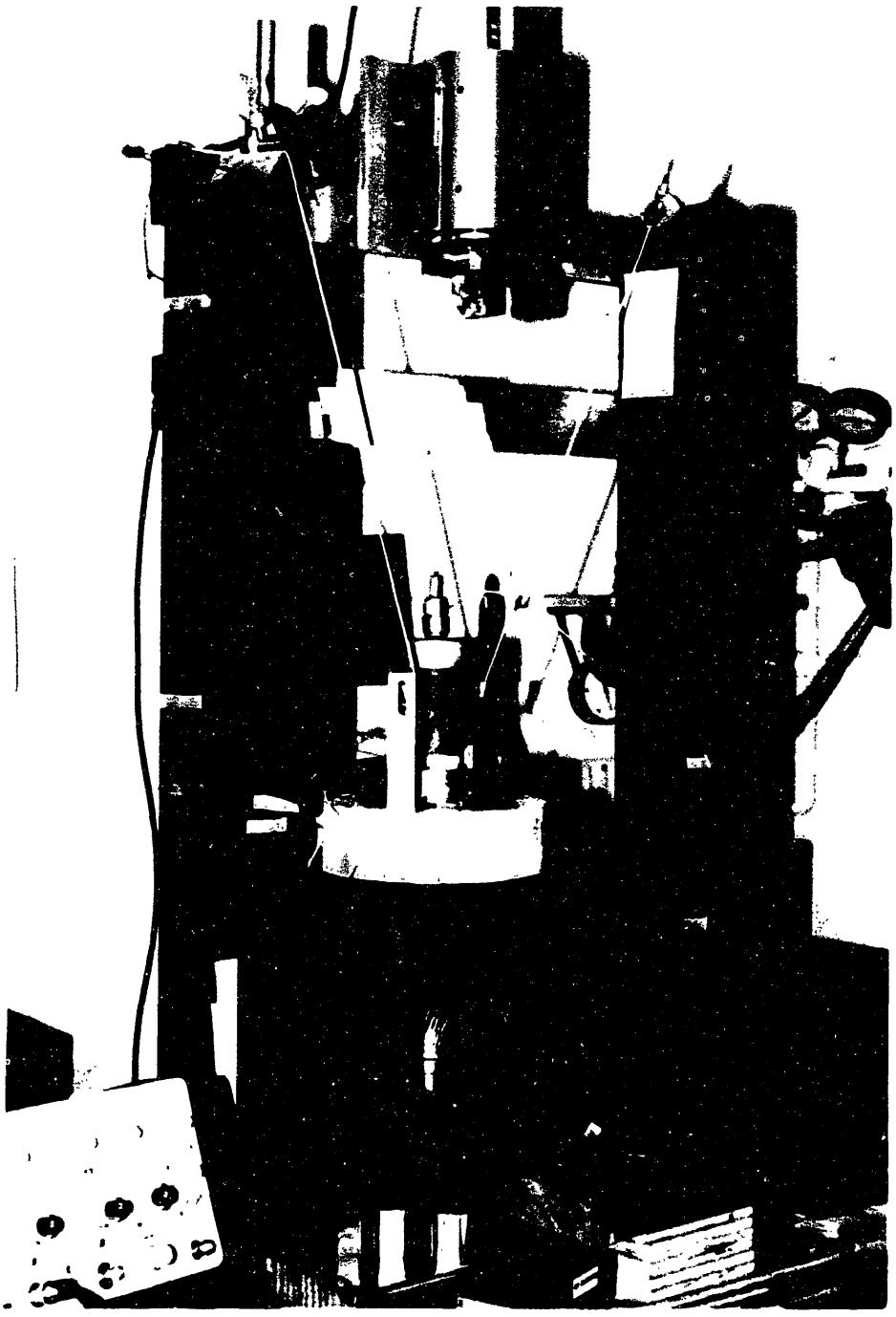

Figure 1.4, Existing NBS low frequency calibration system.

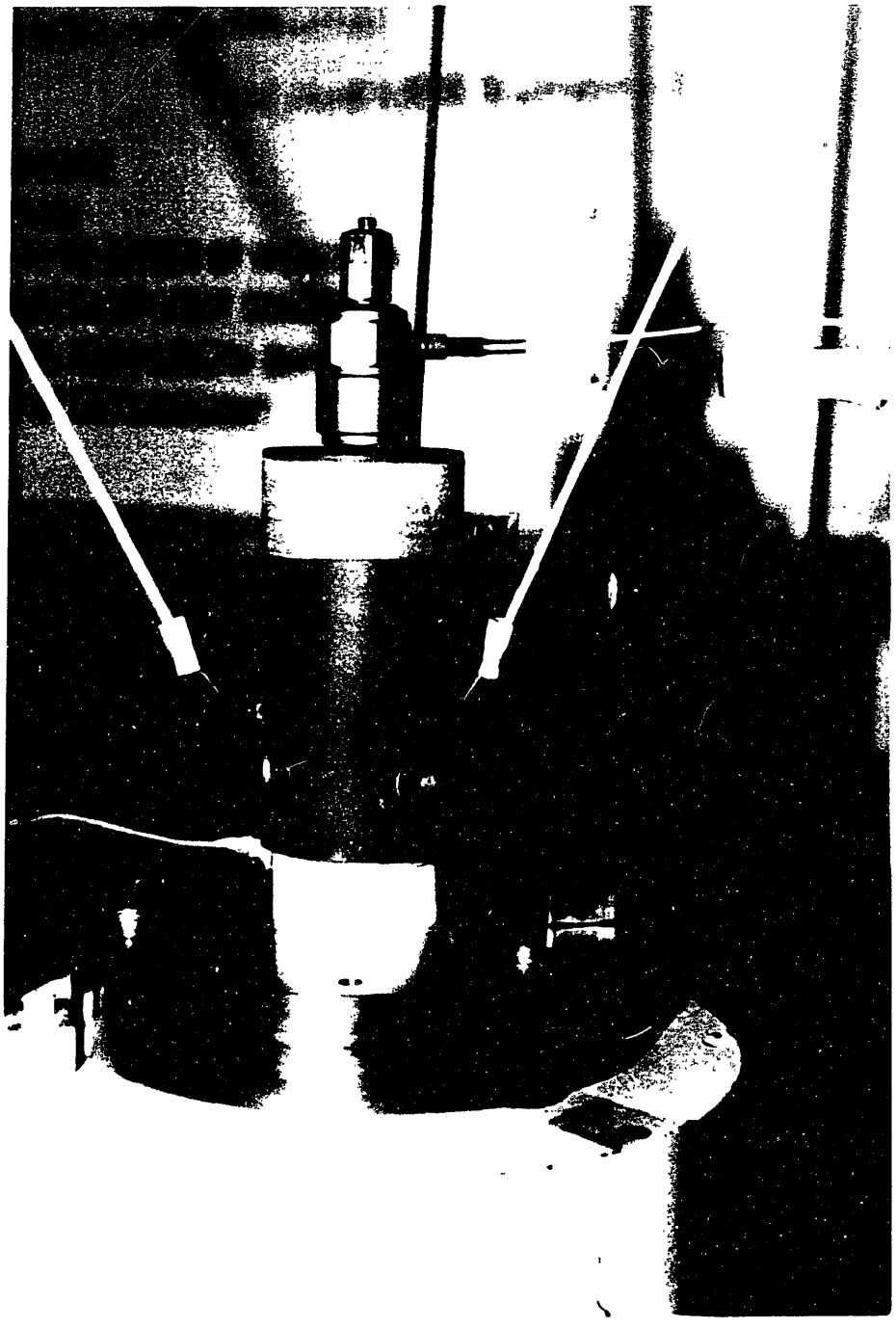

Figure 1.5, Existing NBS low frequency calibrator.

increase to values greater than 1% possibly due to the overhead suspension system. As a result calibrations can be completed with the current NBS exciter to only ±1% uncertainty.

1.5 Research Goals for the New Calibrator

The goal of this thesis is to develop a vibration exciter having a frequency range of 1 to 100 Hz and the ability to calibrate accelerometers with less than ±0.1% uncertainty [8,15]. The cross axis motion and distortion must be reduced by an order of magnitude to less than 0.1% in order to meet this goal. Secondary goals are to achieve a 6 inch double amplitude displacement at 1 Hz and a 3 g acceleration at 100 Hz. If possible, the vibration exciter should handle accelerometers weighing up to 1 or 2 lbs, allowing for calibration of larger seismic accelerometers. Also, both absolute and comparison calibrations should be possible with the new exciter. Conceptually the exciter will consist of: an actuator and amplifier to develop the sinusoidal motion, a linear air bearing and hardware to mount the test accelerometers, instrumentation for reading accelerometer voltage outputs, a laser interferometer for measuring displacements and digital computer to collect data and to control the calibration equipment. The research necessary to meet the specifications involves improving the bearing and actuator systems in order to gain the higher accuracies needed in accelerometer calibrations; and to integrate these systems with an appropriate control and data acquisition system to give ease of operation.

The problems with the NBS exciter and solutions that this research will address are:

a) Large (1%) cross axis motion - The current NBS air bearing was designed and built in 1971. This research will study current air bearing design technology to determine if a new air bearing design needs to be developed or if a commercially available precision air bearing will achieve less than 0.1% cross axis motion under load over the bandwidth.

b) Limited displacement amplitude - A larger displacement is desired so that the frequency can be varied while holding the acceleration constant for determining bandwidth characteristics of accelerometers. H.-J. von Martens from the Office of Standardization, Metrology and Quality Control, German Democratic Republic has developed a low-frequency rectilinear vibration exciter capable of a 1.0 meter double amplitude displacement with 0.5% to 1.5% uncertainty in the absolute calibration of accelerometers [16]. This research project is on a much smaller scale with the maximum double amplitude displacement desired at 6.0 inches, but with much greater accuracy.

c) Non-optimal design - A new design that does not incorporate an overhead suspension system will aid in reducing distortions. The use of a horizontal linear slide does not require a gravitational restoring force and allows the suspension system to be eliminated from the design.

d) Limited Acceleration and Frequency - The maximum acceleration is limited to 1.5 g's in the 2 to 50 Hz frequency range. Outside of this frequency range, the NBS exciter does not satisfy the required accuracies.

This thesis shall supply mechanical design in the form of shop drawings and theoretical verification of performance for a machine to calibrate accelerometers. An experimental verification will also be preformed. The mechanical components, sensors and control system will be integrated into a working prototype. In summary, the proposed accelerometer calibrator should meet the following specifications:

1) System Bandwidth - 1 to 100 Hz
2) Minimum Double Amplitude Displacement - 6 inches
3) Cross axis motion - 0.1% over bandwidth
4) Harmonic Distortion - 0.1%
5) Peak Accelerations - up to 3 g's
6) System accuracy - 0.1%
7) Constant Acceleration over bandwidth

Since the motion is sinusoidal, we can derive that the maximum velocity is 20 in/sec at 1 Hz. It is impractical to use the 3 g peak acceleration as the constant acceleration over bandwidth. This would require a 40 inch double amplitude displacement and a 200 inch/sec maximum velocity, a specification that would be difficult to obtain. Therefore, 0.3 g constant acceleration will be used which at 1 Hz corresponds to a 6 inch double amplitude displacement. At 100 Hz, the

0.3 g acceleration gives a 600 microinch double amplitude displacement. For 0.1% system accuracy, the measurement sensor to be able to resolve to greater than 0.1% of the double amplitude displacement or 0.6 microinches. For 0.1% cross axis motion, off axis motion must be less than 0.6 microinches. A summary of the derived specifications are as follows:

Minimum velocity: 20 inches/second
Sensor resolution: 0.6 microinches
Cross axis motion: 0.6 microinches.

These specification are plotted in Figure 1.6 to show the operation regions of the proposed calibrator verses the existing calibrator. The remainder of this thesis addresses these design goals. Chapter 2 analyzes available technology that can be applied the design. Chapter 3 gives a theoretical analysis of the proposed design from Chapter 2. Chapter 4 describes the prototype calibrator and experimental results.

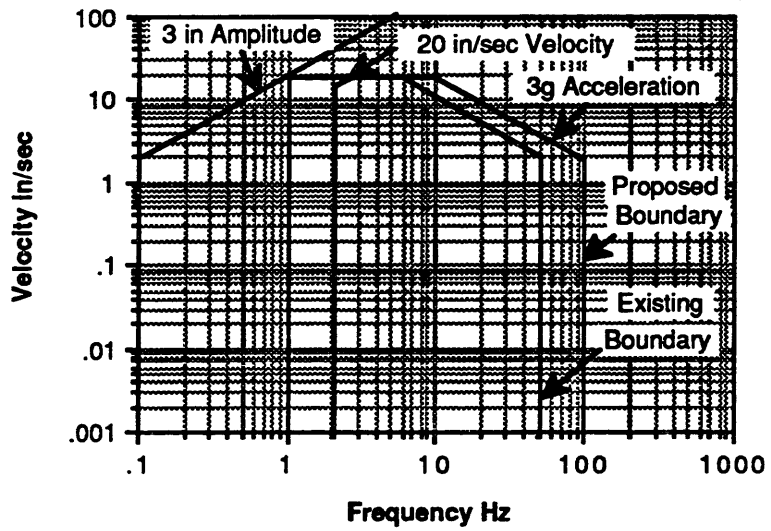

Figure 1.6, Operating regions of the existing and proposed calibrator.

Chapter 2
Calibrator Design

2.1 Overview of Design Issues

The guiding factors in this calibrator design are cost, accuracy and geometric constraints. As accuracy requirements increase, costs increases substantially [17]. The cost of microinch accuracies can be minimized by employing commercially available parts. The geometry confines the design to be a linear motion system driven by a linear actuator. Traditional linear motion systems use cast iron ways or linear roller bearings for support and accuracy while they are driven with ball screws. This chapter will analyze the available linear actuators, linear bearings systems and linear displacement transducers that could be used to meet the calibrator design specifications. A design based upon these components will be proposed at the end of the chapter as the solution to the calibrator design problem. The remaining chapters will cover a theoretical analysis of the design and detail the experimental results of a prototype.

2.2 Analysis of Linear Actuators

Linear actuators used to position linear motion systems include lead screws or ball screws, capstan drives, linear motors, hydraulic cylinders, wire drives, piezoelectric actuators and electrodynamic drives. Each linear actuator will be evaluated for use in the calibrator.

2.2.1 Ball Screws

Ball screws have been the traditional linear actuators in the machine tool industry. A good design involving ball screws requires a careful selection of parameters such a length, bearing supports, lead, diameter and accuracy rating. A discussion of these parameters and how they relate to the calibrator design follows.

Ball screws are capable of great accuracies but at the sacrifice of speed. The calibrator design requires both. The high speed motion requires high acceleration rates that result in greater ball screw deflections and increased servo settling times. The positioning accuracy of a ball screw is increased by using two preloaded ball nuts to reduce the backlash. The two nuts are typically separated by a spring to reduce the axial clearance of the ball screw to zero. Under high accelerations, the spring can deflect: consider a spring stiffness of 1,000,000 lbf/in, if a one pound axial load is applied the spring can deflect one microinch. This compliance decreases the servo system stiffness, resulting in increases settling times.

The calibrator's sinusoidal motion places the ball screw in tension for one direction of travel and compression in the other. This constant cyclic loading quickly fatigues the ball screw and creates backlash. The existing NBS calibrator has been operational since 1971, a life of 17 years. Typically the calibrator will run for 2 hours per calibration. Assuming one calibration week per year, the life of the calibrator is approximately 1700 hours. The selection of the fatigue life for a ball screw must be equivalent to the life of the existing calibrator. In addition, the bearing supports and ball screw diameter must be sufficient to prevent a buckling of the screw under a

compressive load and the reaching of the critical ball screw rotation speed (taken as 80% of the angular speed that is resonant with the natural frequency of the screw shaft [18]).

The primary errors within a ball screw are the lead error and straightness error. The lead error is a linear error component associated with one revolution of the screw. This error is minimized when end point feedback is used as opposed to using a rotatory encoder coupled to the end of the ball screw. The straightness error is also called a wobble or periodic error. This is a deviation from straight line travel and will cause unwanted side loads when coupled to a linear slide. The alignment between a ball screw and linear slide is critical as shown in Figure 2.1. For motions near the bearings, the lateral rigidity of the ball screw increases, causing increased side loadings as represented in Equations 2.1(a) and 2.1(b). Laterally compliant couplings are used to reduce the geometric errors associated with coupling ball screws to linear slides [19,20]. These devices can improve the positioning accuracy but at the sacrifice of speed because there are axial complaint. Temperature changes in the environment and heat generated in the ballnut due to friction will cause thermal growths within a ball screw. This naturally affects the accuracy of the positioning system.

Ball screws work well for quasistatic conditions, for highly precise and dynamic conditions such as for the calibrator, a ball screw would not be recommended.

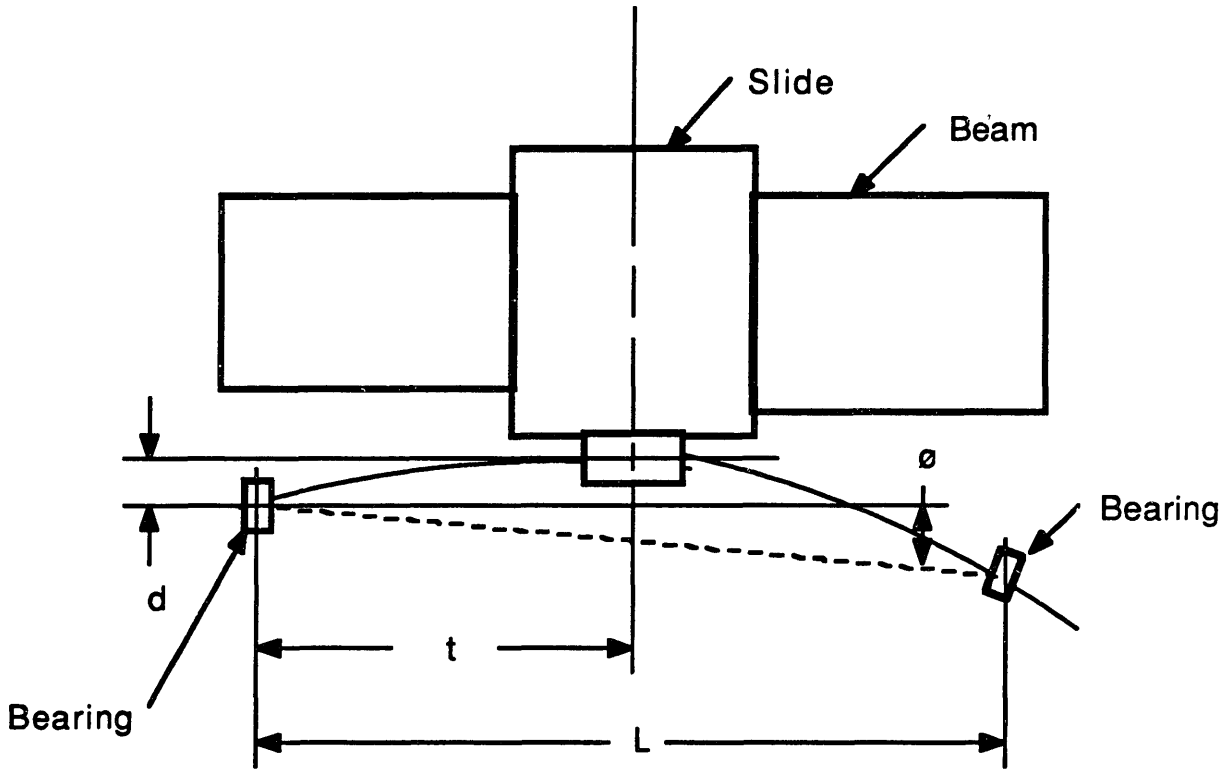

A) Case of Fixed-Fixed Bearings:

$$\delta = \frac{3EIL^3(d-t\theta)}{Gt^3(L-t)^3+3EIL^3} \qquad 2.1(a)$$

B) Case of Fixed-Free Bearings:

$$\delta = \frac{3EI(d-t\theta)}{Gt^3+3EI} \qquad 2.1(b)$$

δ; Slide error perpendicular to motion.

d; Screw offset due to miss-alignment of front bearing.

θ; Miss-alignment angle of screw (radians).

L; Length between supports.

t; Distance slide from front bearing.

E; Young's moduls of screw.

I; Moment of Inertia of screw $\left(I = \frac{D^4}{64} \right)$.

D; Screw diameter.

G; Bearing stiffness perpendicular to motion assuming beam and slide rigidity infinite.

Figure 2.1, Miss-alignment of a ball screw and linear slide.

2.2.2 Capstan Drives

Capstan drives are very similar to rack and pinion drives, the difference is friction between the capstan and drive rod as shown in Figure 2.2 converts rotatory to linear motion much like the a rack and pinion uses meshed gears [21]. The capstan is typically direct driven by a brushless DC motor. High precision bearings fixture the capstan and guide. The advantage of the capstan drive is there is no backlash like that associated with geared drives. High precision capstan drives use hand lapped capstans, drive rods and guides for greatest accuracy. However, with time these components will wear out.

The linear velocity v of the drive rod is:

$$v = R\omega \qquad (2.2)$$

where R is the capstan radius and ω is the angular velocity of the motor. At low speeds, a brushless DC motor will cog resulting in a torque ripple. To obtain smooth linear motion at low speeds, the motor must run at high speeds which requires the capstan radius to be small. The linear force F of the drive rod is:

$$F = \tau/R \qquad (2.3)$$

where τ is the motor torque assuming no slippage. The calibrator design acceleration rate is of 3 g's. Using Newtons law, where m is the mass of the drive rod and load plus the rotor, capstan, guide inertia, the friction force F can be calculated. This is also the linear drive force. The dynamic coefficient of steel on steel unlubricated is $\mu = 0.4$. The

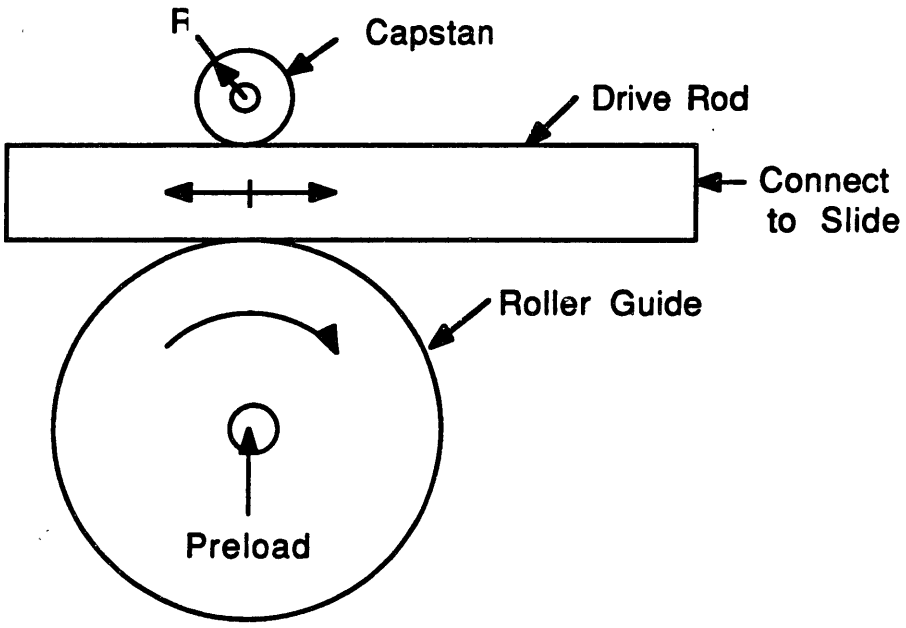

Figure 2. 2, Capstan drive schematic.

minimum capstan preload F_p to prevent slippage under 3 g acceleration rates is:

$$F_p = F/\mu \qquad (2.4)$$

$$F_p = ma/\mu \qquad (2.5)$$

For example, a mass of 5 lbm requires a capstan preload of F_p = 37.5 lbf. As the mass increases, a higher preload is necessary to prevent slippage which ultimately results in more wear of the mechanical components.

Miss-alignment between the drive rod and linear slide can effect the systems' accuracy similar to coupling a ball screw with one bearing support to linear slides. In addition, the drive rod becomes a loaded column in one direction of travel. The drive rod size must be minimized for weight without sacrificing stiffness. A capstan drive could be utilized in the calibrator design, but is not recommended.

2.2.3 Linear DC Motors

Linear DC motors are becoming more accurate, cost effective and reliable linear actuators. Because a linear DC motor is a force transducer, there is no theoretical limit to the motors' resolution [22]. Tests run by the Cranfield Unit for Precision Engineering demonstrated that a linear motor can position a load to within 0.4 microinches of a commanded position. The resolution of the feedback transducer is usually the limiting factor in the system [23]. Linear DC motors developed by Anorad Corporation, Northern Magnetics and Inland Motor

have achieved positioning accuracy better than one microinch. Speed control to 0.0001 in/sec has also been achieved. The linear DC motors are capable of 4 g accelerations and 100 in/sec speeds. The length of travel can be as long as 20 feet [24,25,26].

A linear DC motor connects directly to the linear slide eliminating flexible couplings, backlash and bearing supports. Alignment is still an critical issue however. The high performance and reliability of rotatory brushless DC motor technology has been applied to the linearized versions. There are no contacting parts within a brushless motor: brush wear, arcing and EMI generation are not a problem. Therefore, integrity and cost of the motion system can be greatly improved by using a brushless linear DC motor.

Linear DC motors have very fast servo responses allowing for servo bandwidths in excess of 30 Hz depending on the weight of the driven system, correspondingly low settling times and high servo stiffness. The maximum obtainable velocity is a function of the terminal voltage, the IR drop and the back emf of the motor. The maximum obtainable acceleration is a function of the current rating and the force constants of the motor. Heat dissipation in the armature is affected by three factors: ambient temperature, armature mounting and length of motion. Forced cooling, liquid or air, will increase the heat dissipation and thus can increase motors continuous force rating.

There are two configurations of linear motor's: moving coil and moving magnet as shown in Figure 2.3. The moving coil configuration has the advantage of less moving weight and no cogging like the moving magnet configuration [22]. The result is smoother motion and better response. The moving magnet configuration has a high attractive force

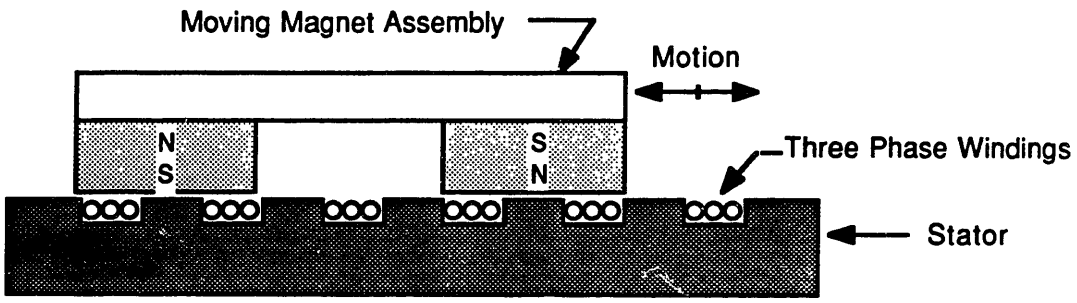

A) Moving magnet linear motor.

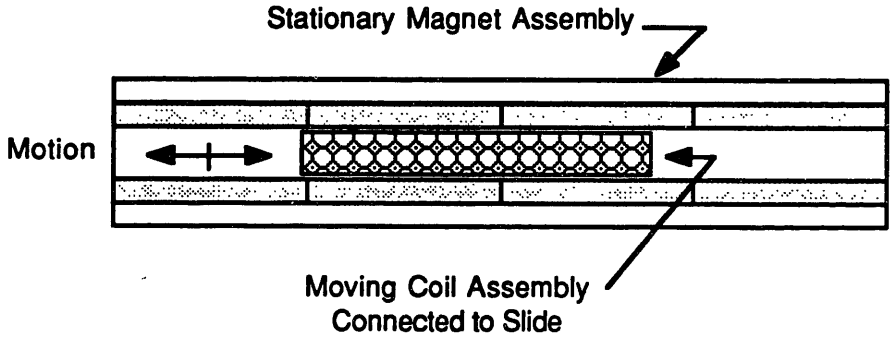

b) Moving coil linearmotor

Figure 2.3, Linear DC motor configurations.

between the moving magnet and the coil. This attractive force can be several hundred pounds and must be compensated for in the bearing design or with a balanced magnet design so that an air gap of 0.005 to 0.015 inches is maintained. Variations in the air gap during motion will cause motor force perturbations.

A "off-the-shelf" linear electric motor will satisfy the calibrator design based on the manufactures specifications. An Anorad linear Brushless DC motor with moving coil will be used in the prototype calibrator design. This motor was chosen because of its high force to weight ratio of 7.2, the moving coil design that has limited cogging and the brushless design that eliminates brush wear and has no sliding or contacting parts that could generate noise or vibrations.

2.2.4 Hydraulic Cylinders

Hydraulic cylinders have very high force capabilities but limited speed capabilities. Consider a 1.0 in^2 piston and a typical fluid line pressure of 2000 psi, in order to reach the design speed of 20 in/sec, the hydraulic pump must be rated at 20 in^3/sec or 5.2 gallons/min. An average hydraulic pump would meet these specifications, but its noteworthy that a 2000 lbf is an exaggeration of the force requirements. If the pressure level is decreased, than the flow rate must be increased for a constant tubing diameter. In designing a hydraulic system such as the above, careful fluid flow analysis must be made when sizing the tubing diameter. The tubing size along with pressure and flow rate determines if a laminar or turbulent flow exists. Turbulent flows along with vibrations generated in the pump can cause excessive noise levels in the accelerometer measurements.

In addition to requiring a hydraulic cylinder and pump, a hydraulic servo value is needed for flow control along with a fluid reservoir and filters. Hydraulic systems require expensive components in order to implement an actuator and for this application, the cost of these components plus the excessive force capabilities eliminate it as a viable design option. Note, hydraulic systems are used in the modal testing of large structures where the force capabilities can be met with no other means. For the small high cycle calibrator, hydraulic cylinders are a poor choice as an actuator.

2.2.5 Wire Drive Systems

A wire drive system uses a pretensioned wire driven by a motor-pulley combination to position a linear slide. The positioning accuracy is affected by the stiffness of the wire much like flexible couplings affect accuracy in ball screws. The stiffness K of the wire is:

$$K = AE/L \qquad (2.6)$$

where A is the cross sectional area of the wire, E is the modulus of elasticity and L is the wire length. The longitudinal natural frequency f_n can be estimated as:

$$f_n = (K/m)^{1/2}/(2\pi) \qquad (2.7)$$

$$f_n = (AE/(mL))^{1/2}/(2\pi) \qquad (2.8)$$

where m is the mass of the slide. Taking the wire length L as 6 inches, the slide mass m as 5 lbm, assuming a steel wire with E of 30E6 psi

and a natural frequency f_n of 150 Hz (50 Hz greater than the desired bandwidth), the wire cross sectional area must be greater than 0.028 in^2. This equates into a wire diameter of 0.19 inches which is large considering it must wrap around various pulleys. In general a pulley diameter needs to be 200 time the wire diameter to prevent a permanent set in the wire [27]. Obviously a pulley diameter of 38 inches makes the wire drive excessively large and subsequently is ruled out for use in the calibrator design. Several factors to address if the wire drive is used under different circumstances: the fatigue life of the wire. under the required pretension and the resulting structural deflections.

2.2.6 Electrodynamic drives

The theory of operation of an electrodynamic drive is based on the Lorentz force equation:

$$\underline{F} = \underline{B} \times \underline{I} \qquad (2.9)$$

where F is the force, B is the flux density of the magnetic field and I is the current in the conductor. The displacement of an electrodynamic drive is limited by the size of the magnetic poles producing the field and the force is limited by the maximum current the conductor can withstand as shown in Figure 2.4.

As stated in Chapter 1, most calibrators to date use custom made electrodynamic drives. One such drive has been built with a 39 inch displacement and peak acceleration of 1.2 g [16]. No suitable commercial electrodynamic drives are available. Acoustic Power

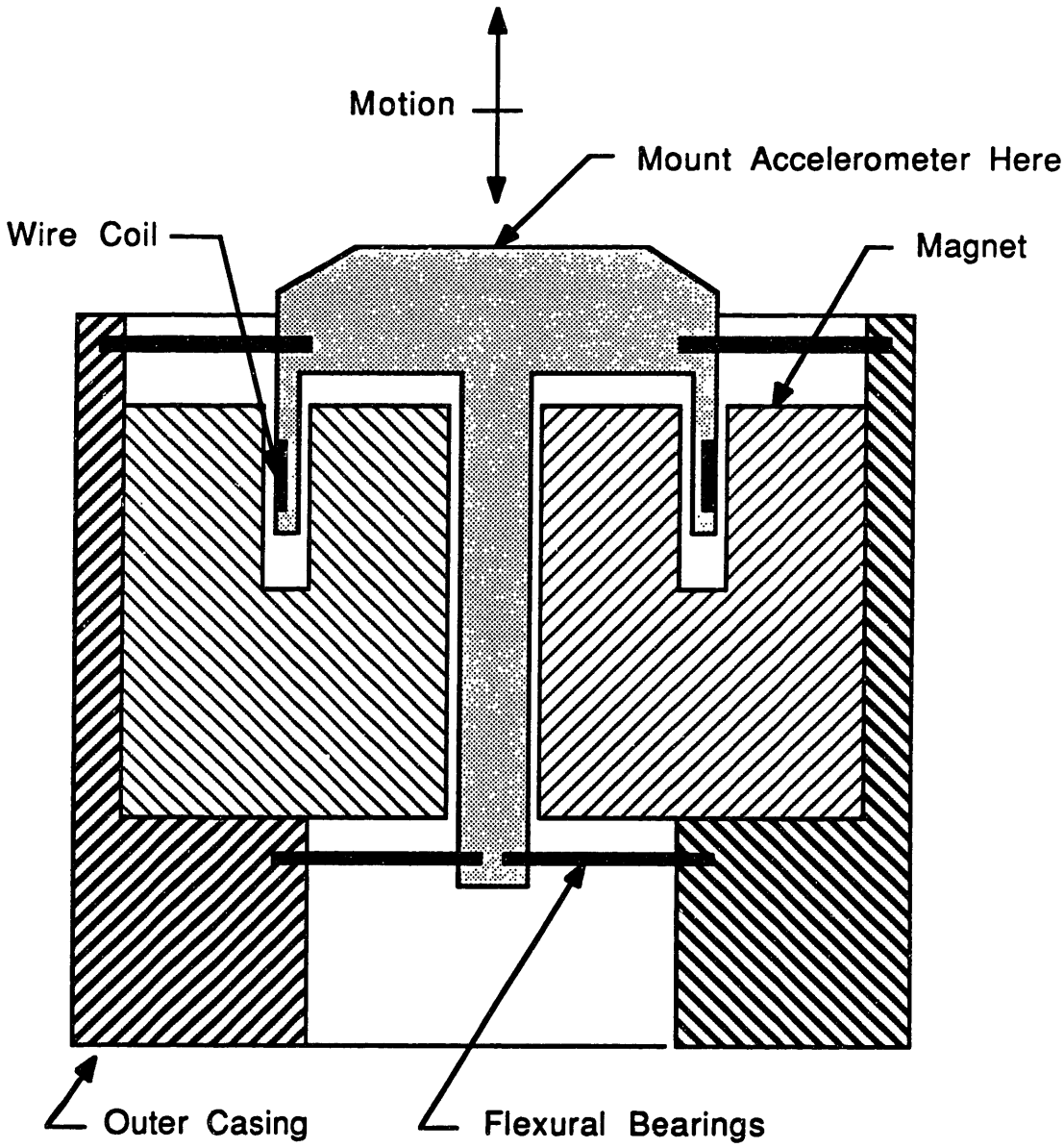

Figure 2.4, Electrodynamic drive assembly.

Systems, Inc. [28] comes close with their model 113-AB shaker used for modal analysis of structures. It has a 6.0 inch displacement, 200 Hz bandwidth and no load acceleration of 0.25 g's. Calibrators have been built around electrodynamic drives for years and have been proven reliable and successful. A custom made electrodynamic drive would thus be used if no other alternative (e.g. linear DC motors) existed.

2.2.7 Piezoelectric Drives

Piezoelectric stacks and piezoelectric inch worm motors are capable of sub microinch resolution, but are incapable of large displacements at high speeds with current technology [29]. Subsequently, they are unsuitable for the calibrator design.

2.2.8 Comparison of Linear Actuators

A comparison of linear actuators is given in table 2.1. The linear electric motor has the best positioning accuracy and axial force combination than the other actuators. Thus the linear DC motor was chosen as the actuator for the calibrator design. A ball screw has excellent positioning accuracy but is limited by its axial force and acceleration. The electrodynamic drive is a good actuator but only over small displacements. The wire, piezoelectric, capstan and hydraulic drives are not suitable for the calibrator design.

2.3 Analysis of Linear Bearing Systems

From the design specifications, the cross axis motion or straightness error must be minimized to 0.6 microinches for a 600 microinch travel. Straightness greater then the design value shows up

Table 2.1 Characteristics of Linear Actuators.

	Ball screw	Capstan drive	Linear motor	Hydraulic cylinder	Wire drive	Electro-dynamic	Piezo-electric
Axial Stiffness	Δ	◊	Δ	•	≈	◊	≈
Back-lash	Δ	•	•	•	≈	Δ	≈
Position accuracy	•	Δ	•	Δ	≈	Δ	Δ
Speed variation	◊	◊	◊	≈	≈	Δ	≈
Periodic errors	≈	◊	◊	◊	Δ	Δ	≈
Axial force	Δ	≈	•	•	◊	Δ	≈
Length of travel	◊	◊	Δ	≈	Δ	≈	≈
Cost	◊	◊	Δ	≈	Δ	Δ	◊

•	Excellent
Δ	Good
◊	Average
≈	Poor

as an error in the accelerometer's output. The bearing stiffness must be maximized to reduce static and dynamic loading errors. A low friction bearing system is desired for controllability and long life. Described below are bearings currently used in precision mechanical systems.

2.3.1 Ball Bearings

Precision ball bearing components with microinch smoothness are available but at considerable expense. Diamond turning and coordinate measuring machines are examples of systems with microinch accuracies that utilize ball bearings or roller bearings. Microinch accuracies are only achievable in temperature controlled environments and at low speeds. The friction in the rolling parts is undesirable from the controls and wear stand point. At low speeds, the roller elements may slip, not roll, due to friction. When the roller element does start to roll, the transition can show up as spikes in some displacement transducers. For the above reasons, ball or roller bearings are not suitable for the calibrator design.

2.3.2 Polymeric Bearings

Polymeric bearings made from material such as Delrin or Teflon are finding their way into precision mechanical systems. Small polymeric pads are currently used in semiconductor wafer steppers that have microinch resolution. These pads, which are attached to a platen and slide on a precision ground way. The accuracy of the platen is a function of the precision ground way and the dynamic loading. Typically the only preload on the bearing pads is the weight of the

platen The wear characteristics are very good when this loading is minimal. For dynamic loads present in the calibrator design, multiple preloaded bearing pads would be necessary to constrain the slide in five degrees of freedom. This preload causes increased wear in the pad. This bearing technology is still being developed and at this point is not applicable to the calibrator design.

2.3.3 Magnetic

Magnetic bearing technology is a rapidly growing field. For microinch accuracies, the technology is still at a research and development stage with SatCon Technology Corporation in Cambridge, Massachusetts a leader in this field. Magnetic bearings are frictionless because no contact is made between the bearing pad and bearing surface. This gap is maintained using a feedback transducer and closed loop control system. To constrain a linear slide to only one degree of freedom, multiple bearing pads are required. The overall cost is therefore substantial. Current high accuracy magnetic bearing technology preforms well under static conditions or limited range of dynamic motion, but is not practical for long travel dynamic conditions like the calibrator design.

2.3.4 Air bearings

Air bearings are currently used in the NBS and East German calibrators [9,10,16]. A linear air bearing uses the expansion of high pressure air through a jeweled orifice or groove to create a film of air between a stationary guide, commonly referred to as the beam, and the moving slide [18,19,21,30,31]. This film of air prevents contact

between the moving parts and has a stiffness on the order of millions of pounds per inch. The gap between the parts is typically 100 to 200 microinches, larger gaps decrease the stiffness of the air film. On the other hand, smaller gaps are more difficult to manufacture. Air bearings are frictionless and therefore have will not wear. Air bearings have very smooth motion, no rolling elements, making them ideal for a calibrator design, wafer steppers and other precision applications. But if the bearings are not properly designed, they can exhibit instabilities referred to as pneumatic hammer.

A very common air bearing design uses a precision ground beam supported on both ends with a four sided carriage [18,19,21,30,31] shown in Figure 2.5(a). The carriage is attached to an air supply and slides along the beam. The straightness of travel can be good as 0.4 microinches per inch. A design that eliminates the beam sag due to gravity is supported along its entire length as shown in Figure 2.5(b). This bearing rests on a surface plate to achieve maximum straightness of travel. The supported design allows for longer travels, higher payload and higher natural frequencies.

The beams are typically made from either alumina oxide or aluminum, whose material properties are contrasted in Table 2.2. If alumina oxide were used for the construction of the beam, a 30% increase in weight, a 440% increase in the modulus of elasticity and 68% decrease in thermal expansion would result when compared to aluminum. Therefore, the alumina oxide beam would be over four times stiffer than an aluminum beam and less susceptible to thermal gradients. In addition, the internal damping characteristics are better

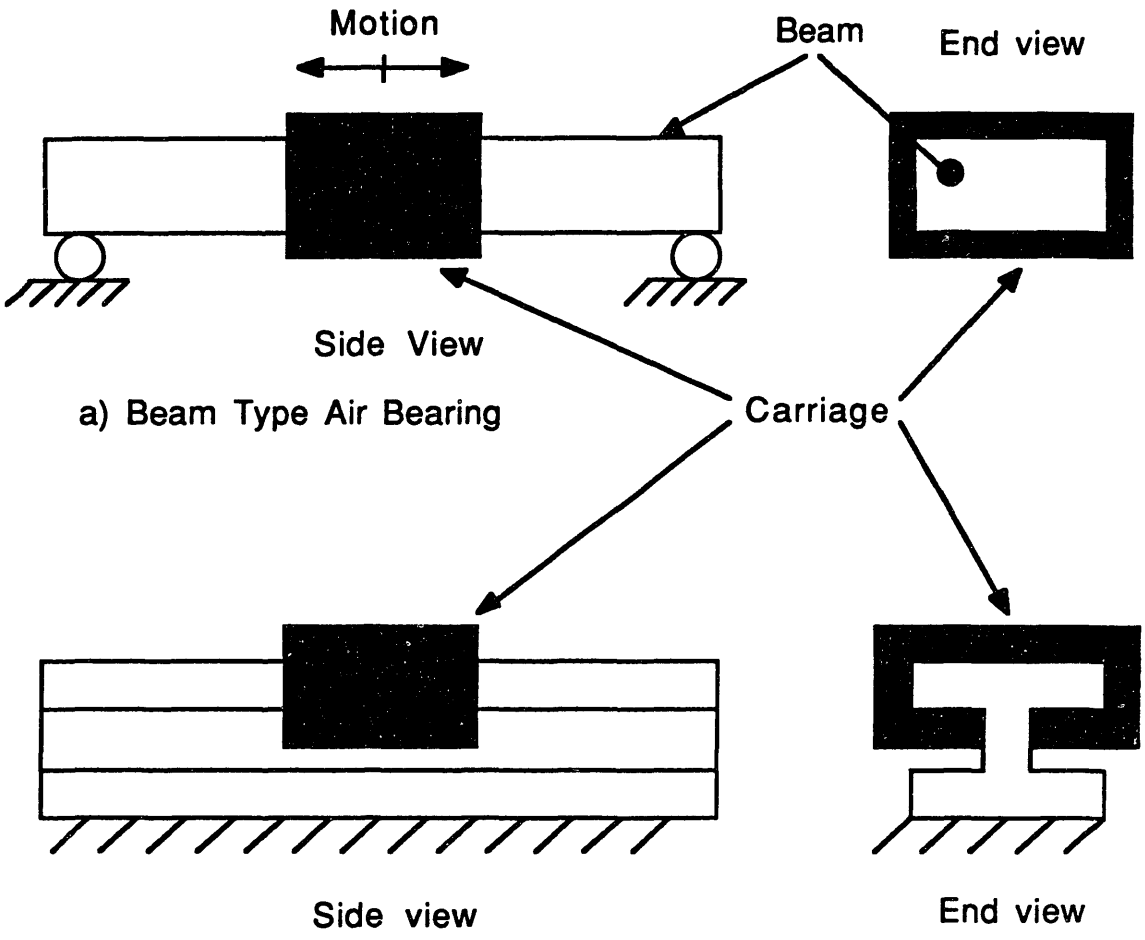

Figure 2.5, Linear air bearing configurations.

Table 2.2 Material properties of alumina oxide and aluminum.

Material	Modulus of elasticity (psi)	Density (lb/in^3)	Thermal expansion (in/in °C)
Alumina Oxide	54 E6	0.13	7.8 E-6
Aluminum	10 E6	0.10	24 E-6

in alumina oxide. Note that alumina oxide, a ceramic material, is more expansive to machine then aluminum.

An air bearing design for the calibrator will be used because of its stiffness, straightness of motion and the availability of off-the-shelf units that have a range of travel up to 78 inches.

2.4 Analysis of Sensor Systems

From the design specifications, the sensor system must be able to resolve axial motion to 0.6 microinches at speeds of 20 in/sec and at acceleration rates of 3gs. For absolute calibrations, the acceleration of the accelerometer was shown to be a function of amplitude and frequency. This sensor will measure the amplitude of displacement and must be traceable to a National Standard at the NBS. To meet this criteria, stabilized laser interferometers used. Below is an analysis of available linear sensor systems and why they fail the design criteria.

2.4.1 Linear encoders

Linear encoders are functionally equivalent to rotary encoders, and have resolutions up to 4 microinches at speeds of 5.9 in/sec [32,33]. This resolution requires 25 times interpolation and 4 times multiplication of the output from a glass scale with grating pitch of 400 microinches. Increased speeds are available at the sacrifice of resolution. Accuracy is ±0.1 micron. Linear encoders are traceable to the NBS, in fact both the NBS and manufactures use laser interferometers to calibrate the glass scales. With respect to the

calibrator design, linear encoders do not have the required resolution and speed capabilities.

2.4.2 Linear Variable Differential Transformers

The linear variable differential transformer (LVDT) is an electromechanical transducer that produces an electrical output proportional to the displacement of a separate movable core. Mechanically an LVDT consists of a small diameter movable core that translates within a casing the contains the primary coil and two secondary coils. The position of the core changes the voltage induced on the secondary coils by the primary coil. The induced voltage of the secondary coil is proportional to position.

While LVDTs have infinite resolution, their resolution is limited practically by the instrumentation used to measure the LVDT's output. Consider an LVDT output range of ±10 volts over a displacement of 6 inches, using a 16 bit analog to digital convertor the measurement resolution is 90 microinches. The LVDT's maximum speed is a function of the transducer's frequency response, manufacture's specifications must be consulted for a particular unit but typically are 200 Hz at -3 db. A LVDT must be calibrated prior to their use, laser interferometer or precision micrometer is typically used for the calibration. An LVDT's linearity is typically ±0.25%, this can be extended to ±0.024% by using an algorithm and technique for transducer linearization [34].

With respect to the calibrator design, a LVDT would not have the required resolution due to the measuring instrumentation and thus could not be used. If a LVDT did have the resolution, calibration uncertainties of the LVDT must be factored into the calibration

uncertainties of the accelerometer: therefore can increase the overall calibration uncertainty.

2.4.4 Inductosyns

A linear inductosyns' geometry is similar to that of a linear encoder. The difference is a inductosyn utilizes inductive coupling between two coils bonded to a strip of metal to form a scale. The coils are a continuous rectangular waveform with cyclic pitch typically 0.1 in. When the scale is excited by a 5-10 KHz signal, $A\sin\omega t$, the outputs from the slider will be

$$S_{13} = B\sin(\omega t)\sin(2\pi X/S) \qquad (2.11)$$

$$S_{24} = B\sin(\omega t)\cos(2\pi X/S) \qquad (2.12)$$

where B is the magnitude, X is a linear displacement, and S is the spacing of the coil waveform. Accuracy of the motion depends on the accuracy of the coil waveform spacing, the best accuracy is typically ±40 microinches. It is possible to obtain higher resolutions using interpolation scheme, but this will decrease the accuracy of the measurement. An inductosyn would not be suitable for the calibrator design because they do not have the accuracy or resolution required.

2.4.5 Potentiometers

Linear potentiometers fail to meet the design criteria on the basis they require calibration and the limitation in the measuring instrumentation's resolution. Resolutions of 1 microinch are achievable with potentiometers over small distances, but they are noisy and wear out over a period of time.

2.4.5 Laser Interferometers

Two types of laser interferometry methods are used to make precise displacement measurements: single frequency fringe counting and optical heterodyne detection. Both methods use the extremely stable and well known wavelength of the Helium-Neon laser light as the reference: stability greater than 1 ppm and λ = 632.8 nm. Absolute calibrations use the displacement amplitude and excitation frequency to determine the accelerometers acceleration rate. The displacement amplitude measurement needs to have an accuracy greater than 0.01% (10 times better than the over all accuracy desired).

A typical fringe counting single frequency laser interferometer calibration set up was shown in Figure 1.1, Figure 2.6 shows the basics of the measurement system. The laser beam passes through a Michelson interferometer where apportion of the beam is split. A reference beam remains in the interferometer while the measurement beam is passed to the retroreflector mounted on the test stand. The beam returns parallel to itself and back through the interferometer where the two beams recombine. Interference fringes occur between the two beams for retroreflector displacements of $\lambda/2$. A photodiode detects the fringes and generates electrical pulses. A counter records the number of pulses n per vibration cycle. The displacement amplitude X equals:

$$X = n\lambda/8 \qquad (2.13)$$

For sinusoidal motion, the peak acceleration A_o is given by:

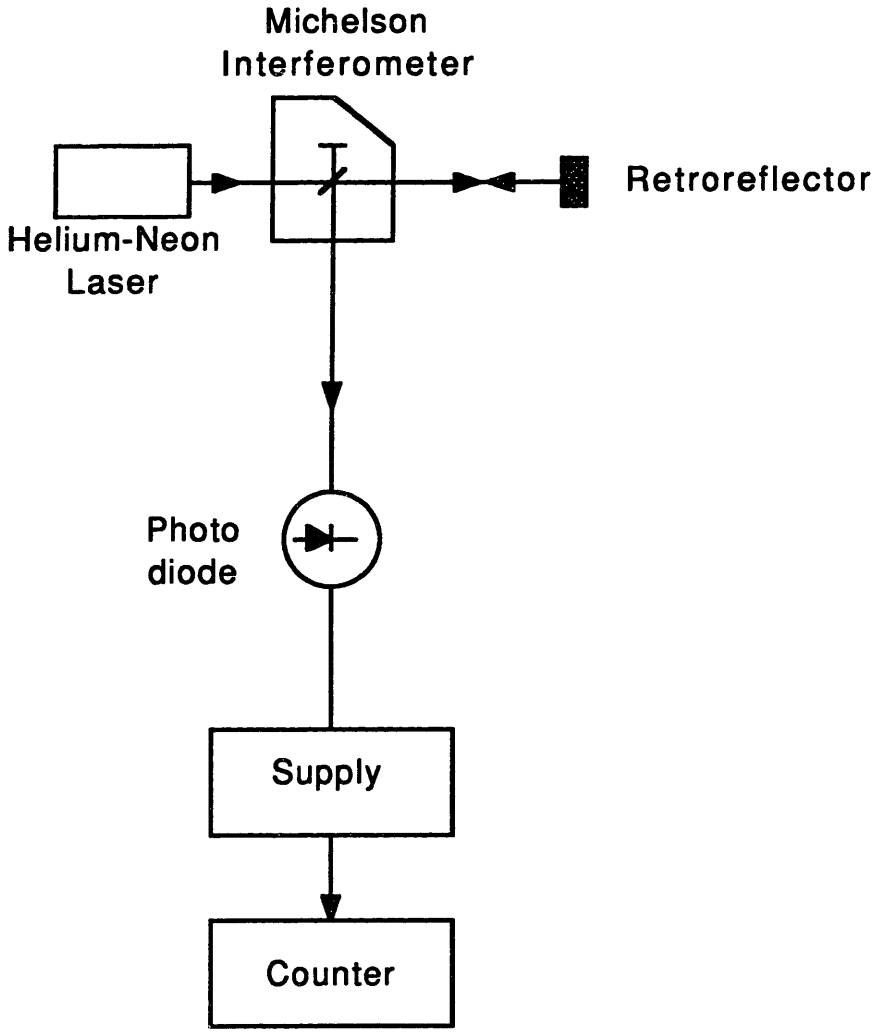

Figure 2.6, Fringe counting laser interferometer system.

$$A_o = (2\pi f)^2 n\lambda/8 \qquad (2.14)$$

where f is the frequency of vibration. An error in the fringe counting occurs when the displacement amplitude is not an integral multiple of $\lambda/2$. At low frequencies where the displacement amplitudes are to be 3 inches, the fringes per cycle would be 480,000 counts. An error of one count results in a 0.0002% error. At high frequencies where the displacement amplitude is 300 microinches, the fringes per cycle would be 48 counts. An error of one count results in a 2% error, 20 times the design accuracy. Clearly, fringe counting method does not meet the design criteria.

An optical heterodyne interferometer, on the other hand, can achieve resolutions of 12 Å. Such laser beams have two orthogonally linearly polarized components that differ in frequency. The laser beams are stabilized to better than 1 part in 10^7 by controlling the temperature of the laser tube and subsequently its length. A constant length laser tube means a constant frequency is maintained (the frequency is related to the wavelength and speed of light). The laser beams are further processed depending upon the scheme chosen by a commercial manufacturing of the laser heads. For more information consult the Zygo Corporation and Hewlett-Packard product literature [35,36,37,38]

The two frequency laser interferometry has proven to be superior to single frequency laser interferometry for over a decade. The main advantage of the two frequency approach is that distance information is carried on AC signals as the phase difference between the frequencies rather than as the amplitude as in the single frequency DC

signal. These two methods are similar to FM versus AM signals. The FM signals have a much higher signal-to-noise ratio with less power required to achieve it. Compared with a single frequency system, the tow frequency system achieves a longer measurement range, greater measurement stability and far less sensitivity to various noise sources that affect a measurement.

During measurement, the laser beam exits the laser head with frequency components F_1 and F_2 and enters an interferometer as shown in Figure 2.7. The interferometer splits the beam at the surface of a polarizing beam-splitter, with frequency F_2 reflected into the reference retroreflector mounted on the interferometer housing. Frequency F_1 is transmitted to the moving retroreflector, then returned to the interferometer where it is recombined with frequency F_2. Both frequencies travel along a common axis to the photodetector in the receiver.

Relative motion between the interferometer and the retroreflector causes a Doppler shifted frequency component ΔF_1. The electronics unit measures the phase change and determines the optical path change, this of course relates to a physical displacement of the retroreflector. Different phase measuring technics are used by the manufactures, Zygo Corporation has achieved resolutions of $\lambda/254$ for a linear interferometer with a maximum slew rate of 70 in/sec and no limit on the acceleration [35,36]. Zygo is the only manufacture able to meet the required specifications for the calibrator as shown in Table 2.3 and subsequently their system will be used in the calibrator design.

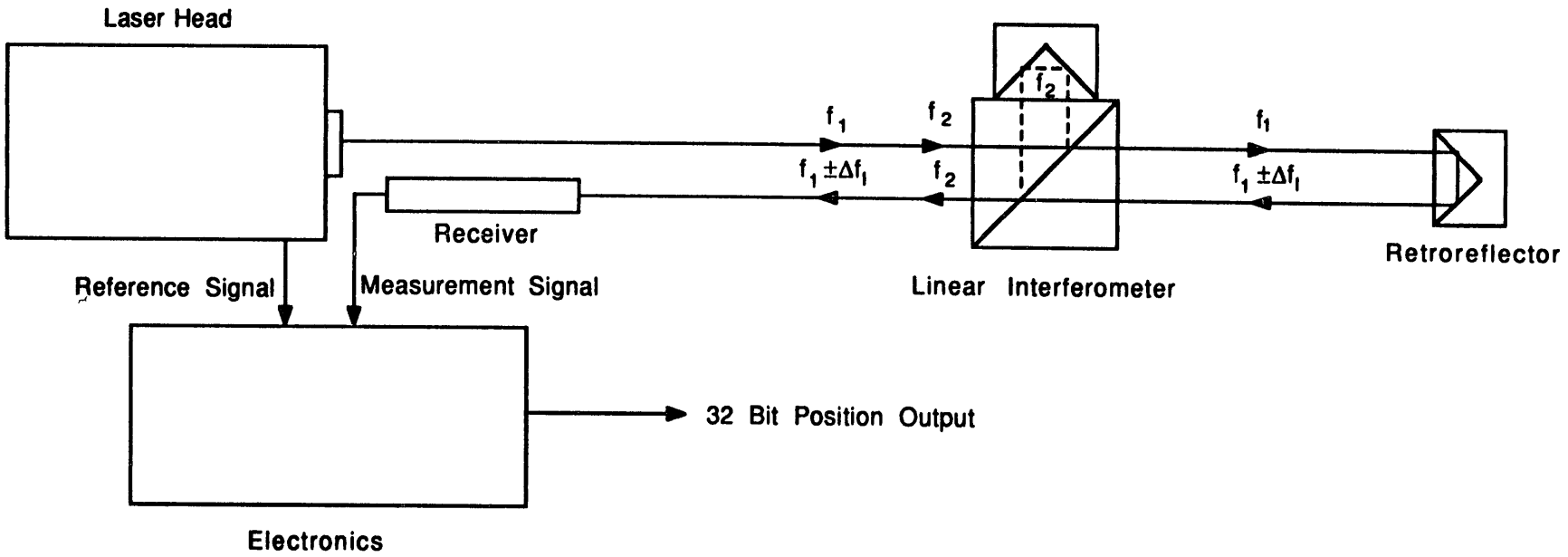

Figure 2.7, Block diagram of optical heterodyne laser interferometer system.

Table 2.3 Comparison of Hewlett Packard and Zygo laser systems.

	HP5527A	Axiom 2/20
Stability	±[0.02 ppm + 0.2 μin]	±[0.01 ppm + 0.1 μin]
Measurement Resolution (Single Pass Interferometer)	0.4 μin	0.1 μin
Measurement Velocity	16 in/sec	70 in/sec
Measurement Acceleration	10 g maximum	no limit
Data Transfer Rates (32-Bit Parallel Output)	1.5 to 2.0 MHz	2.0 MHz
Analog Velocity Output	±10%	±10%
Laser	Helium-Neon	Helium-Neon

2.5 Control Systems

The control system for the calibrator should utilize an accelerometer to obtain acceleration feedback. This is currently available in commercial calibrators such as the Bruel & Kjaer Instruments' model 4294 [39]. A block diagram representation of a proposed control system for the accelerometer calibrator developed herein is shown in Figure 2.8. The difference between the sinusoidal reference signal and acceleration feedback is applied to an amplifier which produces a current in the actuator. The actuator accelerates the carriage where an accelerometer is attached. The accelerometer output signal is then fed back to the controller where is is used to stabilize the control loop.

Real time methods for predicting and compensating for errors in machine tools has been developed [40]. Since it is impossible to build a machine tool without errors, the errors are mapped and corrected with a real time controller. Accuracy enhancements of 20 times has been achieved on a two axis computer numerical controlled turning center. The calibrator design is considerably smaller with fewer components than a machine tool; thus it should be possible to construct the calibrator with the necessary mechanical accuracy, eliminating the need for such a real time compensation scheme.

The overall setup will be controlled by a personal computer as shown in Figure 2.9. The PC will set the reference signal generators frequency and amplitude, measure the accelerometer output with a digital voltmeter and measure the displacement amplitude with the laser interferometer. The PC will then generate a calibration report for the test accelerometer.

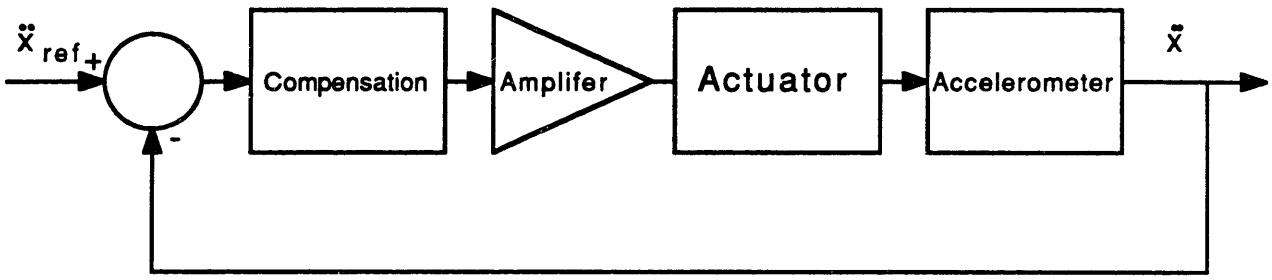

Figure 2.8, Block diagram of acceleration servo system.

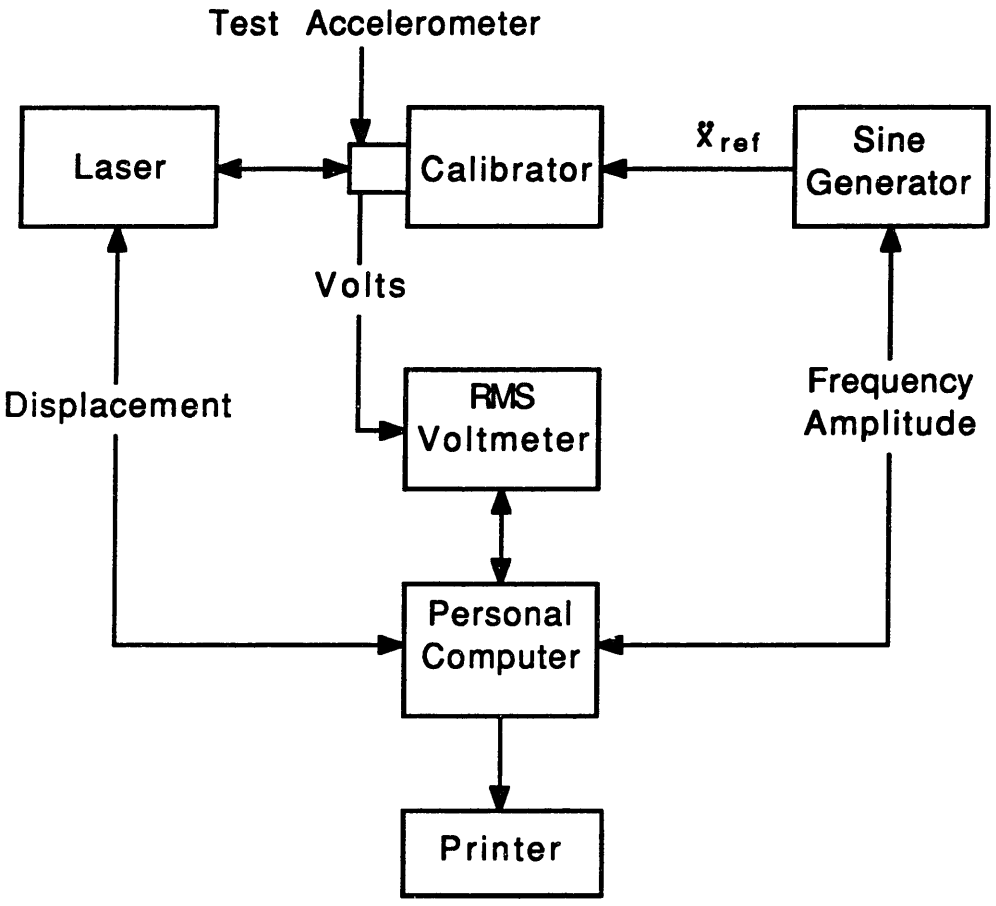

Figure 2.9, Diagram of overall calibration setup.

2.6 Proposed Design Configuration

From the above discussion, the specifications of the calibrator design are best met with the following hardware components: Anorad linear brushless DC motor model LP2 as the actuator, a linear air bearing and Zygo's Axiom 2/20 laser interferometry linear displacement transducer system.

The use of these components allows the specifications to be increased to a 16 inch double amplitude displacement, 8.5 time larger; a 50 in/sec minimum velocity and maximum constant acceleration of 0.8 g over the bandwidth. The disadvantage is the bandwidth is decreased to 22 Hz due to the extra mass of the carriage and mounts. This is acceptable to the NBS since their remains an overlap in this frequency range with other calibration equipment [8]. This design should allow calibrations below 1 Hz: large displacements are required in the low frequency range in order to produce a transducer signal that can be accurately measured.

Several design configurations exist with the above components. The under-over design shown in Figure 2.10 is a simple implementation. The beam of the linear air bearing is supported on both ends with the linear motor's stationary magnet assembly fixtured to a surface plate under the beam. The moving coil assembly of the motor mounts directly under the air bearing carriage. The optics and accelerometer mount directly over the carriage. This design has the disadvantage in that the beam sag due to gravity may result in large cross axis motion as seen by the accelerometer. Also, the motor force vector is not directed through the centroid of the bearing. This causes moment loading on the

air bearing resulting in a rotation of the carriage. By mounting the optics and accelerometers on top of the carriage, any rotation of the carriage is amplified by the distance from the carriage centroid to the accelerometer causing Abbe errors.

The side-over configuration shown is Figure 2.11 uses a supported air bearing to eliminate the beam sag problem. The motor is mounted on the side and the optics remain over the carriage. Again the force vector is not through the centroid, so the moment loading will still cause carriage rotations. A side-side-over configuration shown in Figure 2.12 uses two motors on opposite sides to balance the forces and eliminate the moment loading. The optics remain over the carriage. This design has the disadvantage of requiring two motors, two amplifiers and two controllers with a substantial increase in cost.

A fourth configuration called the inside-over is shown in Figure 2.13. A supported air bearing is used that has slot cut over its full length. The motor magnets would be epoxied to the vertical surfaces of the slot. The motor's moving coil then is mounted underneath the carriage aligned with the slot. The optics remain over the carriage, but could be mounted on both sides of the carriage in a balanced fashion. This design requires one motor which has its force vector aligned with the carriage's centroid to eliminate the moment loading.

The best design is one that produces zero Abbe errors. This is accomplished by having the force vector, optics and accelerometers aligned with the carriage centroid. The designs progress sequentially until the inside-over design comes closest to this criteria. The cost also increases sequentially for these designs. The supported air

bearing is more expensive then the beam air bearing and modifications to a standard bearing would be excessive.

The under-over design is less expensive to implement and is considered the worst case. The analysis of Chapter 3 will focus on determining if such a design could meet the calibrator design specifications.

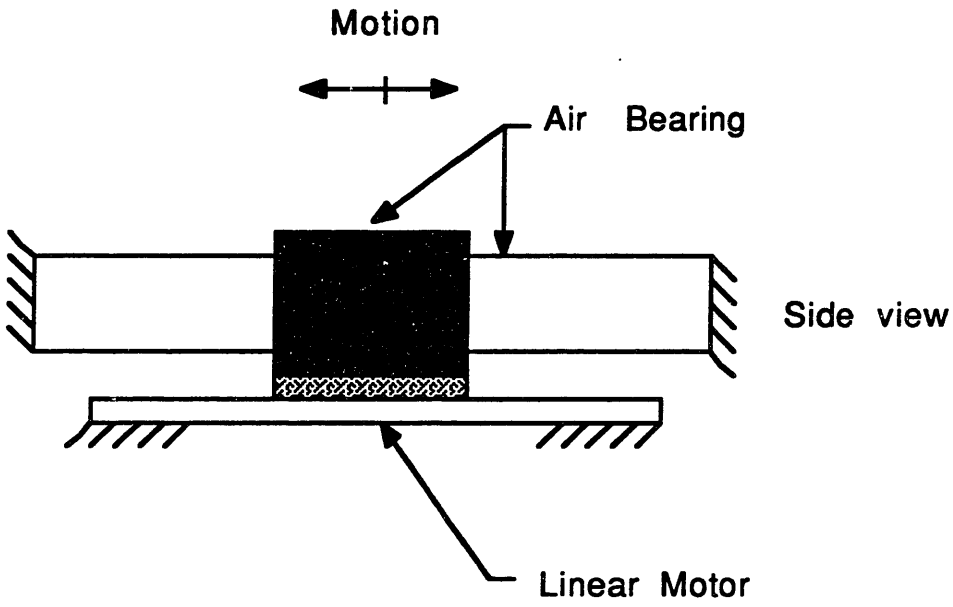

Figure 2.10 The under-over calibrator design configuration.

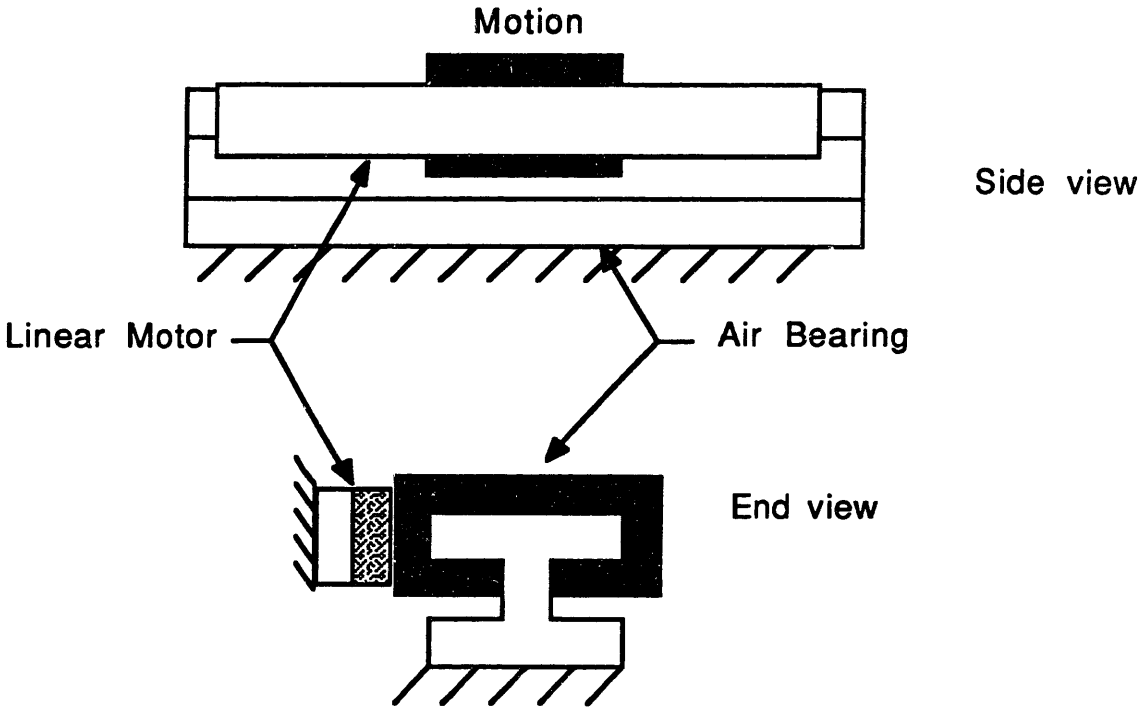

Figure 2.11, The side-over calibrator design configuration.

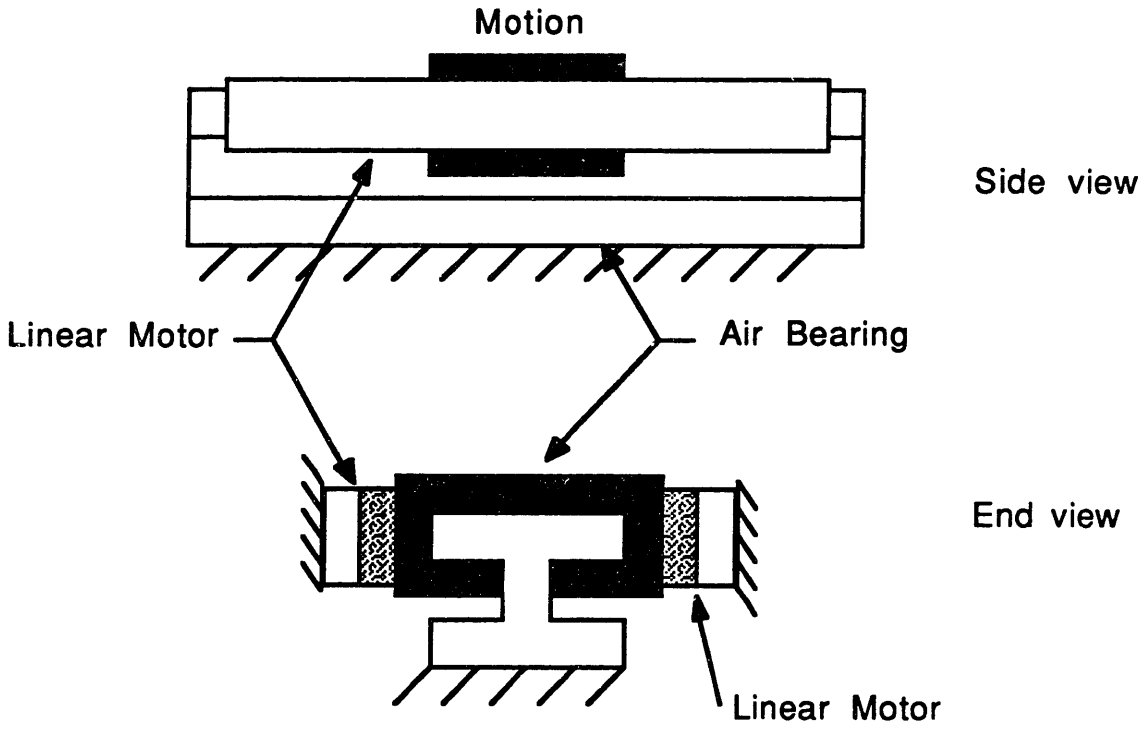

Figure 2.12, The side-side-over calibrator design configuration.

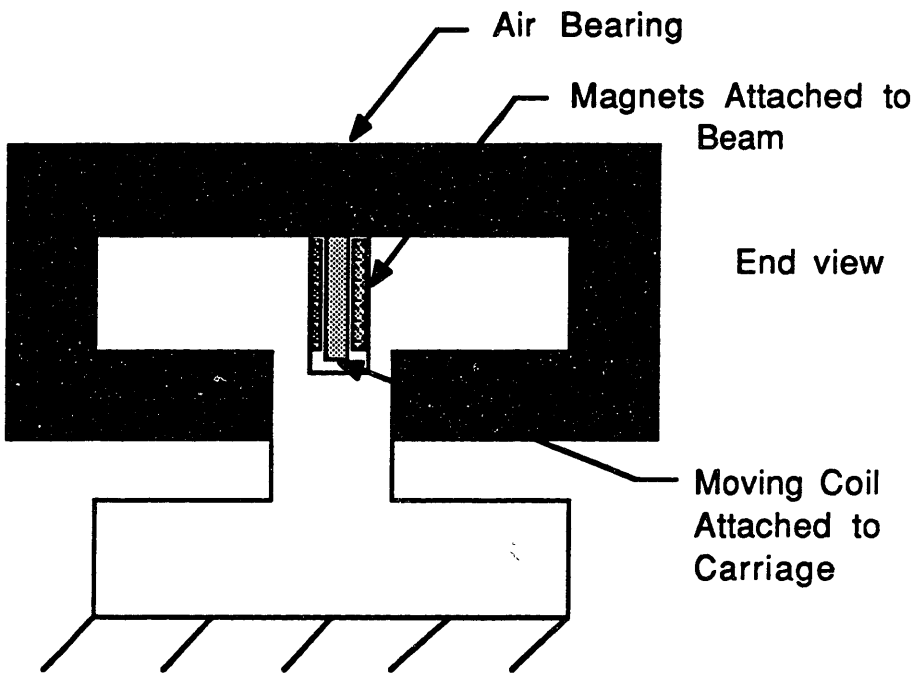

Figure 2.13, The inside-over calibrator design Configuration.

Chapter 3
Theoretical Analysis of Design

3.1 Introduction

The design of the calibrator using standardized components must proceed in an iterative fashion. Factors to be considered include:

- Air bearing model (type and number of carriages, resultant stiffness).
- Error motions at the center of the accelerometer as a function of system geometry, stiffness, and applied loads.
- Frequency and amplitude of operations, and the resultant forces generated in achieving them.
- Environmental fluctuations and the resultant effects on the stability of the calibrator.

While the analysis that follows is generic for a one degree of freedom linear slide, the results focus on using a Dover Instrument model 850-S air bearing with 20 inch travel, Anorad LP2 brushless DC linear motor with continuous force output rating of 18 lbf and Zygo Axiom 2/20 laser interferometer position measurement system with 0.1 microinch resolution and maximum allowable slew rate of 70 in/sec. Such an air bearing was available for loan along with a Zygo Axiom 2/20 laser transducer system.

3.2 Error Budget Analysis

An error budget is a tool used for predicting and controlling the total error of a system at the design stage [41]. Given a system error

design specification such as with the calibrator design, an error budget can be used in a predictive mode to assess error contributions of proposed subsystem designs, leading to a predicted overall system error. Typically the predictive mode is an iterative process.

Two assumptions are made when using an error budget. The instantaneous value of the total error in a specified direction, is the sum of all the individual error components in that direction and the individual errors have physical causes that can be isolated and measured to allow reduction or prediction of the error magnitude. Generating an error budget is a multi-step process with the suggested sequence:

1) Identify **error sources** from the geometry, kinematics, dynamics and environmental effects. The worst case assumptions could be used to determine the error.
2) Determine the **coupling mechanism** that connects an error source to a displacement error at the tool tip (point of interest). For vibrational errors, they can be assumed omnidirectional and estimate the error as the maximum amplitude.
3) **Combine the displacement errors** by category and direction into a single displacement error. When complete detail is known, the resultant displacement error can be a function of position or time. When complete detail is not known, statistical methods can be used to combine errors (e.g. rms error)

Matrix tabulation of the error sources and resultant displacement errors are a convenient way of keeping track of the results. This

bookkeeping method of cause and effect matrices allow the user to pinpoint dominant errors and correct for them in the design.

The error motions associated with each of the six degrees of freedom for a typical machine carriage designed for linear motion along the x-axis is shown in Figure 3.1 [42]. There are six error terms, one for each degree of freedom. Rotations about the Cartesian axes are denoted as $\varepsilon_x(x)$, $\varepsilon_y(x)$ and $\varepsilon_z(x)$ were the rotation axis is indicated by the subscript and the dependence upon carriage position is displayed explicitly. These rotations are typically very small and are referred to as roll, yaw and pitch respectively. The remaining errors terms correspond to linear displacement errors. The positioning error $\delta_x(x)$ is the difference between the commanded position and the actual position. The vertical and horizontal motions of the carriage are referred to as straightness errors. The quantities $\delta_y(x)$ and $\delta_z(x)$ are the "y-straightness of the x-axis" and the "z-straightness of the x-axis" or they can be called "vertical straightness" and "horizontal straightness". Straightness errors are the residuals obtained from the subtraction of the best-fit straight line from the measurement data.

Error budgets for the quasistatic effects, modeled dynamics, unmodeled effects and laser interferometry will be developed in following sections according to the steps outlined above.

3.2.1 Error Budget of Modeled Quasistatic Effects

The quasistatic errors are a function of frequency and amplitude of oscillation and gravity. These error sources cause loads on the calibrator that occur along the X, Y and Z axes and about the X, Y and Z axes as shown in Figure 3.2. The weight of each component of the

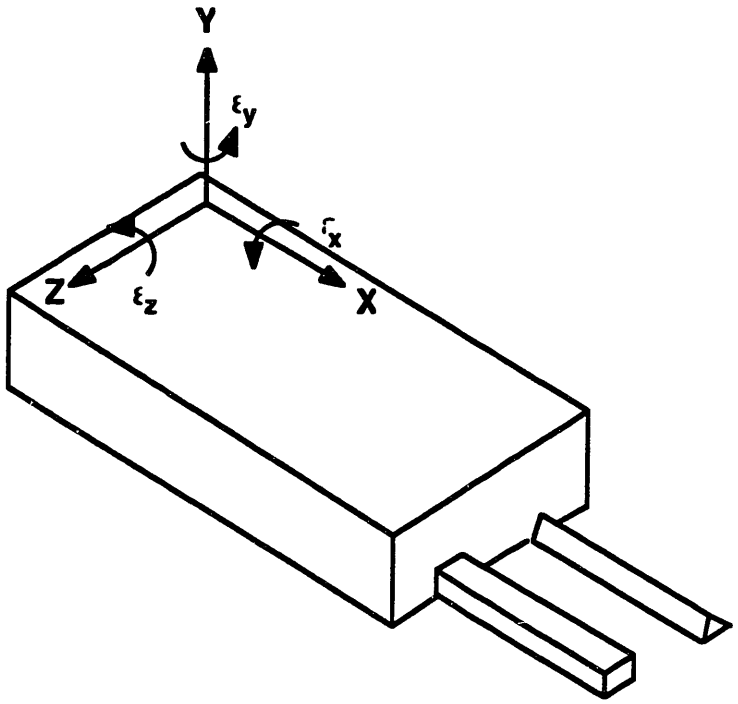

Figure 3.1, A typical machine carriage designed for linear motion along the X-axis.

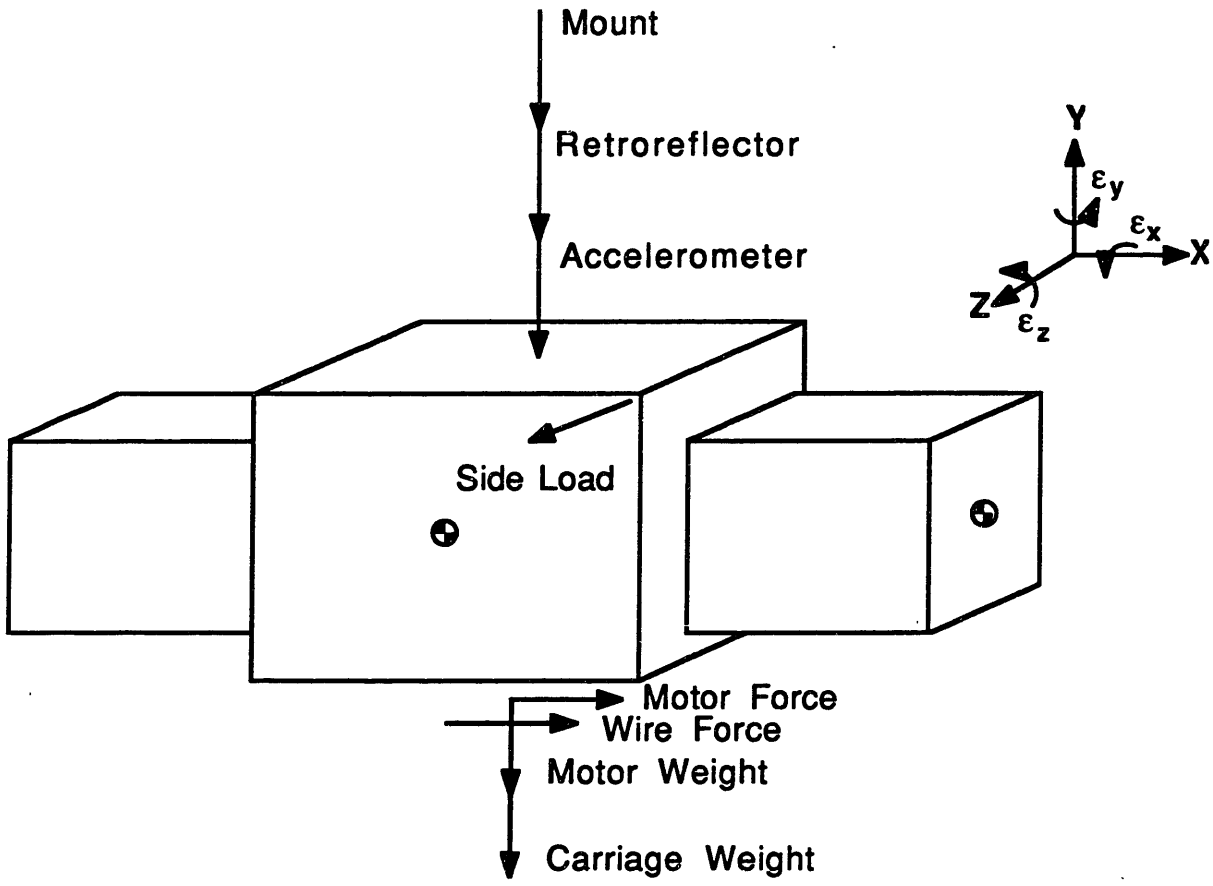

Figure 3.2, Diagram of load sources affecting the accuracy of the calibrator design.

calibrator is considered a load source, this includes the accelerometer, retroreflectors, accelerometer and retroreflector mount, motor and carriage. Also to be included is the motor force, which is a function of frequency and amplitude of oscillation according to:

$$F_m = m_s a = -m_s X_o \omega^2 \sin(\omega t) \quad (3.1)$$

$$x = X_o \sin(\omega t) \quad (3.2)$$

$$F_m = -m_s \omega^2 x \quad (3.3)$$

where F_m is the motor force, m_s is the mass of the accelerometer, retroreflectors, accelerometer and retroreflector mount, motor and carriage, x is the position of the carriage with respect to zero being the point about which the oscillation occur (the zero point is the center of travel on the air bearing slide) and ω is the frequency of oscillation in radians per second. Two additional load sources are: a umbilical load assumed to be 15% of the motor force and a side load assumed to be 15% of the accelerometer and retroreflector mount weight. These loads are an effort to account for the motor and air cabling effects on the carriage's accuracy. Loads offset from the centroid of the carriage will produce moments assumed to be about the centroid. Table 3.1 summarizes the load sources into their resultant forces.

The coupling mechanism that links the error sources to the displacement error is a result of the geometry of the calibrator, and elastic deflections. The displacement errors for the air bearing beam and carriage are summed together vectorially. These errors determine the accelerometer errors which defines the accuracy of the calibrator. The accelerometer errors are rotations of the accelerometer and displacements motions of the accelerometer that are not axial with it's sensitive axis. Formulation of error matrices for each stage of the

Table 3.1, Relationship between load sources and resultant forces effecting the calibrator design as a function of frequency, amplitude and gravity.

	Acceler-ometer	Retro-reflector	Mount	Motor Force	Motor Weight	Umbilical Force	Carriage weight	Side load
F_x	0	0	0	$M_s\omega^2x$	0	$-M_s\omega^2x15\%$	0	0
F_y	$2M_ag$	$2M_rg$	$M_{mn}g$	0	M_mg	0	M_cg	0
F_z	0	0	0	0	0	0	0	$0.15M_{mn}g$
M_x	0	0	0	0	0	0	0	$0.15M_{mn}gb_y$
M_y	0	0	0	0	0	$-0.15M_s\omega^2xa_z$	0	$0.15M_{mn}gb_x$
M_z	0	0	0	$M_s\omega^2xa_y$	0	$-0.15M_s\omega^2xa_y$	0	0

analysis follows, the general format is the horizontal heading of the error matrix is the cause of an error and the vertical heading is the resultant error at the accelerometer. Summing the individual horizontal components for a given cause yields the magnitude of the resultant error for that particular direction. When forces are the cause of errors, the matrix components will be a function of the stiffness. For error motions (e.g. slide straightness errors), the matrix component will be a function of the geometry involved.

3.2.1.1 Stiffness of Beam and Carriage

The beam is assumed to be an isotropic elastic beam of constant rectangular cross section and constant material properties. It is assumed to be simply supported at its ends in order to avoid thermally overconstraining it. The fully supported bearing is assumed to have a relative infinite lateral stiffness. The rotational and lateral stiffness for the beam of length $\ell = \ell_1 + \ell_2$, subject to forces and moments applied at $x = \ell_1$ respectively:

$$K_{\alpha F} = \frac{3EI(\ell_1 + \ell_2)}{\ell_1 \ell_2 (\ell_2 - \ell_1)} \tag{3.4}$$

$$K_{\delta F} = \frac{3EI(\ell_1 + \ell_2)}{\ell_1^2 \ell_2^2} \tag{3.5}$$

$$K_{\alpha M} = \frac{3EI(\ell_1 + \ell_2)}{\ell_1^2 + \ell_2^2 - \ell_1 \ell_2} \tag{3.6}$$

$$K_{\delta M} = \frac{3EI(\ell_1+\ell_2)}{\ell_1\ell_2(\ell_2-\ell_1)} \tag{3.7}$$

where E is the modulus of elasticity and I is the moment of inertia of a rectangular beam. The deflection or rotation is at a position $x = \ell_1$.

The lateral and rotational stiffness for the simply supported beam subject to the gravitational sag of its own weight W are:

$$K_{\alpha W} = \frac{24EI(\ell_1+\ell_2)}{\ell^3-6\ell\ell_1^2+4\ell_1^3} \tag{3.8}$$

$$K_{\delta W} = \frac{24EI(\ell_1+\ell_2)}{\ell_1(\ell^3-2\ell\ell_1^2+\ell_1^3)} \tag{3.9}$$

where E is the modulus of elasticity and I is the moment of inertia of a rectangular beam. The deflection or rotation is at a position $x = \ell_1$.

The torsional stiffness of the beam is given by:

$$K_{\alpha X} = \frac{(\ell_1+\ell_2)GK}{\ell_1\ell_2} \tag{3.10}$$

where G is the shear modulus and K is given by [43]:

$$K = ab^3\left[\frac{16}{3} - 3.36\frac{b}{a}\left(1-\frac{b^4}{12a^4}\right)\right] \tag{3.11}$$

the width of the beam is 2a and the height is 2b. The rotation is at a position $x = \ell_1$. Table 3.2 summarizes the stiffnesses of the beam, as a function of position, due to the resultant forces, resultant moments.and gravity. For the given load sources, using Tables 3.1 and 3.2, the deflections and rotations of the beam can be computed and the error contributions to the accelerometer predicted.

Table 3.2, Relationship between resultant forces and error motions of the air bearing beam as a function of position.

	F_x	F_y	F_z	M_x	M_y	M_z	Weight of beam, W
$\delta_{xb}(x)$	0	0	0	0	0	0	0
$\delta_{yb}(x)$	0	$\frac{3B(\ell_1+\ell_2)}{\ell_1^2\ell_2^2}$	0	0	0	$\frac{3B(\ell_1+\ell_2)}{\ell_1\ell_2(\ell_2-\ell_1)}$	$\frac{24B(\ell_1+\ell_2)}{\ell_1(\ell^3-2\ell\ell_1^2+\ell_1^3)}$
$\delta_{zb}(x)$	0	0	$\frac{3B(\ell_1+\ell_2)}{\ell_1^2\ell_2^2}$	0	$\frac{3B(\ell_1+\ell_2)}{\ell_1\ell_2(\ell_2-\ell_1)}$	0	0
$\varepsilon_{xb}(x)$	0	0	0	$\frac{(\ell_1+\ell_2)GK}{\ell_1\ell_2}$	0	0	0
$\varepsilon_{yb}(x)$	0	0	$\frac{3B(\ell_1+\ell_2)}{\ell_1\ell_2(\ell_2-\ell_1)}$	0	$\frac{3B(\ell_1+\ell_2)}{\ell_1^2+\ell_2^2-\ell_1\ell_2}$	0	$\frac{24B(\ell_1+\ell_2)}{\ell^3-6\ell\ell_1^2+4\ell_1^3}$
$\varepsilon_{zb}(x)$	0	$\frac{3B(\ell_1+\ell_2)}{\ell_1\ell_2(\ell_2-\ell_1)}$	0	0	0	$\frac{3B(\ell_1+\ell_2)}{\ell_1^2+\ell_2^2-\ell_1\ell_2}$	0

A similar analysis is applied to the carriage has one degree of freedom and five degrees of freedom constrained by air springs. Using Tables 3.1 and 3.3, the deflections and rotations of the beam can be computed and the error contributions to the accelerometer predicted. The stiffness values for the carriage are supplied by the manufacture and are listed in Table 3.5. The structural stiffness of the carriage was neglected because the cross sectional moment of inertia of the carriage is 15 times that of the beam. Thus only the deflections and rotations of the carriage associated with the compliance of the air bearing film is considered.

An option to increase the carriage stiffness would be to use two carriages on the beam. With this configuration, the two pitch stiffnesses add linearly, and the lateral stiffness act as an additional effective pitch stiffness component. Given that the distance between the center of the carriage is ℓ_c, the total effective pitch stiffness as a function of the individual carriage stiffness are:

$$K_{Ptotal} = 2K_{Pcarriage} + \frac{\ell_c^2 K_{Lcarriage}}{2} \qquad (3.12)$$

3.2.1.2 Air Bearing Beam Configuration

A beam type design has the fundamental advantage of being able to be mounted kinematically. Kinematic mounting can decrease the chance of distortion due to environmental effects such as heat from the motor causing differential expansion and bending. The principal problems with a beam type design are its lower natural frequency and higher lateral deflection (cross axis motion). The choice of beam

Table 3.3, Relationship between resultant forces and error motions of the air bearing carriage as a function of position.

	F_x	F_y	F_z	M_x	M_y	M_z
$\delta_{xc}(x)$	$K_{\delta x}$	0	0	0	0	0
$\delta_{yc}(x)$	0	$K_{\delta y}$	0	0	0	0
$\delta_{zc}(x)$	0	0	$K_{\delta z}$	0	0	0
$\varepsilon_{xc}(x)$	0	0	0	$K_{\varepsilon x}$	0	0
$\varepsilon_{yc}(x)$	0	0	0	0	$K_{\varepsilon y}$	0
$\varepsilon_{zc}(x)$	0	0	0	0	0	$K_{\varepsilon z}$

materials can make a significant difference in these quantities. For example, a beam made from alumina oxide has a specific stiffness (ratio of modulus of elasticity to density) 4 times greater than aluminum. Thus the deflections of the beam could be reduced to one quarter the deflections for the aluminum beam and the natural frequency could be increased by 2 times.

A fully supported design would utilize bearing rails rigidly fastened to an effectively rigid mass, such as a master flat. The flat would have to be lapped (or scraped) to a flatness better than that of the minimum required cross axis motion. If the flat were kinematically mounted on vibration mounts, it could result in a stiffer more accurate machine. The latter point, of course, depends on thermal compatibility of the rails and the flat.

The simply supported aluminum beam configuration is the most economical, it is an off the shelf item and will be used if possible.

3.2.1.3 Abbe Errors in the System

When the beam and carriage deflect, the translational errors sum directly. The effect of angular deflections of the beam and carriage causes Abbe errors in the Y and Z direction which causes cross axis motion of the accelerometer.

Figure 3.3 shows the geometry of the system, where the X and Y dimensions a and b are the distances of the center of the accelerometer to the center of the stiffness of the carriage. The latter is usually located at the geometric cross section center of the beam. Angular deflections ε of the slide are assumed about this point.

The horizontal Abbe error δ_X in the x-y plane is:

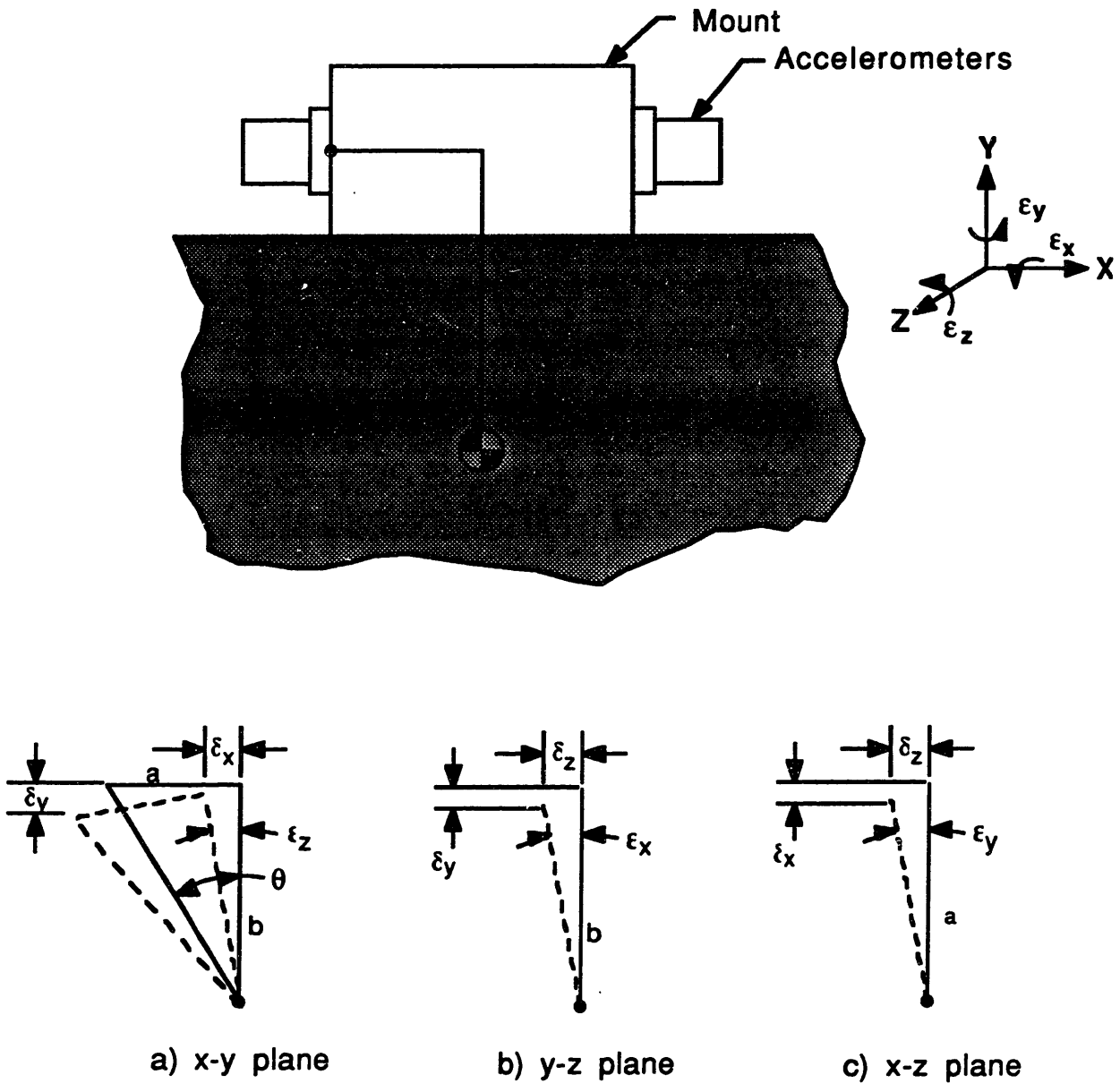

Figure 3.3, Accelerometer mounting Abbe errors.

$$\delta_x = -\sqrt{a^2 + b^2}\,[\sin(\theta+\varepsilon_z) - \sin\theta] \qquad (3.13)$$

A good design will minimize the sensitivity of δ_x by making θ small, so:

$$\lim_{\theta\to 0} \delta_x = -\varepsilon_z\sqrt{a^2+b^2} \qquad (3.14)$$

The horizontal Abbe error δ_x in the x-z plane is:

$$\delta_x = a(1-\cos(\varepsilon_y)) \qquad (3.15)$$

for small angles this can be approximated by:

$$\delta_x = \frac{a\varepsilon_y^2}{2} \qquad (3.16)$$

The vertical Abbe error δ_y in the x-y plane is:

$$\delta_y = -\sqrt{a^2 + b^2}[\cos(\theta + \varepsilon_z) - \cos\theta] \qquad (3.17)$$

Once again, it is wise to make $\theta \to 0$, so:

$$\lim_{\theta\to 0} \delta_y = -\theta\varepsilon_z\sqrt{a^2+b^2} \qquad (3.18)$$

Thus the vertical Abbe error can be effectively eliminated if $\theta = 0$. The vertical Abbe error δ_y in the y-z plane is:

$$\delta_y = b(1-\cos(\varepsilon_x)) \qquad (3.19)$$

for small angles this can be approximated by:

$$\delta_y = \frac{b\varepsilon_x^2}{2} \qquad (3.20)$$

The horizontal Abbe error δ_z in the x-z plane and y-z plane is:

$$\delta_z = b\sin(\varepsilon_x) + a\sin(\varepsilon_y) \qquad (3.21)$$

for small angles this can be approximated by:

$$\delta_z = b\varepsilon_x + a\varepsilon_y \qquad (3.22)$$

In general, given angular deflections ε_x, ε_y, ε_z beam and carriage, the resultant motions seen by the accelerometer in the X, Y, and Z direction are summarized in Table 3.4. The error motions δ_{yac}, and δ_{zac} of the accelerometer are cross axis motions errors or can be referred to as straightness errors and are the errors most concerned about in the design. The error motion δ_{xac} of the accelerometer will be minimized by the fact that the retroreflector for the laser interferometer is mounted next to the accelerometer.

3.2.1.4 Computational Results

A computer program was written to evaluate Tables 3.1 thru 3.4 for three cases: a simply supported design with an aluminum beam, a simply supported design with an alumina oxide beam and a fully supported design with an alumina oxide beam. For the fully supported case, the modulus of elasticity was set to 10 times that of alumina oxide to simulate elastic foundation mounting. For each cases, 10 different bearings were available for analysis. The results in Figures 3.4 thru 3.9 are based on the dimensions and stiffness of the Dover 850-S bearing, the model available for use in the prototype. The results are based on the maximum double amplitude of 16 inches, acceleration of 0.82 g's and a frequency of 1 Hz. The results are comparable through out the bandwidth and acceleration range.

Figures 3.4 and 3.5 show the beam displacements and rotations as a function of position. The graviational sag and carriage weight cause a maximum 275 microinch displacement for the simply supported aluminum beam and 60 microinch displacement for alumina oxide beam. The deflection of the fully supported beam is essentially zero. The

Table 3.4, Relationship between air bearing beam and carriage error motions to accelerometer error motions as a function of position.

	X	Y	Z	ε_x	ε_y	ε_z
$\delta_{xac}(x)$	$\delta_{xb}(x)+\delta_{xc}(x)$	0	0	0	$\frac{a(\varepsilon_{yb}(x)+\varepsilon_{yc}(x))^2}{2}$	$-\sqrt{a^2+b^2}\,[\sin(\theta+\varepsilon_{zb}+\varepsilon_{zc})-\sin\theta]$
$\delta_{yac}(x)$	0	$\delta_{yb}(x)+\delta_{yc}(x)$	0	$\frac{b(\varepsilon_{xb}(x)+\varepsilon_{xc}(x))^2}{2}$	0	$-\sqrt{a^2+b^2}\,[\cos(\theta+\varepsilon_{zb}+\varepsilon_{zc})-\cos\theta]$
$\delta_{zac}(x)$	0	0	$\delta_{zb}(x)+\delta_{zc}(x)$	$b(\varepsilon_{xb}(x)+\varepsilon_{xc}(x))$	$a(\varepsilon_{yb}(x)+\varepsilon_{yc}(x))$	0
$\varepsilon_{xac}(x)$	0	0	0	$\varepsilon_{xb}(x)+\varepsilon_{xc}(x)$	0	0
$\varepsilon_{yac}(x)$	0	0	0	0	$\varepsilon_{yb}(x)+\varepsilon_{yc}(x)$	0
$\varepsilon_{zac}(x)$	0	0	0	0	0	$\varepsilon_{zb}(x)+\varepsilon_{zc}(x)$

Table 3.5 Properties of the calibrator design.

Air Bearing Dimensions		
X_{beam}	8.5	in
Y_{beam}	5.45	in
Z_{beam}	7.0	in
$X_{carriage}$	31.0	in
$Y_{carriage}$	3.0	in
$Z_{carriage}$	5.0	in
Air Bearing Stiffness		
$K_{\delta y}$	1,800,000	lb/in
$K_{\delta z}$	960,000	lb/in
$K_{\varepsilon x}$	1,500,000	lb-in/rad
$K_{\varepsilon y}$	2,400,000	lb-in/rad
$K_{\varepsilon z}$	4,300,000	lb-in/rad
Air Bearing Carriage Moment of Interia		
I_{xx}	193	in^4
I_{yy}	234	in^4
I_{zz}	251	in^4
System Natural Frequency		
Lateral	124	Hz
Rotational	120	Hz
Total Weight of carriage	18.9	lb

maximum z-axis displacements are 45 microinches for the simply supported aluminum beam caused by the imposed umbilical load. The x-axis rotations are negligible. The y-axis rotations have a range of ±4 microradians while the x-axis has a range of ±15 microradians caused by the moment loads produced by the motor force, umbilical force and side load.

Figures 3.6 and 3.7 show the carriage displacements and rotations as a function of position. Displacements along the y-axis and z-axis are constant due to the constant loads. The x-axis rotation is constant for the same reason. The rotations about the y-axis and z-axis are a result of the moment loads caused by the motor force, umbilical force and side load.

Figures 3.8 and 3.9 show the accelerometer displacements and rotations as a function of position. The x-axis displacements are due to rotations about the y-axis and z-axis as show in Table 3.4. The y-axis and z-axis displacements are the cross axis motion. Subtracting the residuals from the best-fit straight line from the predicted displacements gives a maximum cross axis motion along the y-axis as 76 microinches, 16 microinches and 2 microinches for cases one thru three respectively. Along the z-axis, the maximum cross axis motion is 9 microinches, 4 microinches and 1 microinch for cases one thru three respectively. The rms cross axis motion is 5 ppm, 1 ppm and 0.2 ppm for cases one thru three respectively. In all cases, the cross axis motion was less than the maximum allowed by the design criteria.

An error due to the rotation of the accelerometer occurs about the y and z axis as a result of the beam and carriages rotations. This error equals the acceleration times the sine of rotation. For case one,

the error is 1 ppm and 5 ppm for the rotations about the y and z axis respectively. For cases two and three, the rotational errors of the beam are small and do not cancel the carriage rotational errors. This rotational error is a result of the moment loads caused by the motor force, umbilical force and side load. These rotations can be reduced by driving the carriage through its centroid or using two motors to balance the forces, producing zero moments on the carriage as explained in Section 2.6. A second less accurate linear slide could run parallel to to the calibrator, with its motion coordinated, relieve the umbilical forces imposed on the carriage. A third method to reduce the rotation errors is to use a stiffer carriage. All three methods along with a fully supported air bearing beam design are available with current technology and could be utilized to eliminate the rotation errors caused by the dynamic loads.

3.2.1.5 Modeled Dynamics

There are an infinite number of natural frequencies of the system, but only the fundamental frequency is of interest here. A conservative first order estimate can be obtained if the system is modeled as a two degree of freedom linear system. The first mass can be represented by a concentrated mass, applied at the point along the beam at which we wish to find the natural frequency. That gives an equal deflection as is caused by the distributed mass of the beam. The lowest natural frequency, and thus the limiting factor for the designs, will occur when the mass acts at the most flexible point which is the center of the beam. For lateral vibration of the beam, the deflection at the center caused by the beam's own weight is:

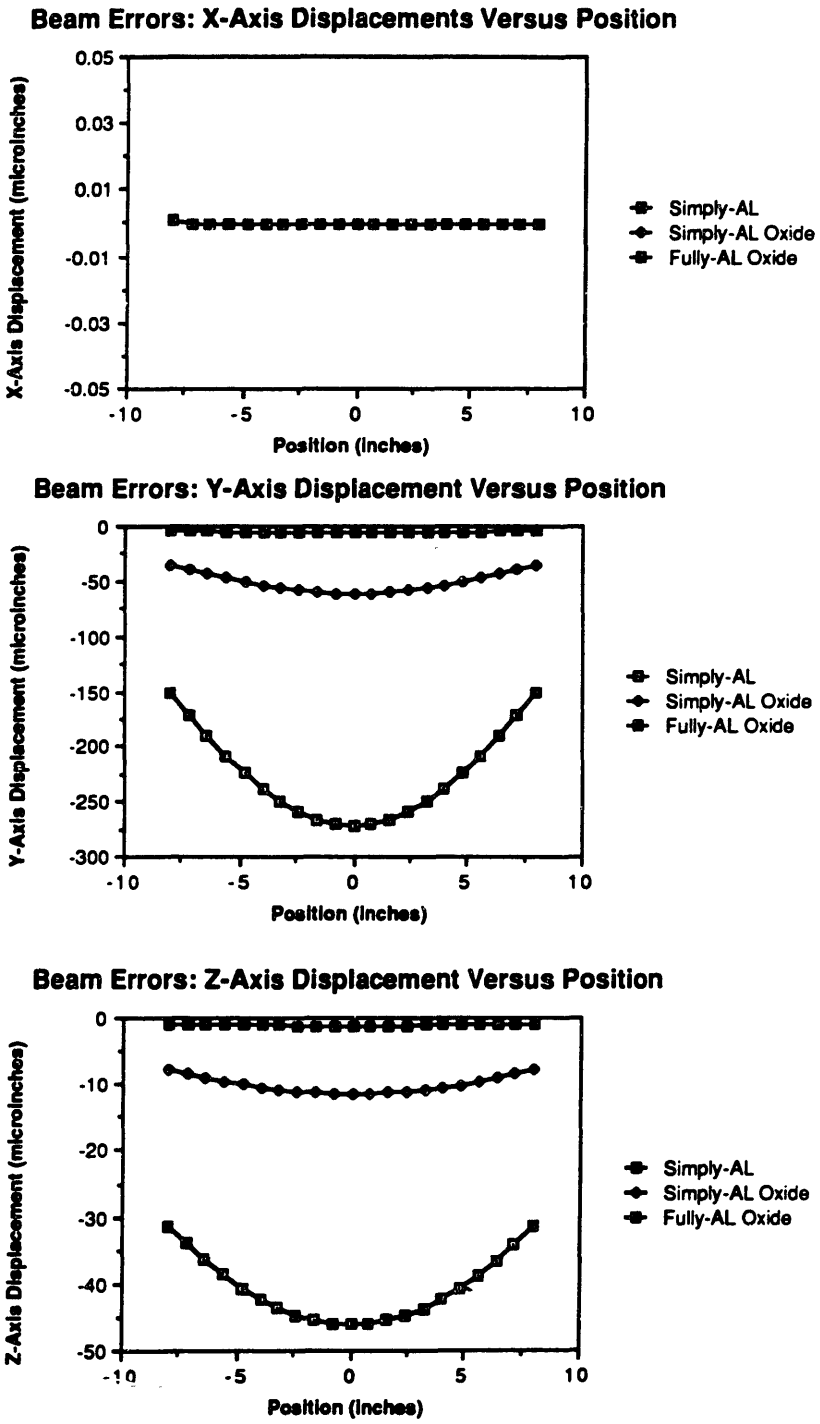

Figure 3.4, Beam displacement errors,
for 1 Hz frequency, 8 inch amplitude and 0.82 g acceleration.

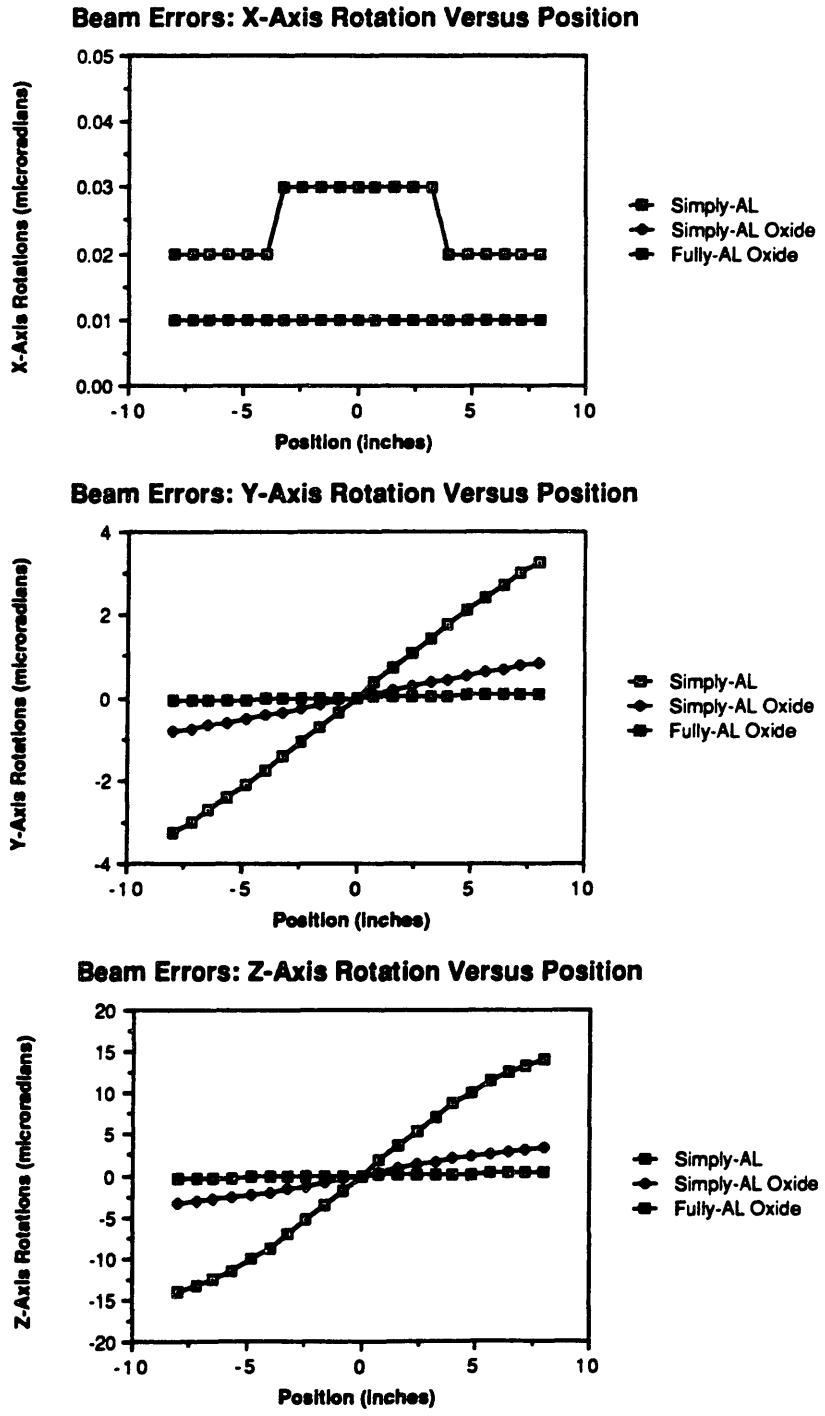

Figure 3.5, Beam rotation errors
for 1 Hz frequency, 8 inch amplitude and 0.82 g acceleration.

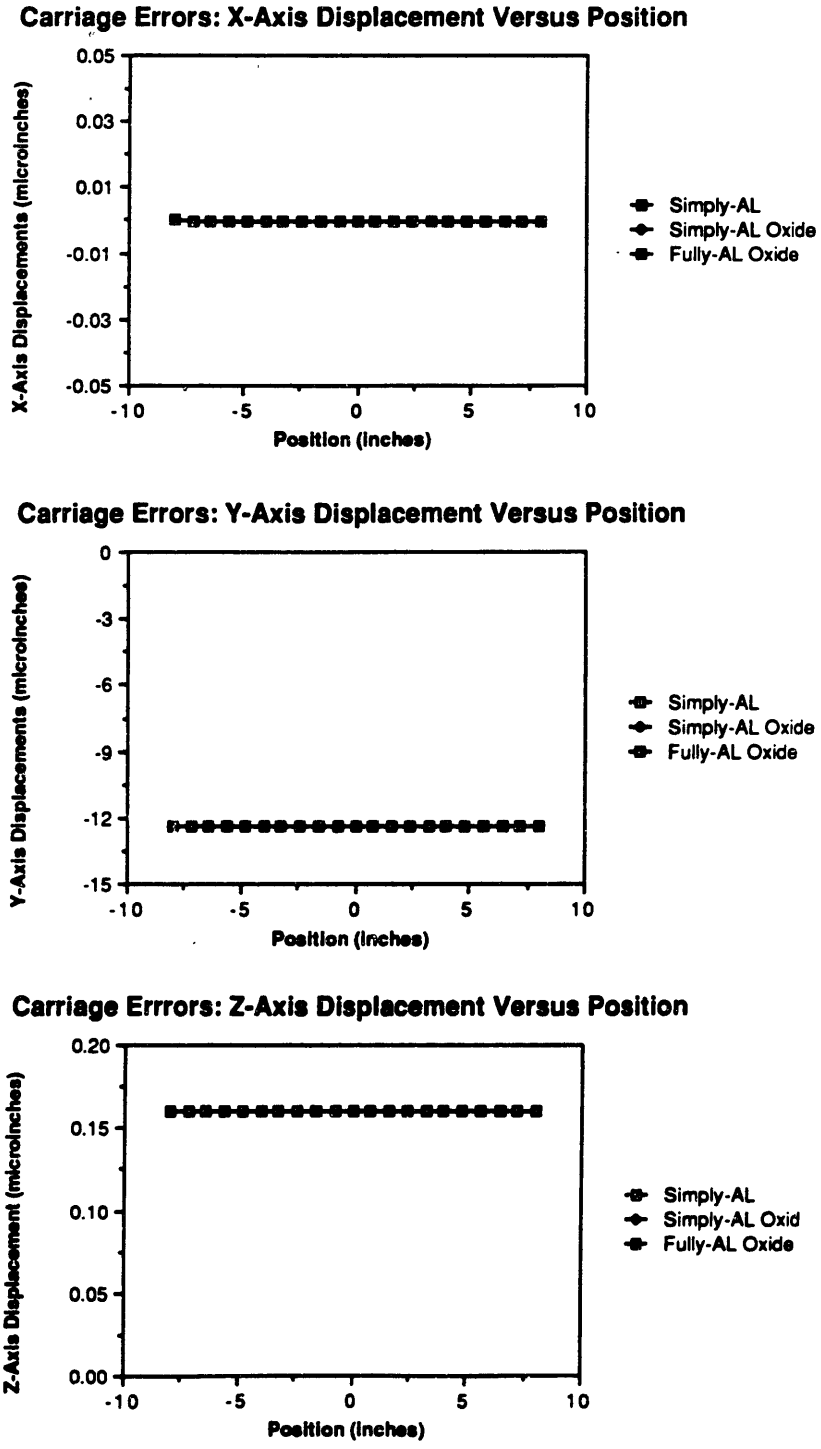

Figure 3.6, Carriage displacement errors
for 1 Hz frequency, 8 inch amplitude and 0.82 g acceleration.

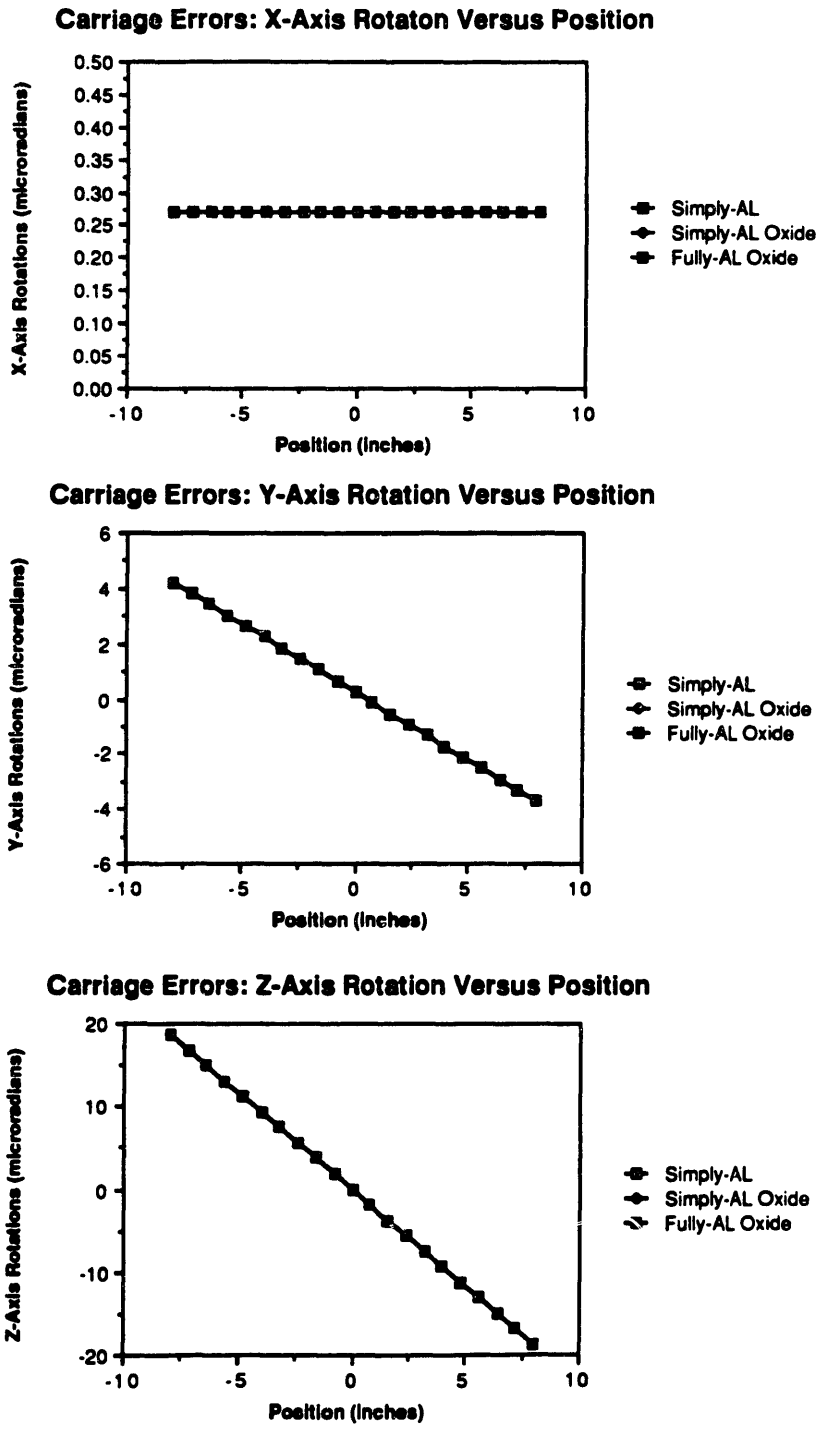

Figure 3.7, Carriage rotation errors
for 1 Hz frequency, 8 inch amplitude and 0.82 g acceleration.

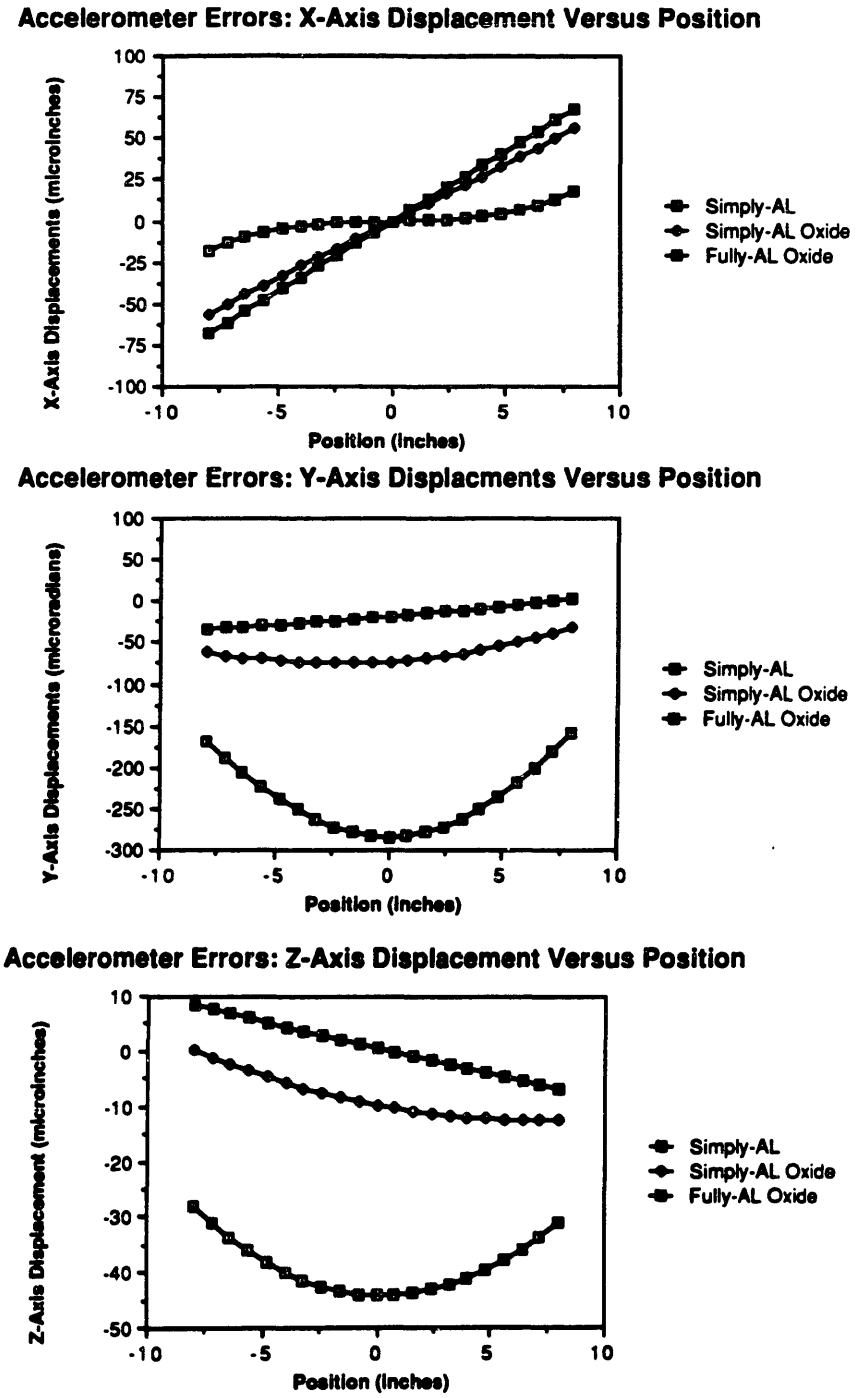

Figure 3.8, Accelerometer displacement errors for 1 Hz frequency, 8 inch amplitude and 0.82 g acceleration.

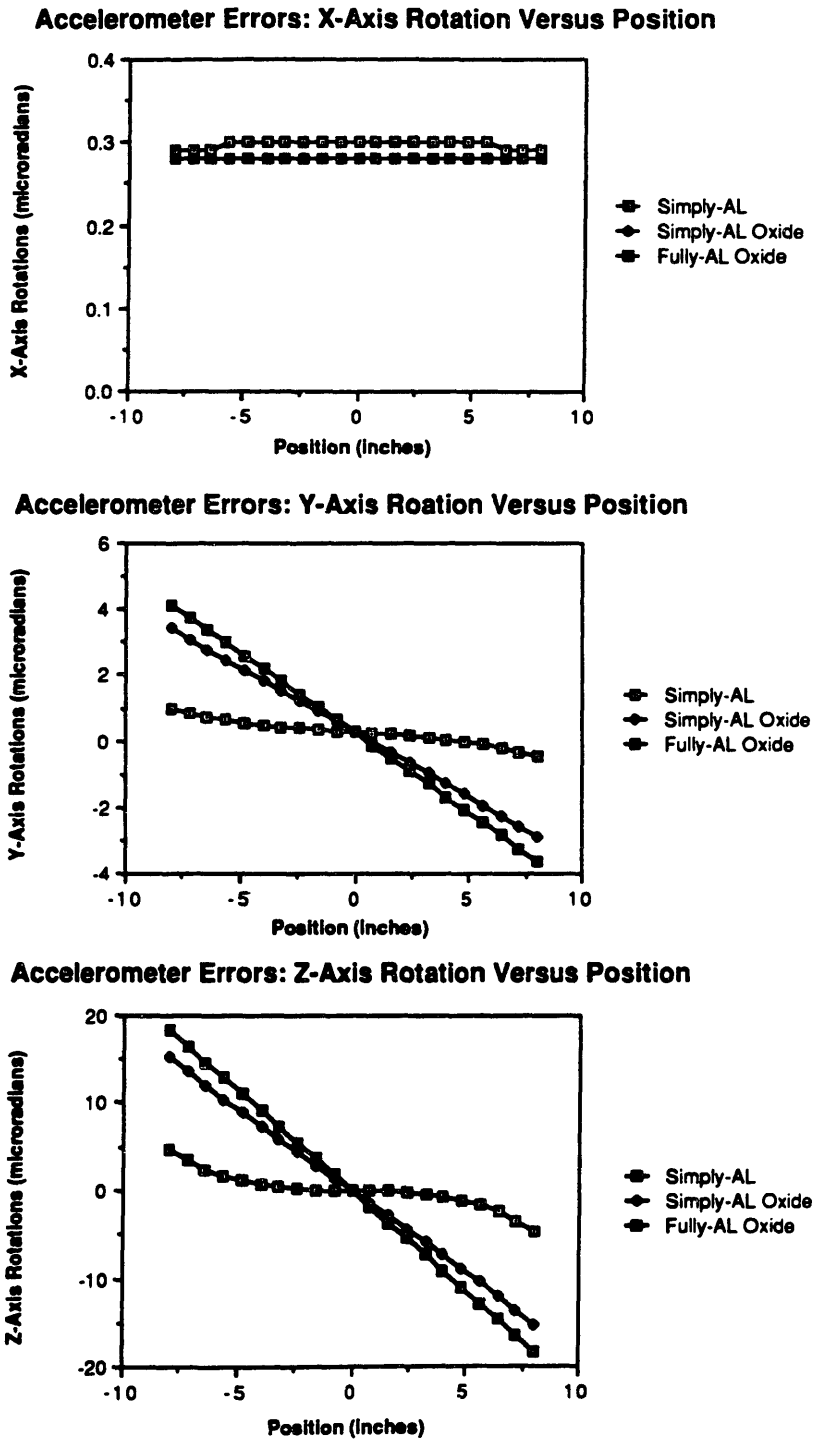

Figure 3.9, Accelerometer rotation errors
for 1 Hz frequency, 8 inch amplitude and 0.82 g acceleration.

$$\delta_{bw} = \frac{5M_{beam}\ell^3}{384EI} \tag{3.23}$$

The equivalent mass concentrated at the center of the beam that will cause the same deflection is found from (3.5) and (3.23) to be:

$$M_{eq} = \frac{5M_{beam}}{8} \tag{3.24}$$

Note that for this loading configuration, at the center of the beam the slope is equal to zero. Thus when the pitch natural frequency is calculated, effects of lateral motion can be ignored. At other points along the beam, however, coupling would occur.

The second spring is the lateral stiffness of the slide obtained from Table 3.5 of air bearing lateral stiffnesses. The second mass is that of the slide which includes all mounting hardware and the accelerometers.

For the unforced two degree of freedom system, the equations of motion are:

$$\begin{bmatrix} M_{eq} & 0 \\ 0 & M_{slide} \end{bmatrix} \begin{bmatrix} \ddot{X}_1 \\ \ddot{X}_2 \end{bmatrix} + \begin{bmatrix} K_{beam}+K_{slide} & -K_{slide} \\ -K_{slide} & K_{slide} \end{bmatrix} \begin{bmatrix} X_1 \\ X_2 \end{bmatrix} = 0 \tag{3.25}$$

Assuming a harmonic solution in for X_1 and X_2, and equating the two expressions found for the mode fraction X_2/X_1, the natural frequencies are found from the determinant of:

$$\text{Det} \begin{bmatrix} K_{beam}+K_{slide}-M_{eq}\omega^2 & -K_{slide} \\ -K_{slide} & K_{slide}-M_{slide}\omega^2 \end{bmatrix} = 0 \tag{3.26}$$

Expanding and collecting terms, a quadratic with coefficients a, b, and c is obtained:

$$a = M_{eq}M_{slide}$$

$$b = -[M_{slide}(K_{beam}+K_{slide})+K_{slide}M_{eq}]$$

$$c = K_{slide}K_{beam}$$

The fundamental frequency for the system is thus:

$$\omega_1 = \sqrt{\frac{-b-\sqrt{b^2-4ac}}{2a}} \qquad (3.27)$$

The pitch natural frequency is found in a similar manner. The pitch stiffness for the beam and slide are given by Equations 3.6 and 3.12 respectively. The equivalent inertia of the beam is found assuming that the effective length of the beam is equa[illegible]e distance between the two points, on the simply supported beam that is twisted by a moment at the center, where the slope is zero. The general expression for the slope of a simply supported beam with an applied moment is:

$$\alpha = \frac{M}{EI}\left\{\frac{X^2}{2l} - \left\langle X - \frac{\ell}{2}\right\rangle - \frac{\ell}{24}\right\} \qquad (3.28)$$

When $X < \ell/2$(the left side of the beam), the slope is zero when

$$X_1 = \frac{\ell}{2\sqrt{3}} \qquad (3.29)$$

The equivalent length of the beam is thus:

$$\ell_{eq} = \ell(1-1/\sqrt{3}) \qquad (3.30)$$

The equivalent moment of inertia of the beam is thus:

$$I_{eq} = \frac{M_{beam}\ell^2(1-1/\sqrt{3})^3}{12} \qquad (3.31)$$

The results are summarized in Table 3.5. For the simply supported beam, the first mode lateral natural frequency is 124 Hz. and the rotational natural frequency as 120 Hz.

3.2.2 Error Budget of Unmodeled Effects

Two other possible sources of errors are floor vibrations and thermal errors. Errors due to floor vibrations can be minimized by using pneumatic vibration isolation equipment. Furthermore, the floor vibrations would excite the beam in the vertical direction and would be seen as cross axis motion errors by the accelerometer. This error must be determined experimentally. The second possible error is thermal expansion due to thermal gradients produced by the motor or as a result of room temperature variations. The prototype configuration has the accelerometer and retroreflector mounted as far as possible from the motor heat source and is located in a laboratory where the temperature variations are estimated as ±1.5° F. For a temperature change of 3° F, the beam expansion would be 0.001 inches. An over constrained beam subjected to this temperature change would warp or buckle causing straightness errors. The prototype configuration has the beam mounted such that it is unconstrained in the longitudinal direction allowing the beam to thermal expand and not warp. Thus no error is associated with the thermal expansion of the beam.

3.2.3 Error Budget of Laser Interferometry

In order to verify the predicted performance of the calibrator, a metrology system with better than 10 parts per million accuracy is needed. The Zygo Axiom 2/20 laser transducer system is able to

measure angular and straightness errors along with linear displacement measurements with an accuracy on the order of one ppm. This section will formulate an error budget for these measurements.

3.2.3.1 Environmental Errors

The accuracy of the laser interferometry system depends largely on the operational environment. The factors to consider are: index of refraction, air turbulence, deadpath error and material temperature.

The wavelength of the laser is known to better than 1 part per million in a vacuum, but the wavelength in air is shorter because the velocity of light in air is less that in a vacuum. Temperature, humidity and barometric pressure effect the index of refraction, the ratio of the wavelength in a vacuum to air, of the laser and must be known in order to compensate the measurements values. A linear measurement value obtained from the Axiom 2/20 system equals:

$$d = \frac{N\lambda}{n254} \qquad (3.32)$$

where N is number of counts, n is the index of refraction and λ is the wavelength of the laser. A typical value for the index of refraction in a laboratory environment at 68° F is n = 1.00027. When the number of counts is 1000 (0.0001 inches), the compensated value is 999.73 a difference of only 0.027%. Therefore the index of refraction n becomes critical for large displacements and if repeatability is to be maintained between data sets.

The exact index of refraction can be computed to an accuracy of 0.1 part per million using Edlen's formula [44]:

$$n = 9.74443P\left[\frac{1+10^{-6}P(26.7-0.187T)}{0.934915+0.0020388T}\right] - 1.089\cdot10^{-3}Re^{0.032015T} \qquad (3.33)$$

where T is the air temperature in degrees Fahrenheit, P is the barometric air pressure in inches of mercury and R is the relative humidity in %. From Edlen's formula, a change in air pressure has the greatest effect on the index of refraction. These quantifies must be measured accurately in a laboratory setting before measurements are taken. Problems arise when the index of refraction changes such as during a machining operation. The changes in the index of refraction from an initial value can be monitored with a refractometer [45].

The room where the calibrator is located has no windows and only one door opening into an interior hall way. The temperature is regulated to approximately 68° ± 1.5° F. It is anticipated that the index of refraction will change very little during measurements, but a refractometer will still be used to monitor changes in the index of refraction for verification. A change in temperature over the range specified could give an error in the index of refraction of approximately 0.002%.

In a machine shop environment, air turbulence or inhomogeneity of the air in the optical measuring path will reduce the amount of signal at the receiver and can show up as a change in the index of refraction [46]. The turbulence is usually caused by variations in air temperature, rapidly moving parts or air showers. Thus where laser interferometers are used on machine tools, the optical measuring path is enclosed in bellows to reduce this problem [47]. The design of the a shield or bellows must be such that impulse of air or turbulence is not created within the shields or bellows themselves from their collapsing

and stretching motions. This would be eliminated if the bellows were evacuated. It will not be necessary to use bellows on the calibrator since it is not in a harsh machine tool environment. There is a possibility that turbulence will be generated by the calibrator as it oscillates. This can be determined using a hot wire anonometer.

Localized heat sources (e.g. motors, pumps, etc.) will effect the geometric accuracy of a machine. This is prevalent when the point of operations does not coincided with the point of measurement. In the calibrator design, the heat source, the motor, is located below the optical measuring path with the 3X5 inch air bearing beam in between. The beam is fixed at one end and clamped at the opposite end to allow for thermal expansion. Expansion of the beam will not cause measurement errors since the retroreflector is mounted right next to the accelerometer. The linear interferometer is also mounted as close to the retroreflector as possible in order to minimize the deadpath error. The deadpath error is introduced because of an uncompensated length of laser light between the interferometer and retroreflector. The error equals the length of the deadpath times the stability of the laser times the change in temperature. The Zygo laser is stable to ±0.01 part per million. For the calibrator design, the worst case deadpath length occurs for large travels and equals 20 inches giving a deadpath error of ±0.2 microinches. For short travels, the carriage will be position as close to the interferometer as possible to minimize this error.

3.2.3.2 Angular Measurement Errors

A differential plane mirror interferometer (DPMI) will be used to measure the angular rotations about the Y and Z axis (yaw and pitch) as seen by the accelerometer. A description of the test set up is found in Chapter 4. The pitch resolution of the DPMI angular measurement optics is ±0.029 microradians over a range of ±2300 microradians [44]. The error in this case is one resolution unit or ±0.029 microradians. A yaw rotation of less than ±580 microradians will cause an error of less than one resolution unit. Rotations about the X-axis or roll will not cause an error in the pitch measurement. From Figure 3.9, the pitch and yaw rotations for each axis are less than ±20 microradians and subsequently an error of will be associated with the angular measurements. Note that translations do not affect the angular measurements made with the DPMI.

3.2.3.3 Straightness Measurement Errors

Straightness measurements will be made with a Zygo Axiom 2/20 straightness interferometer, a description of the test setup is in Chapter 4. The accuracy of the straightness measurements is ±20 microinches with a resolution of ±0.8 microinches [48]. The accuracy of the interferometer fails to meet the requirements. The principle error is caused by the flatness of the mirrors (±14 microinches). The alternative is to use an optical straight edge and plane mirror interferometer that would have an accuracy of ±1 microinch [49]. Using a DPMI, the accuracy could be increased to ±0.1 microinch. No real optical straightedge is perfectly straight, the errors of the straightedge are mixed with the errors the machine being measured.

The straightedge can be calibrated by a reversal technique. A similar approach is suggested to calibrate the Zygo straightness interferometer to improve the accuracy.

3.2.3.4 Linear Measurement Errors

Miss-alignment between the optical measuring path and the axis of motion will result in an error between the measured displacement P-P" and the actual distance traveled P-P' as shown in Figure 3.10. This is referred to as a cosine error and is represented by:

$$\text{error (ppm)} = (1 - \cos\theta)10^6 \qquad (3.34)$$

From Figure 3.8 the maximum displacement is 300 microinches from straight line travel P'-P" for a measured displacement P-P" of 10 inches. The angle θ is given by:

$$\theta = \tan^{-1}(300 \text{ microinches}/10 \text{ inches}) \qquad (3.35)$$

evaluating Equation 3.34 gives a cosine error of 4 parts in 10^{-10}. The cosine error is insignificant in the calibrator design.

For the calibrator, the Abbe offset is 1.75 inches as shown in Figure 3.11. The maximum yaw for the accelerometer assuming rotation about the centroid of the carriage from Figure 3.9 is 4 microradians. The resultant Abbe error is 7 microinches. This error is below the 10 parts per million requirement. This error can be reduced by using two retroreflectors to obtain an average displacement of the accelerometer or 3.5 microinches. As described in Section 3.1.2.4, the rotation errors that cause this Abbe error can be eliminated thus yielding zero Abbe error due to pitch. No Abbe errors occur for pitch rotations since the retroreflectors and the accelerometer are mounted in the same vertical plane.

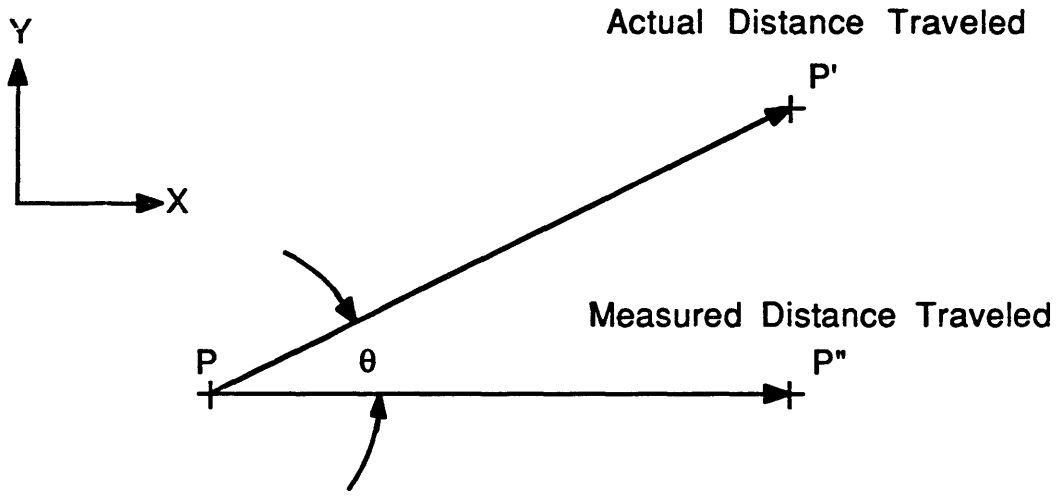

Figure 3.10, Cosine error representation.

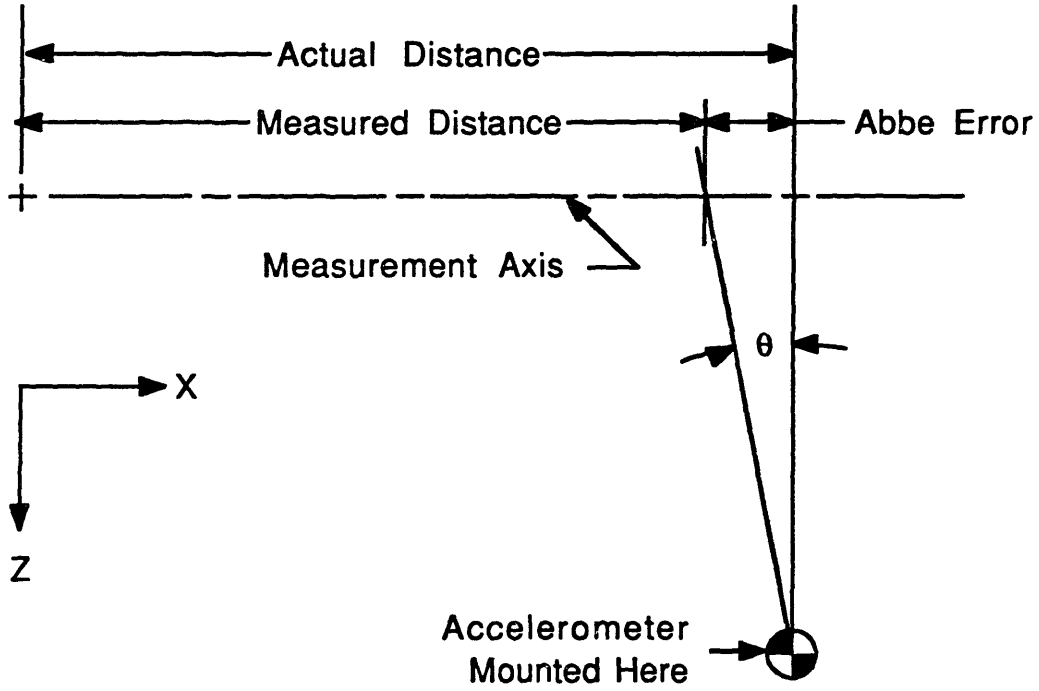

Figure 3.11, Abbe error representation.

3.2.4 Error Budget Summary

Table 3.6 gives a summary of the error budget results for the prototype calibrator. The root mean square error is 10 ppm and the sum of the errors is 19 ppm. The average of the two is 14.5 ppm. Typically, the actual error falls between the rms error and sum of errors. Two error sources, harmonic distortion and mechanical and environmental vibrations, are not included since they must be determined experimentally.

The rms error can be significantly reduced, to one ppm, by a several design changes that would reduce the dominant errors: the cross axis motion, accelerometer pitch and Abbe error due to yaw. By utilizing a fully supported beam, the z axis rotations of the beam are eliminated along with the y displacements associated with the beam sag and the weight of the carriage. Thus the cross axis motion is reduced to 0.2 ppm of travel. Using a balanced motor configuration and strain relieving the umbilical cables significantly reduces the moment loads placed on the carriage. Thus, the pitch and yaw rotations of the carriage that cause the accelerometer pitch errors and Abbe errors due to yaw are reduced to nearly zero. The error budget for the high accuracy design is show in Table 3.6. The rms error is one ppm while the sum of errors is 1.4 ppm. This predicted accuracy is 10,000 times better than the existing design.

3.3 Servo System Design

The existing NBS calibrator operates as an open loop system. Therefore the system's accuracy is susceptible to drift in the analog

Table 3.6 Summary of error budgets
Results for prototype calibrator and high accuracy design.

	Simply Supported Prototype	T-base Design	
Cross Axis Motion	5	0.2	ppm of travel
Cross Axis Motion Measurement	1	0.1	ppm of travel
Accelerometer Pitch Error	5	0	ppm of travel
Abbe Error due to yaw	7	0	ppm of travel
Deadpath	0.01	0.01	ppm of travel
Harmonic Distortion	*	*	
Mechanical or enviromental vibration	*	*	
Sinusoidal Reference Signal	<1	<1	ppm of frequency
Displacement Measurement Cosine Errors	0	0	
Index of Refraction	0.1	0.1	ppm
Root Mean Square Error	10	1.0	ppm
Sum of Errors	19	1.4	ppm
Average RMS and Sum of Errors	14.5	1.2	ppm

* To be Measured

amplifier and harmonic distortion (primarily second and third order harmonics) [7,8,9,10,11,12,13,14]. The amplifier drift causes the amplitude of oscillation to vary during the calibration. By allowing the calibrator to warm up for serval minutes and averaging over a large number of cycles, this error can be reduced to below 1%. Also, the harmonic distortion is caused by miss alignment of the moving coil and the overhead elastic suspension system. Proper alignment and closing a acceleration loop around the system could eliminate this uncertainty [39]. This section addresses the need for a closed loop system and develops a servo design for the prototype calibrator.

The calibrator is modeled as a mass directly driven by a fixed field DC servo motor. The differential equations governing the motion are:

$$V_t = i_m R + \frac{di_m}{dt} L + e_{emf} \qquad (3.36)$$

$$e_{emf} = K_{emf} \text{velocity} \qquad (3.37)$$

$$F_m = K_f i_m \qquad (3.38)$$

$$F_m = ma \qquad (3.39)$$

where V_t is the terminal voltage of the motor, i_m is the motor current, R is the motor resistance (2.8 ohms), L is the motor inductance plus the amplifier inductance required to minimize the current ripple (4.74 mhenrys), e_{emf} is the back emf voltage, K_{emf} the back emf constant (11.8 volts/m/sec), F_m is the motor force, K_f is the motor force constant (13.35 N/amp), m is the mass of the moving system (8.61 Kg) and a is the acceleration of the mass. Evaluating the motor transfer function, using Equations 3.36 through 3.39 gives:

$$G(s) = \frac{\text{Velocity}}{\text{Volts}} = \frac{327}{s^2 + 591s + 379} \qquad (3.40)$$

The prototype calibrator was run open loop at frequencies of 1, 3 and 8 Hz with double amplitudes of 2.6 inches, 0.9 inches and 0.031 inches respectively as shown in Figure 3.12. At 1 and 3 Hz, the drift is caused by the umbilical forces on the carriage: the umbilical force pulls the carriage in the positive direction, increasing the amplitude, while restrain the carriage in the negative direction, decreasing the amplitude. At 8 Hz the drift in not as obvious perhaps due to the small amplitude and limited number of cycles shown. The result is that a closed loop servo system is necessary for eliminating the effects of the umbilical forces.

The compensator $G_c(s)$, for the closed loop servo system is a lead-lag network with the following transfer function:

$$G_c(s) = \frac{K(1 + T_1 s)(1 + T_2 s)}{(1 + \alpha_1 T_1 s)(1 + \alpha_2 T_2 s)} \qquad (3.41)$$

Generally, a phase margin of 30° to 60° acceptable for a second order system. The open loop frequency response of the uncompensated motor and load is shown in Figure 3.13 (a). The system is overdamped with a bandwidth of approximately 1 Hz (bandwidth at -3 db of DC gain). An iterative approach was taken to find the poles and zeros of the compensator. The results are shown in the open loop frequency response of the compensated motor and load in Figure 3.14 (b). The phase margin is 40°, the gain margin is 40 db and the bandwidth is 22 Hz.

The closed loop transfer function H(s) is:

$$H(s) = \frac{G_c(s)G(s)}{1 + G_c(s)G(s)} \qquad (3.42)$$

The closed step response of H(s) is shown in Figure 3.14. The 35% peak overshoot is typical of a 40° phase margin system. The 2% settling time is 0.13 seconds and the rise time is 0.025 seconds. The compensator is an analog network that accepts velocity feedback from an accelerometer with unity gain. Due to modeling errors and the fact that the parameters of the compensator can change with temperature gradients, the actual compensator will differ from the modeled compensator. Thus the actual hardware compensator will have to be fine tuned.

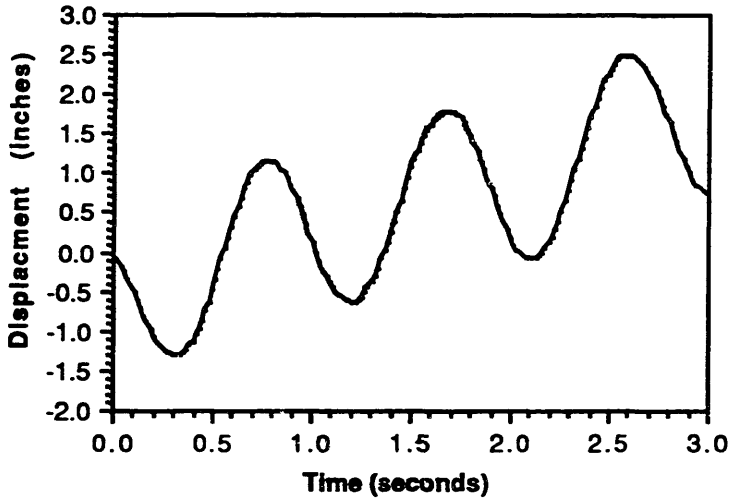

a) System response at 1 Hz.

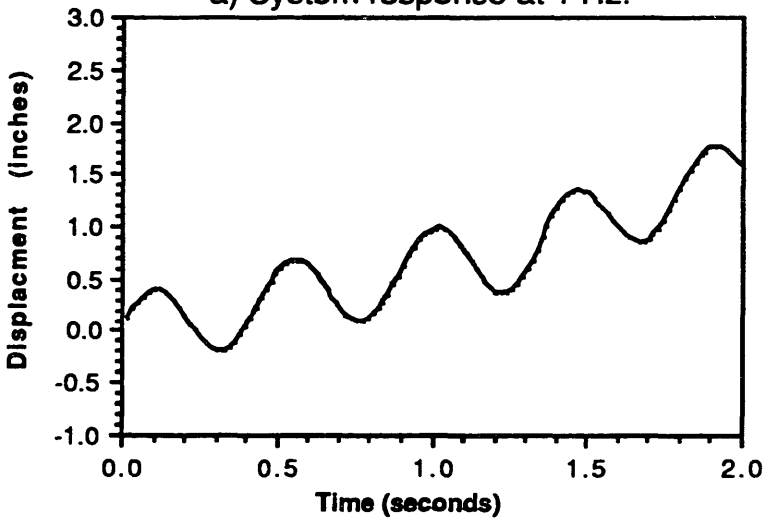

b) System reponse at 3 Hz.

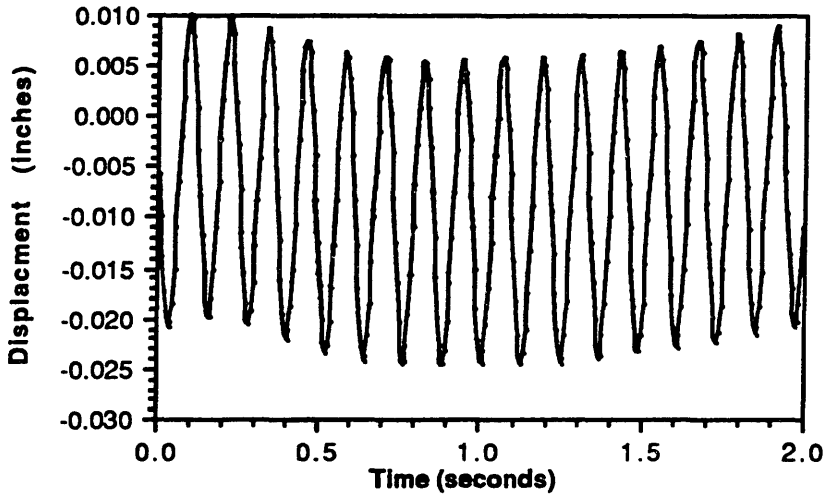

c) System Respones at 8 Hz.

Figure 3.12, Open loop frequency response of prototype calibrator.

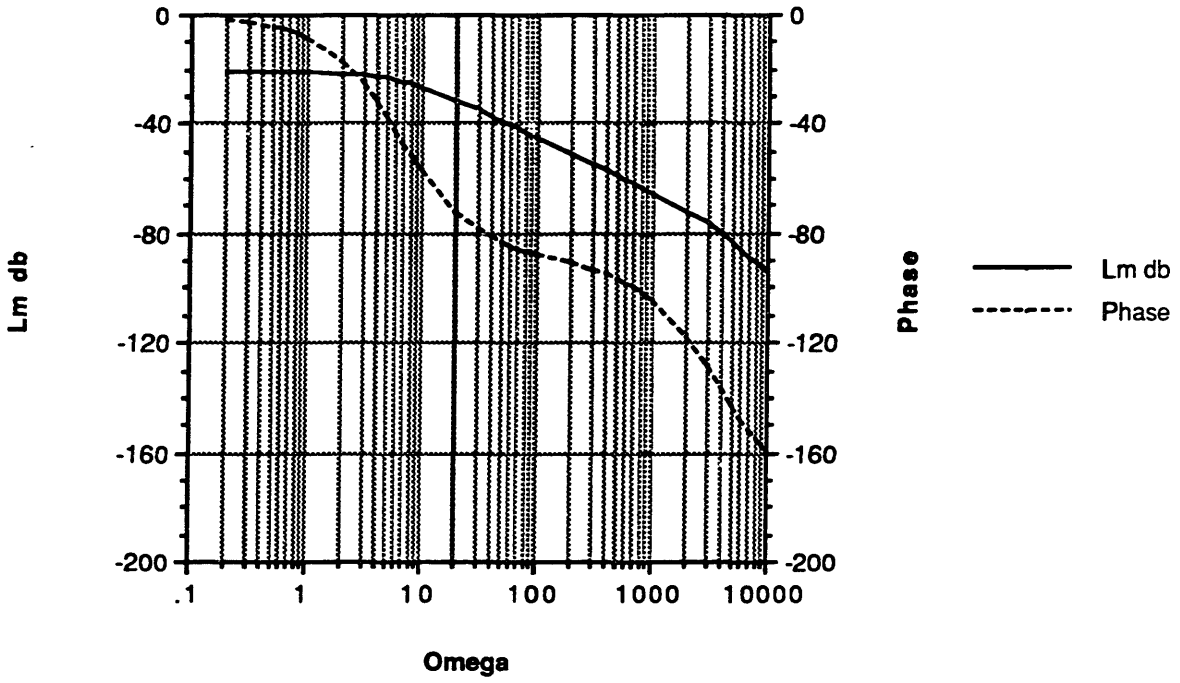

a) Open loop frequency response of motor and load transfer function.

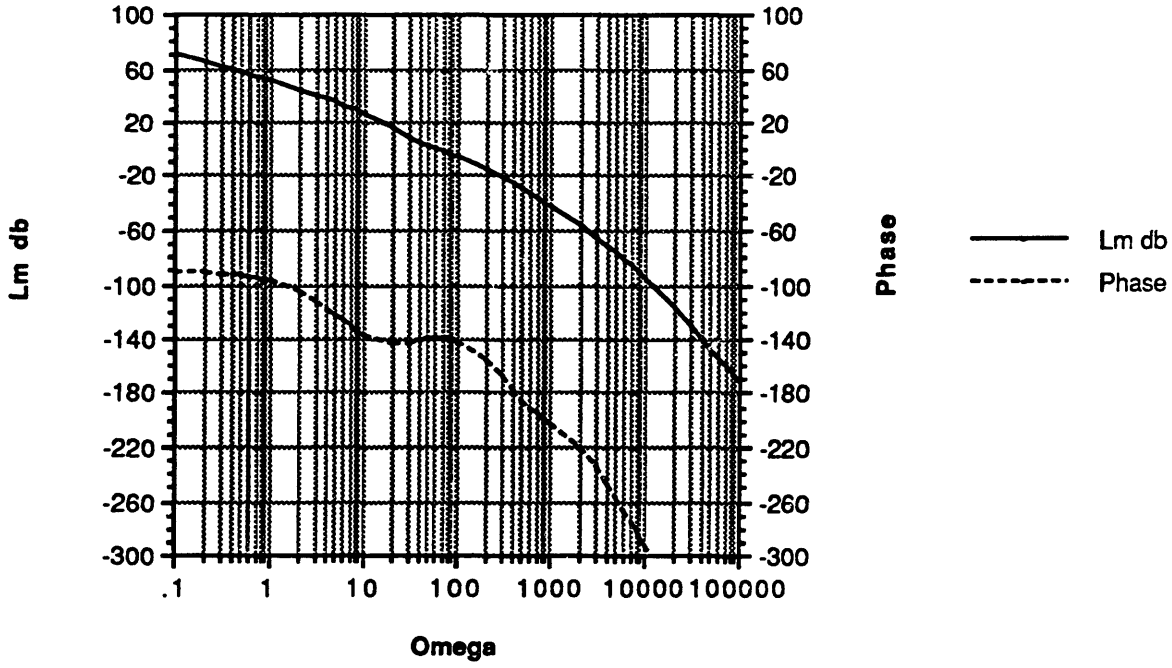

b) Open loop frequency response of motor, load and compensator transfer function.

Figure 3.14, Open loop frequency response of system transfer functions.

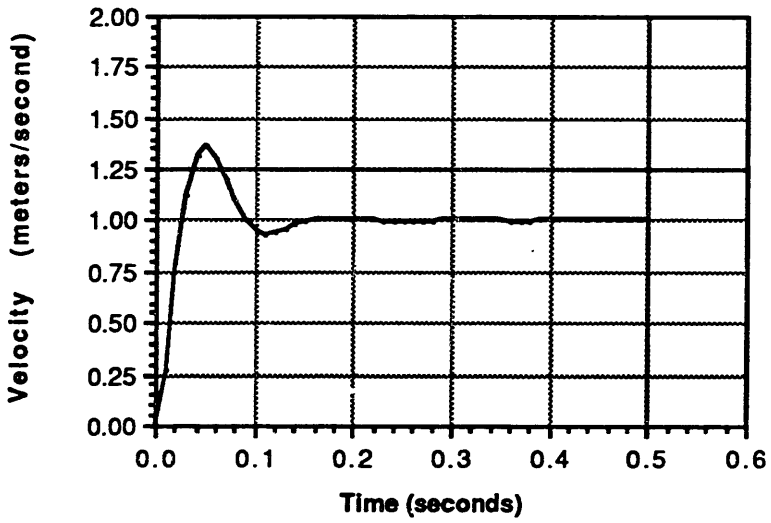

Figure 3.14, Step response simulation of velocity servo loop.

Chapter 4
Experimental Analysis

4.1 Description of Prototype Calibrator

A prototype calibrator was designed and built using the under-over configuration described in Chapter 2 and analyzed in Chapter 3. This prototype uses a Dover Instruments' model 850-S linear air bearing with 20 inch travel. The carriage length is 8.5 inches, width is 7.0 inches and height is 4.5 inches. The beam dimensions are 31.0X5.5X3.0 inches. The carriage weight is 12.7 lbs, the optics mount is 6.3 lbs and the beam weight is 51 lbs. The carriage is driven by an Anorad LP2 brushless linear DC motor that weighs 2.5 lbs. The motor has a peak force output of 48 lbs and rms continuous rating of 18 lbs when using the matched three-phase motor amplifier. The true continuous force rating would be $18\sqrt{2}$ or 25.4. The continuous rating can be increased if auxiliary cooling is used. A Zygo Axiom 2/20 laser interferometer is used to measure the displacement of the carriage. These components represent the basis of the prototype calibrator design as shown in the solid model of Figure 4.1.

This prototype was mounted on a cast iron surface plate that measures 48X22X7 inches and it weighs 250 lbf. The surface plate was chosen because: it is flat to within ±0.0001 inches, old cast iron is dimensionally stable, and a large mass is needed to minimize cross coupling between the slide and the mounting surface. The motor's stationary magnet assembly painted gray is fastened to the surface plate and underneath the air bearing while the moving coil fastens to the carriage as shown in Figure 4.2. The air bearing beam is bolted in

two places to a aluminum block on the near side. Two one inch diameter washers are placed between the beam and the block to give a two point mounting. On the opposite end, the beam is clamped to the mounting block with two Teflon pads acting as an interface between the clamp and the beam surfaces as shown in Figure 4.3. The Teflon pads have a stiffness 10 times that of the beam, minimizing any influence. This configuration comes close to a kinematic mounting. The beam is not constrained in the longitudinal direction which allows for thermal elongation and prevents of warping.

A mount is placed on the center of the carriage to hold two accelerometers and two retroreflectors as shown in Figure 4.4. The two accelerometers would be used for comparison tests and the two retroreflectors maintain an inertial balance. The accelerometers are mounted in the center of the carriage. The mount is counterbored so that the accelerometers mount as close to the centroid of the carriage as possible to minimize Abbe errors caused by rotations of the carriage. The retroreflector mounts on the same horizontal plane of the accelerometer. It is desired to make the displacement measurement as close to the accelerometer as possible to minimize Abbe errors. On the left side, the linear interferometer and receiver are mounted as shown in Figure 4.5. A set of three fold mirrors bend the laser beam from the laser head up to the linear interferometer, this best seen in Figure 4.1.

Two contacting limit switches placed at the ends of travel switch off the motor current when enabled. Two noncontacting inductive sensors are used to position the motor about a home position, remember the laser interferometer is a relative displacement device.

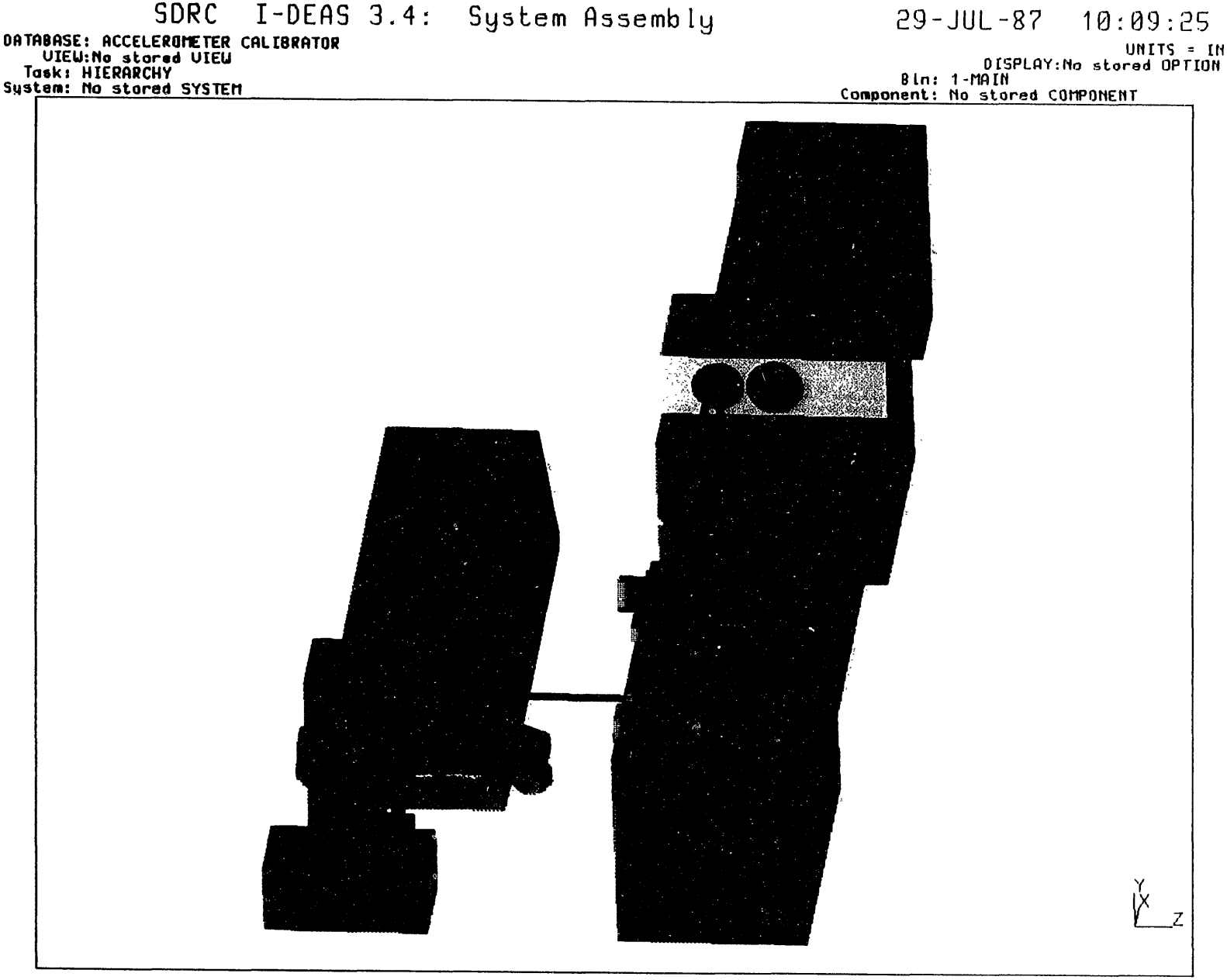

Figure 4.1, Solid model of the prototype calibrator.

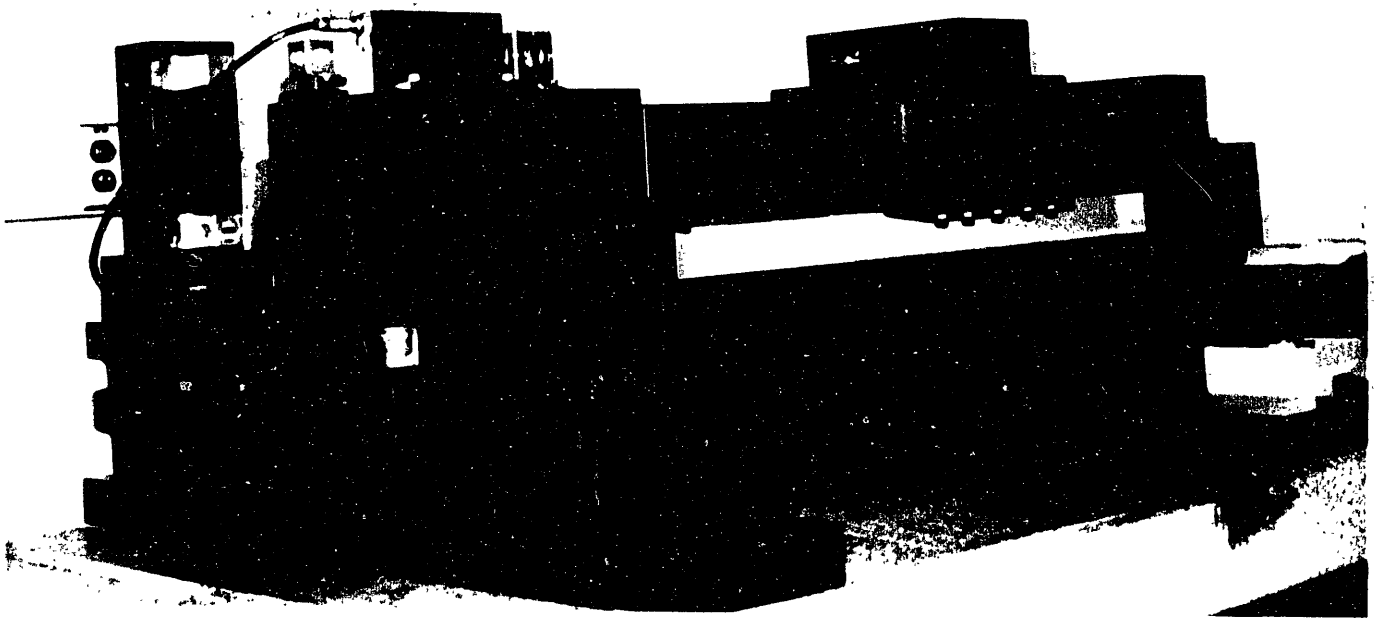

Figure 4.2, Profile view of prototype calibrator.

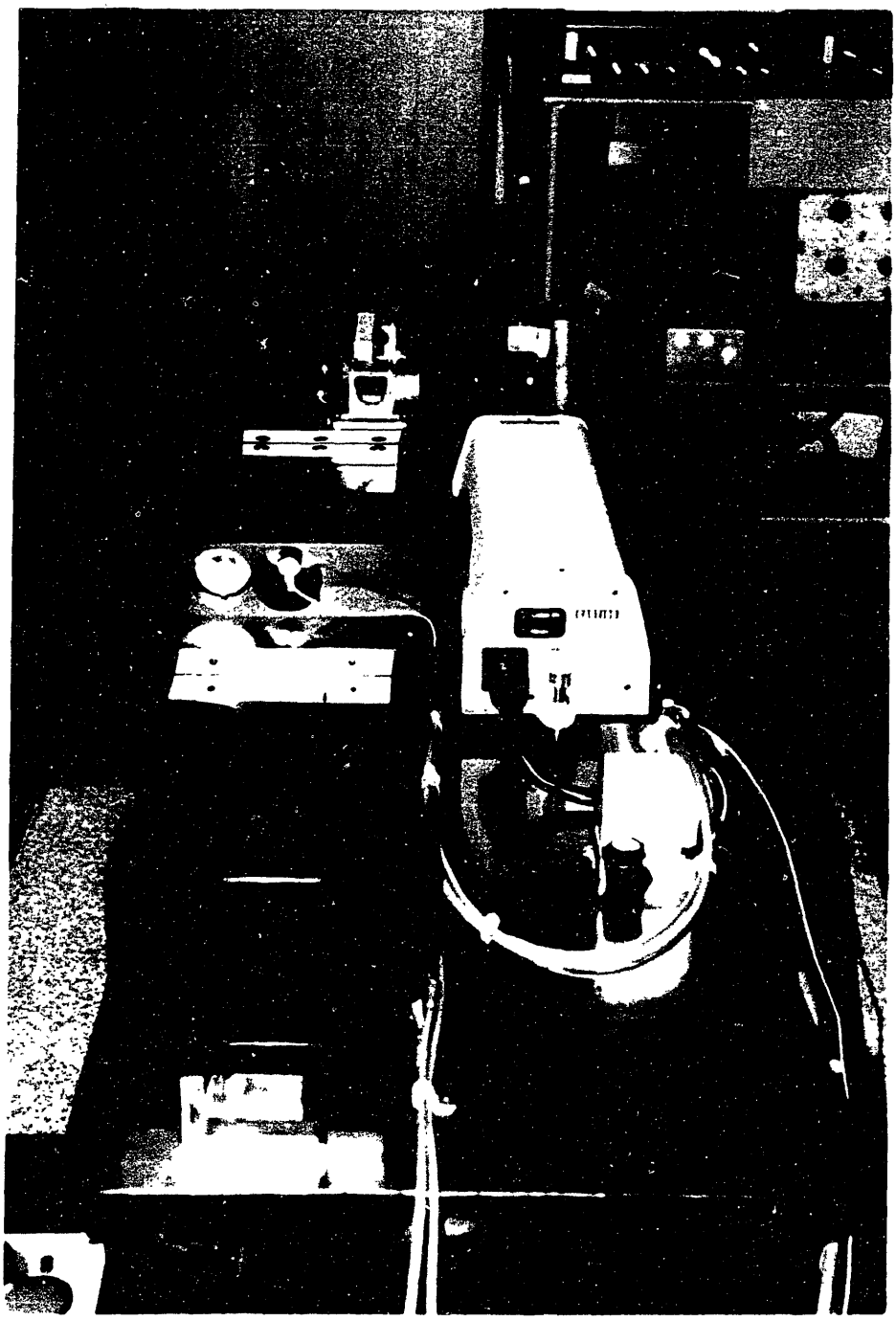

Figure 4.3, Right-end view of prototype calibrator.

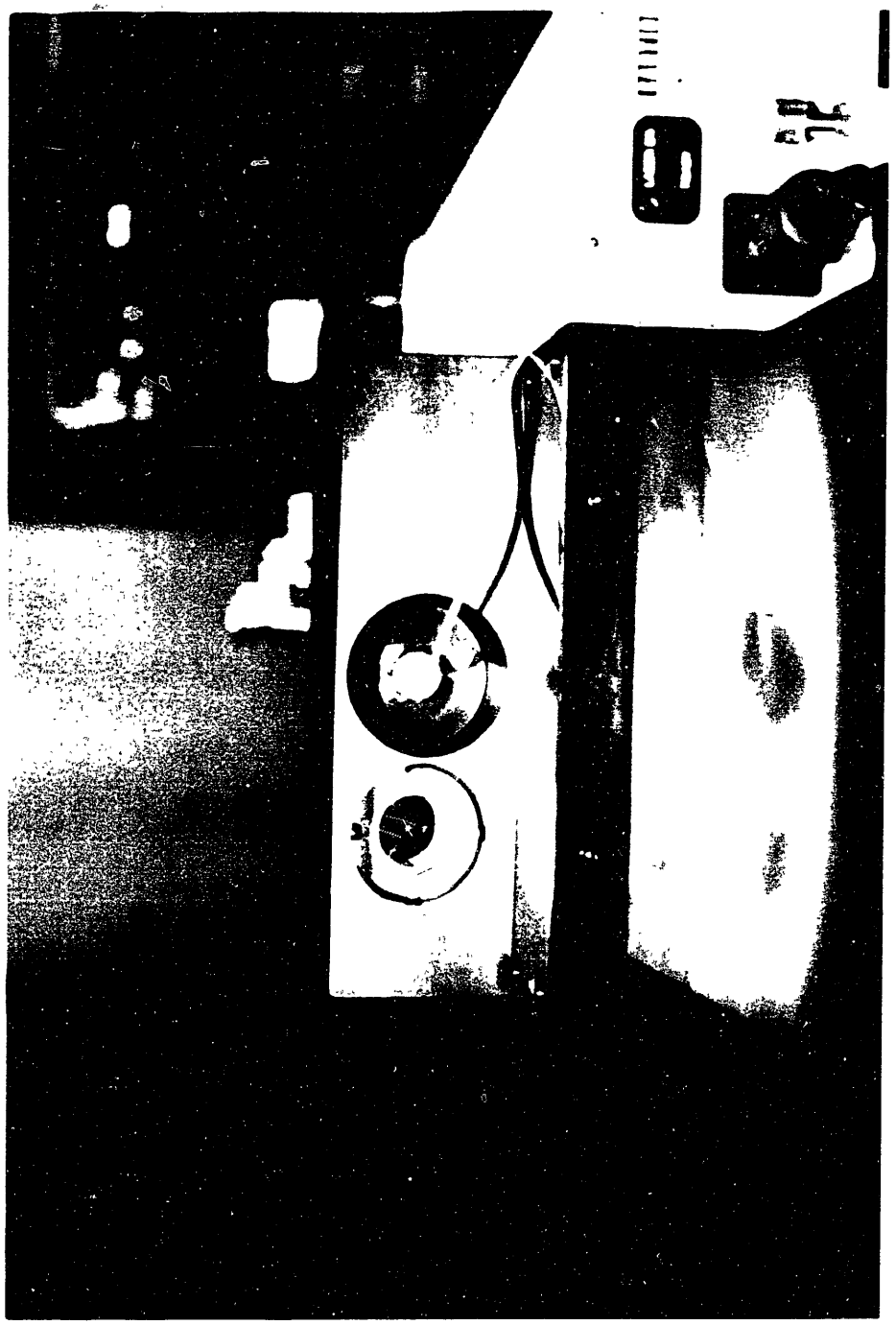

Figure 4.4, View of optics and accelerometer mount.

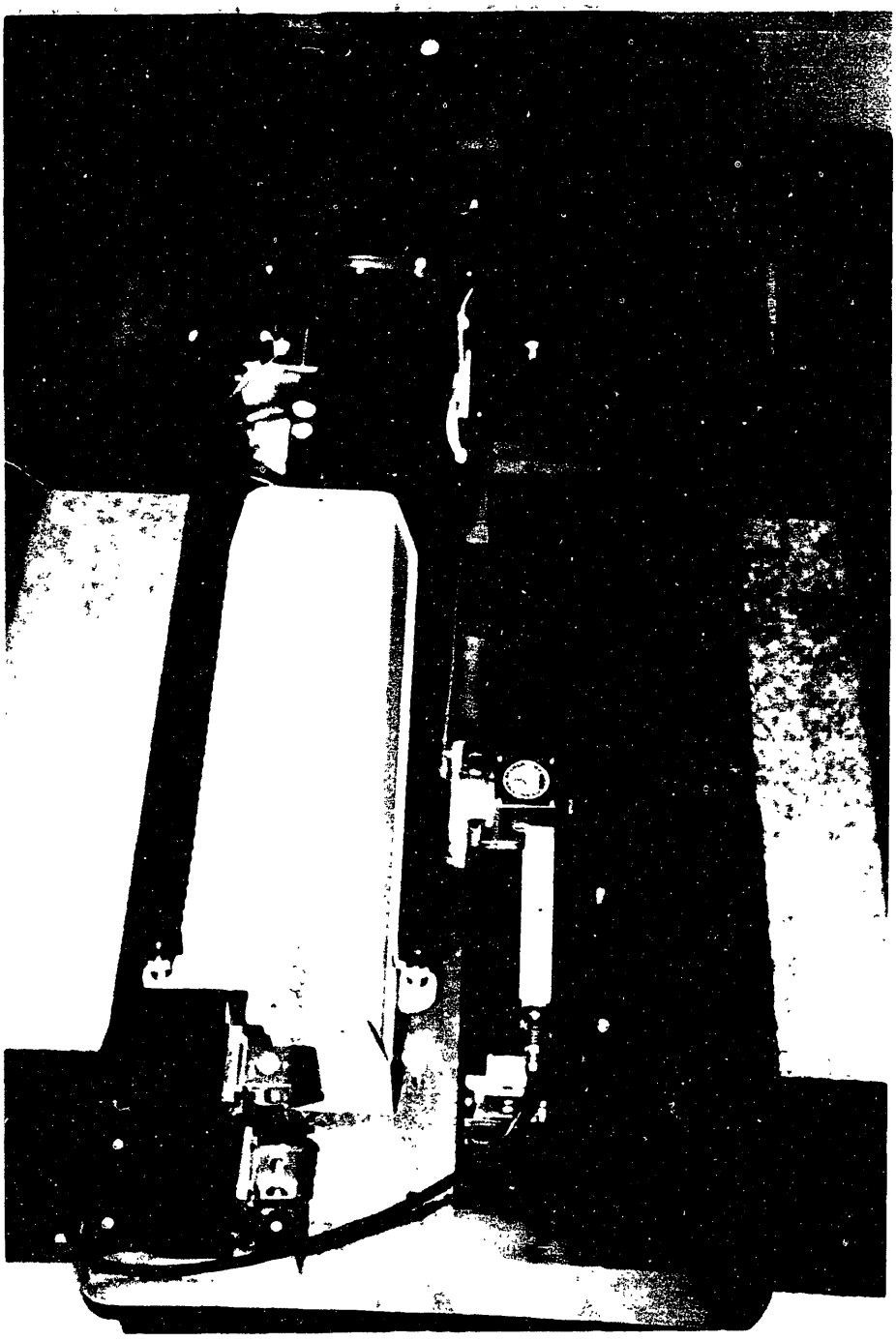

Figure 4.5, Left-end View of the Prototype Calibrator.

The computer will move the carriage to the home position which is typically the center of travel. The motor cables and air supply line are tied together and fastened to a block to strain relief the air bearing carriage. The air supply is filtered and dried before reaching the air bearing. If the influence of the cables adversely affects the carriage's accuracy, a low precision slave linear slide can be added to run parallel to the master slide to relieve the cable forces.

A Hewlett-Packard HP 3522A function generator with -65 dB harmonic distortion and 1μHz accuracy is used to supply the reference sinusoidal waveform. The function generator is IEEE-488 controlled from a Zenith AT compatible personal computer as shown in Figure 4.6. The PC reads the displacement data from the Zgyo instrumentation through a high speed digital interface board developed for the calibrator. This interface use a Data Translation DT2817 32 bit digital I/O card mounted in the PC. A second Data Translation board, a DT2823 with 16 bit A/D's and D/A's, is used for closed loop servo control of the slide using the digital position data from the laser interferometer as feedback. Positioning accuracies of 25 microinches have been achieved at this point. The accelerometer's output signal is read with a digital voltmeter, no specific meter has been chosen for the calibrator at this time.

A minimal of human contact with the carriage is desired during testing. Therefore, a manual control unit that uses a joystick potentiometer to supply a voltage signal to the amplifier was built for ease of manual slide positioning. The manual control unit also contains an emergency stop switch and end of travel indicators. The manual control unit is wired into the electronics control unit with 15 foot

umbilical cord. The electronics control unit is the distribution point for most electrical wiring as shown in Figure 4.6. All the electrical hardware is contained in a rack mount cabinet.

4.2 Verification of Cross Axis Motion

Before the calibrator can be considered as a national standard it must be measured to determine the overall uncertainty. The cross axis motion will be measured using a Zygo straightness interferometer as shown in Figure 4.7. A differential plane mirror interferometer splits the income laser beam into two beams. The beams pass to a prism mounted on the carriage as shown in Figure 4.8. The motions of the prism in the X direction corresponds to displacements in that direction. Rotations and displacements in the remaining five degrees of freedom have only limited affect in the measurement values. A special mount was designed so that the prism is in the same horizontal and vertical plane as the accelerometer so displacements measured will correlate to displacements seen by the accelerometer. The optical path of the laser beams passes to a stationary reference mirror mounted at the end of travel. This straightness interferometer is capable of slew rates of ± 35 in/sec, under special conditions the slew rate can be as high as 95 in/sec. These slew rates will enable real time measurement of the carriage under full dynamic loading (maximum acceleration rates and speeds).

Measurements will be taken over the bandwidth of the calibrator at various amplitudes. This measurements will begin by sending the carriage to the home position. The carriage displacement and straightness will be measured simultaneously using the hardware

developed for this purpose. The straightness interferometer will be rotated from the horizontal to vertical plane to measure both components of the cross axis motion. The residuals of a least squares fit of each axis data will give the cross axis motion. The overall cross axis motion is the maximum square root of the sum of squares of the two axis residuals divide by the displacement amplitude. The design value was to be less than 0.1%.

The measurements will be preformed in June 1988. The measurement hardware will not be ready until then and the results will be published in a supplemental paper.

4.3 Measurement of the Carriage's Angular Rotation

Measurement of the angular rotation of the carriage will be done in conjunction with the straightness measurements. A differential plane mirror interferometer will be used to measure the pitch of the carriage under static and dynamic loading a function of carriage displacement. A plane mirror will be mounted to the optics mount on the slide as shown in Figure 4.9. The yaw of the carriage will be measured using the two retroreflectors mounted on the carriage as shown in Figure 4.10. The yaw will be the difference in displacement measurements divided by the distance between the two retroreflectors. The optical hardware is unavailable until June 1988, at this time the measurements will be completed

4.4 Harmonic Distortion Measurements

A Hewlett Packard HP 3562A dynamic signal analyzer would be used to measure the harmonic distortion of the accelerometer's output. Results unavailable at this time.

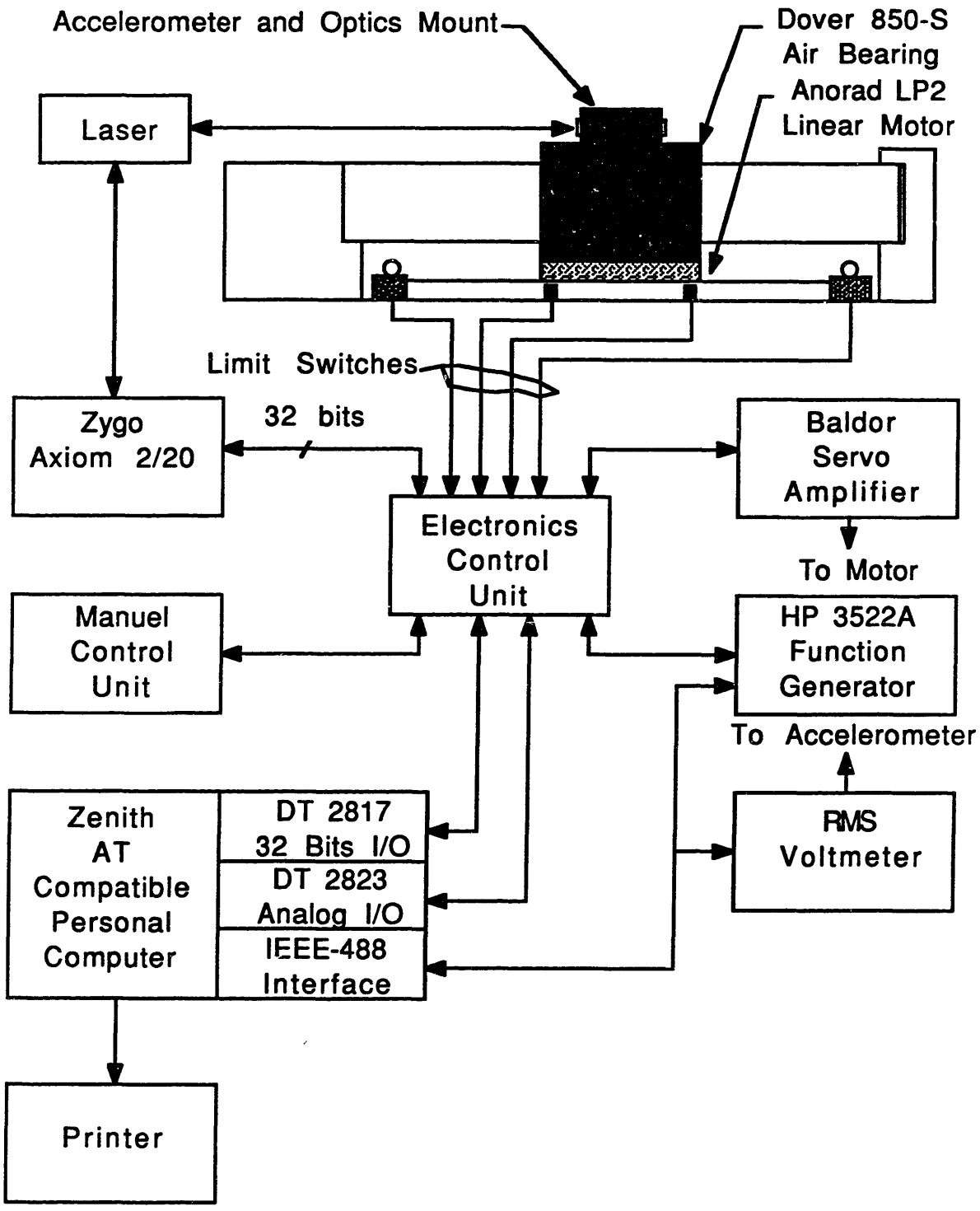

Figure 4.6, Diagram of prototype system hardware.

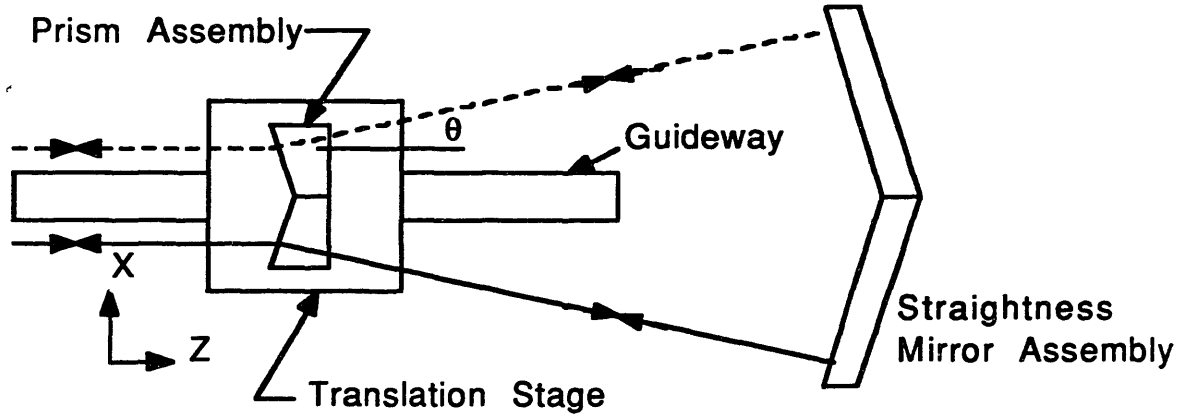

Figure 4.7, Diagram of straightness interferometer used to measure the cross axis motion.

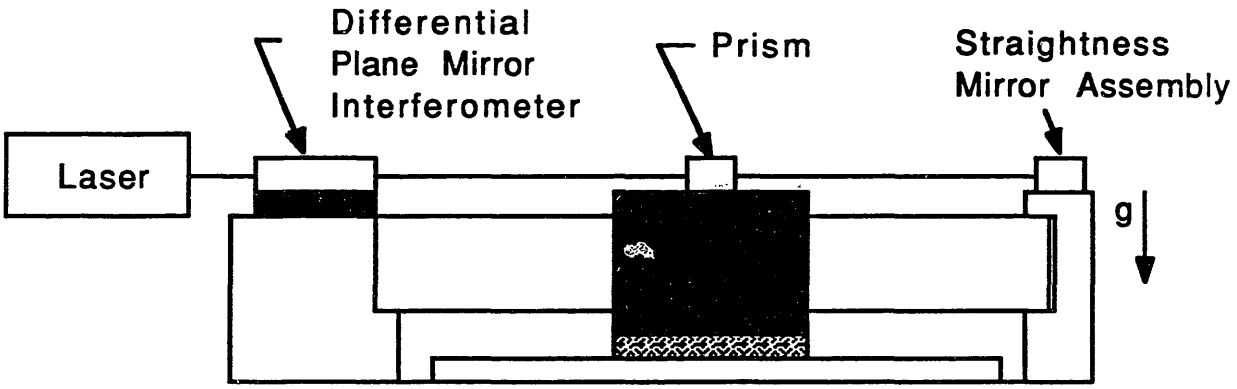

a) Measurement of horizontal straightness.

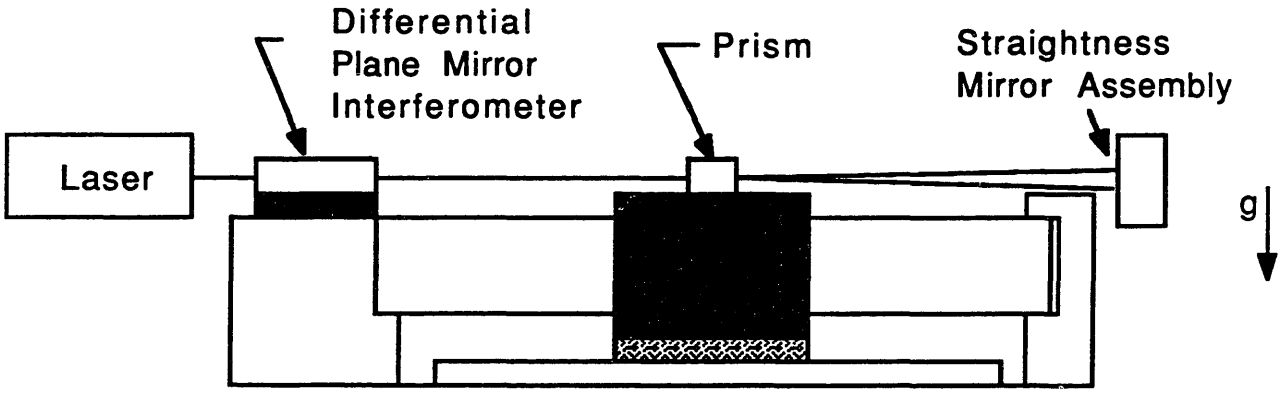

b) Measurement of vertical straightness.

Figure 4.8, Hardware configuration for measuring the cross axis motion.

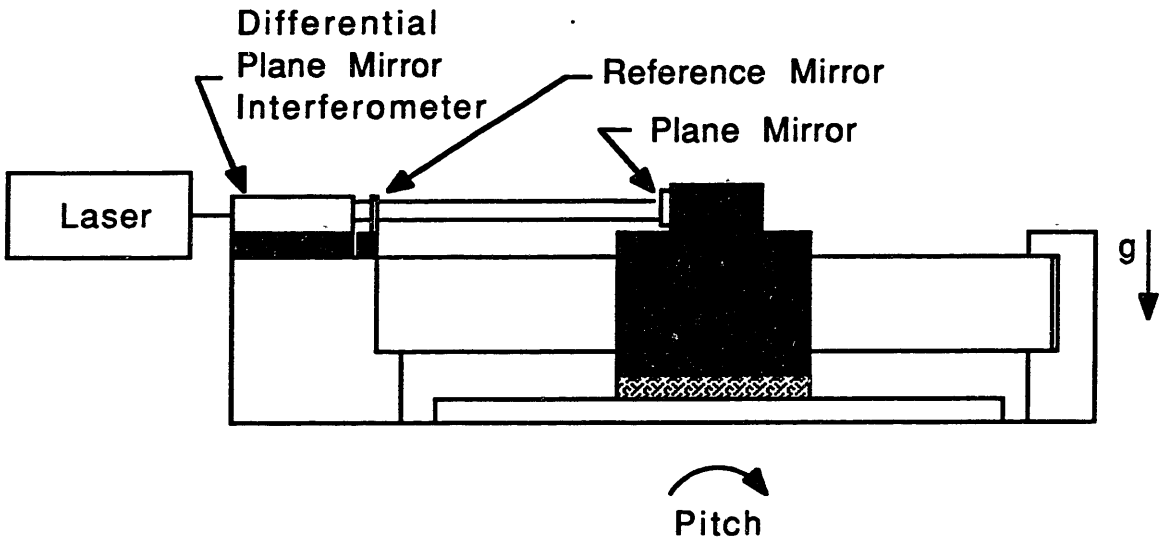

Figure 4.9, Hardware configuration for measuring the pitch of the carriage.

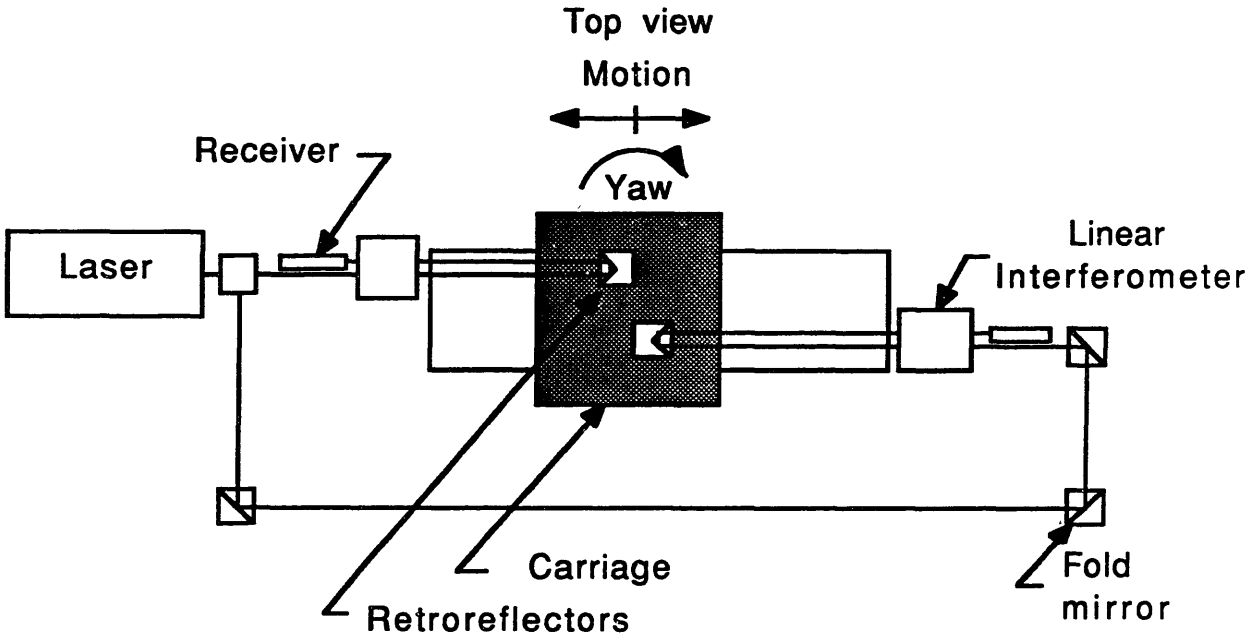

Figure 4.10, Hardware Configuration for measuring the yaw of the carrriage.

Chapter 5
Summary and Conclusions

This thesis presents the design and implementation of a low frequency accelerometer calibration system that will be used to calibrate United States Primary Standard Transducers at the U.S. National Bureau of Standards, Gaithersburg Maryland. In addition, this thesis covers the background research needed to understand accelerometers, their applications, calibration and presents a calibrator design that can achieve a predicted accuracy of 1 part per million, 10,000 times better than the existing calibrator.

Existing calibrator technology was reviewed and limitations were discussed. Design specifications were determined based upon these limitations and the desired specifications developed by accelerometer calibration personnel at the U.S. National Bureau of Standards. The existing and design specifications are presented in Table 5.1 along with with the prototype specifications. The design specifications called for a 3.2 times increase in double amplitude displacement, a 2 times increase in bandwidth and an order of magnitude reduction in cross axis motion and harmonic distortion. Meeting these objectives would have allowed the calibration uncertainty to be reduced by an order of magnitude to ±.0.1%

To meet the design objectives, the available linear actuators, bearings and displacement transducers were analyzed to determine if they could be used to meet the calibrator specifications. It was determined that a commercially available linear air bearing, brushless DC linear motor and laser transducer system could be used in the design

which results in substantial cost savings. Four designs based upon these components were presented as the solution to the calibrator design problem.

Of the four designs, the worst case design has a predicted accuracy of 10 parts per million. A more accurate and substantially more expansive design is presented that has a predicted one part per million accuracy. The worst case design was the least expensive to implement and therefore a prototype of this design was built using the following components: Dover Instruments' linear air bearing, Anorad brushless DC linear motor and Zygo laser transducer system. By utilizing these components, a 8.5 times increase in double amplitude displacement, a 1000 times increase calibrator accuracy and 1/2 times decrease in bandwidth are realized. The decision was made to increase the double amplitude displacement to 16 inches at the sacrifice of the bandwidth. The large double amplitude displacement is required to study the bandwidth characteristics of an accelerometer under a constant peak acceleration, this is not possible with existing calibrators.

A detailed experimental analyzes is in progress to verify the predicted specifications of the prototype. The results will be published at a later date. The prototype calibrator will also be used to study precision high speed servo loops which have applications to next generation machine tools. Up on completion of the experimental analysis, provided the results meet the required specifications, this prototype calibrator will be used in the daily accelerometer calibrations offered to industry by the U.S. National Bureau of Standards.

Future calibrator research could focus on increasing the double amplitude displacement to 2 meters. The hardware components are available but at substantial costs. With a 2 meter calibrator, lower calibration frequencies with high acceleration rates would be possible. Also, the idea of using signal processing techniques (Fast Fourier Transforms) on the high resolution laser displacement data and corresponding accelerometer output to determine the accelerometer's sensitivity could be investigated further.

Table 5.1 Existing, design and prototype calibrator specifications.

Calibrator Specifications	Existing	Design	Prototype
System Bandwidth, Hz.	1 to 100	1 to 100	1 to 22
Minimum Double Amplitude Displacement, inch.	1 7/8	6.0	16.0
Cross axis motion over bandwidth.	1.0%	0.1%	0.001%
Harmonic Distortion.	1.0%	0.1%	*
Peak Accelerations, g.	1.5	3.0	2.0
System accuracy.	1.0%	0.1%	*
Constant Acceleration over bandwidth, g.	N/A	0.3	0.8

* to be measured

References

1 K. Yee and D. S. Blomquist, "An on-line Method of Determining Tool Wear by Time-Domain Analysis", Tech. Paper MR82-901, Soc. Mfg. Engrs., Dearborn, Mich., 1982.

2 Newport Corporation, Fountain Valley, CA. Product literature.

3 Barry Wright Corporation, Watertown, Massachusets, private communication.

4 Hewlett Packard, Palo Alto, CA 94303-0890, "The Fundamental of Modal Testing", Application note 243-3.

5 T. R. Licht and H. Andersen, "Trends in Accelerometer Calibration", Bruel & Kjaer Technical Review, no. 2, 1987.

6 International Standard Organization, ISO 5347, "Methods of Calibration of vibration and shock pick-ups", was to be published in 1987.

7 B. F. Payne and C. Federman, "An Automated Fringe Counting Laser Interferometer for Low Frequency Vibration Measurements".

8 M. R. Serbyn and B. F. Payne of NBS, private communication.

9 T. Dimoff and B. F. Payne, "Application of Air Bearings to an Electrodynamic Vibration Standard", Journal of Research of the National Bureau of Standards, vol. 67c, no. 4, October-December 1963.

10 T. Dimoff, "Electrodynamic Vibration Standard with a Ceramic Moving Element", The Journal of the Acoustical Society of America, vol. 40, no. 3, September 1966.

11 B. F. Payne and M. R. Serbyn, "An application of parameter estimation theory in low Frequency Accelerometer Calibrations"

12 R. S. Koyanagi, "Development of a Low-frequency-vibration Calibration System", Experimental Mechanics, vol.15, no. 11, pp. 443-448, November 1975.

13 "Computer Automates Calibration of Accelerometers"; NBS Technical News Bulletin, pp. 264-265. November 1971.

14 S. Levy, A. E. McPherson, and E. V. Hobbs, "Calibration of Accelerometers", Journal of Research of the National Bureau of Standards, vol. 41, pp. 359-369. November 1948.

15 D.S. Blomquist of NBS, private communication.

16 H. J. von Martens, "Representation of Low-frequency Rectilinear Vibrations for High-accuracy Calibration of Measurement Instruments for Vibration", Proceedings of the Second Symposium of the IMEKO Technical Committee on Metrology-TC8, pp. 203-215. Budapest 1983.

17 G. P. Sutton, "Economics of Accuracy", Technology of Machine Tools, Volume 5: Machine Tool Accuracy, ch. 9.3. Lawrence Livermore Laboratory, University of California. Oct. 1980.

18 NSK, Elmhurst, IL 60126. Product Literature Linear Motion Products.

19 Toto, National Machine Systems, Inc., Orange, CA 92665. Product literature and precision ceramics technical data.

20 A. H. Slocum and B. N. Damazo, "Design of a Ball Nut Coupling, a device used to Reduce Geometric Errors in Linear Slides Driven by Lead Screws", work in progress.

21 Fox International, Inc., Hayward, CA 94545. Linear Air Bearing product literature.

22 A. Chitayat, "Brushless DC Linear Motors", Motion, pp.22-23. September/October 1987.

23 B. L. Triplett, "Linear Motors Combine Muscle with a Fine Touch", Machine Design, pp. 94-97, 7 May 1987.

24 Anorad Corporation, Hauppauge, NY. Product Literature.

25 Inland Motor, Defense Products Group, Radford, VA. 24141. DC Linear Motor Application Guide. March, 1986.

26 Northern Magnetics Inc., Van Nuys, CA 91406. D.C. Linear Motor product literature.

27 J.E. Shigley, Mechanical Engineering Design, 4th ed.,New York: McGraw-Hill, 1983.

28 Acoustic Power Systems, Inc. Carlsbad, CA 92008. Electro-Seis Model 113-AB Shaker.

29 Burleigh Instruments, Fishers, NY. Product Literature.

30 Dover Instrument Corporation, Westboro, MA 01581. Linear Air Bearing product literature.

31 Professional Instruments Company, Minneapolis, MN 55416. Product literature.

32 Heidenhain Corporation, Elk Grove Village, IL 60007. Product Literature model LID 310.

33 Dynamic Research Corporation,Wilmington, MA 01887-2193. Product Literature.

34 J. V. Moskaitis and D. S. Blomquist, "A Microprocessor-Based Technique for Transducer Linearization", Precision Engineering, vol. 5 no. 1, 1983.

35 Zygo Corporation, Middlefield, CT 06455, Product Literature Axiom 2/20.

36..Zygo Corporation, Middlefield, CT 06455, Axiom 2/20 user manuel.

37 Hewlett Packard, Palo Alto, CA. 94303-0890. Product Literature Hp 5527A Laser Position Transducer.

38. R.C. Quenelle and L. J. Wuerz, "A New Microcomputer-Controlled Laser Dimensional Measurement and Analysis System", Hewlett-Packard Journal, pp.3-13, April 1983.

39 Bruel & Kjaer Instruments, Marlborough, MA. 01752. Product Literature Type 4294, Calibration Exciter.T

40 M. A. Donmez, "A General Methodology for Machine Tool Accuracy Enhancement Theory, Application and Implementation", Ph.D Thesis, Purdue University 1985

41 R. R. Donaldson, "Error Budgets", Technology of Machine Tools, Volume 5: Machine Tool Accuracy, ch. 9.14. Lawrence Livermore Laboratory, University of California. Oct. 1980.

42 R. J. Hocken, "Quasistatic Machine Tool Errors", Technology of Machine Tools, Volume 5: Machine Tool Accuracy, ch. 3.0. Lawrence Livermore Laboratory, University of California. Oct. 1980.

43 R. J. Roark and W.C Young, Formulas for Stress and Strain, 5th Ed, McGraw-Hill: New York, 1975.

44 B. Edlen, "The Refractive Index of Air", Metrologia, 1966, 2, 71.

45..G. E. Sommargren, "A New Laser Measurement System for Precision Metrolgy", Presented at the 1986 Precision Engineering Conference, Novemeber 5-7, 1986, Dallas Texas.

46 N. Bobroff, "Residual errors in laser interferometry from air turbulence and nonlinearity", Applied Optics, Vol. 26, No. 13, 1 July 1987.

47 Hewlett-Packard Application Note 197-2, "Laser and Optics, 5501A Laser Transducer".

48 Zygo Corporaton, Application Bulletin, Axiom 2/20 Straightness Interferometer.

49 W. T. Estler, "Calibration and Use of Optical straightedges in the Metrology of Presicion Machines", Optical Engineering, 24(3), pp. 372-379. May/June 1985.

Appendix

A) Error Analysis Program

B) Equipment Costs

Appendix A

Error Analysis Program

Program Error.pas was written in Turbo pascal to generate plots of the error components associated with linear air bearings. Specifically, standard Dover air bearings are analyzed as uniform simply supported elastic beams under the load of its carriage and Anorad LP2 linear brushless DC motor. A variable load can be applied to represent the effects of different optical mounts and accelerometer mounts. In addition, the program computes the natural frequency of the system for the various loading conditions.

```
{P15000}
program  Error(input,output);
{ Brad Damazo, Massachusetts Institute of Technology          }
{ Rm 1-050, 617-253-0448, 10/18/87                            }
{ Program Error analyzes the errors of Dover linear           }
{ Air Bearing slides as a function of load. The               }
{ slide dimensions and stiffnesses are from Dover             }
{ Instrument Corp. 617-366-1456, bulletin no. 274             }
{ and their "Product Bulletin"                                }
{                                                             }
{              Glossary:                                      }
{ Slide - refers to air bearing moving table                  }
{ Beam  - refers to stationary base of air bearing            }
{ Coordinate system -                                         }
{                        Y,Ry                                 }
{                        |                                    }
{                        |                                    }
{                        |                                    }
{                        |_____________ X,Rx                  }
{                      /                                      }
{                    /                                        }
{                  /                                          }
{               Z,Rz                                          }
{                                                             }
```

```
{ Note, all bearing data is entered within the program}
{ for easy access and simplifation.                    }
{ All dimensions in inches, linear stiffness in lb/in  }
{ rotational stiffness in in-lb/rad. All stiffnesses   }
{ are assumed linear.                                  }

{I typedef.sys}
{I graphix.sys}
{I kernel.sys}
{I windows.sys}
{I axis.hgh}
{I polygon.hgh}
{I findwrld.hgh}
{$I dummy.inc}

CONST
    Number_of_Bearings = 10;
    Number_of_Points   = 1;
     Density_AL = 0.1; {lbm/in**3}
     E = 10.3E6; {lbf/in**2}
     G =  3.8E6; {lbf/in**2}
    Scale_Factor = 1.0;
    Percent_Side = 0.15;
    Percent_Wire = 0.15;
     Retroreflector_Weight = 0.0938;
    Motor_Weight = 2.5;
    Multiplier = 1E6;

TYPE
   String80   = STRING[80];
  Tags      = STRING[10];
  Dimensions = RECORD
                 X,Y,Z : REAL;
           END;
  Dimension1 = RECORD
                 X,Y,Z1,Z2 : REAL;
           END;
  DOF      = RECORD
                 X,Y,Z,Rx,Ry,Rz : REAL;
           END;
  DOFARRAY  = RECORD
                 X,Y,Z,Rx,Ry,Rz : ARRAY[1..Number_of_Points] of REAL;
           END;
```

```
  Setup    = RECORD
                Slide_Dim        : Dimension1;
                 Beam_Dim,Inertia  : Dimensions;
               Numbers          : Tags;
               Stiffness        : DOF;
                Starting_Load,
                 TotalInertia,
                Natural_Frequency,
                 Composite_Natural_Frequency,
                  Accelerometer_Errors,
               Beam_Error,
               Slide_Error      : DOFARRAY;
                AirBearing_Weight : REAL;
                 System_Error : ARRAY[1..Number_of_Points] of REAL;
              AD,BD,SD : ARRAY[1..21,1..8] of REAL;

          END;

VAR
   Model        : ARRAY[1..Number_of_Bearings] of Setup;
  Load       : DOFARRAY;
  Q,U,Ua,Uc,
   Increment    : INTEGER;
   Outfile      : TEXT;
   GapLength,
    Amplitude,
    Position,
     Acceleration,
  Frequency    : REAL;
  J,I,C,N,W,Inc: INTEGER;
    Title,
    Axis_labels,
   FileName     : STRING80;
  DA,DB,DS,DT,
   DD,DR        : PlotArray;
  CH         : CHAR;
     Cross_Axis_Motion_range,
     Cross_Axis_Motion_max,
    Cross_Axis_Motion_min : REAL;
   Cross_Axis_Motion     : ARRAY[1..21] of REAL;
   FileIndex    : ARRAY[1..21] of STRING[3];
```

```
PROCEDURE FileIndexData;
BEGIN
      FileIndex[1] := 'at'; FileIndex[8]  := 'bt'; FileIndex[15] := 'st';
      FileIndex[2] := 'ax'; FileIndex[9]  := 'bx'; FileIndex[16] := 'sx';
      FileIndex[3] := 'ay'; FileIndex[10] := 'by'; FileIndex[17] := 'sy';
      FileIndex[4] := 'az'; FileIndex[11] := 'bz'; FileIndex[18] := 'sz';
      FileIndex[5] := 'arx';FileIndex[12] := 'brx';FileIndex[19] := 'srx';
      FileIndex[6] := 'ary';FileIndex[13] := 'bry';FileIndex[20] := 'sry';
      FileIndex[7] := 'arz';FileIndex[14] := 'brz';FileIndex[21] := 'srz';

END;
PROCEDURE Bearing_Data; {All beam lengths based on 20 inch travel}
{with 1 inch for mounting and X length of bearing}
{For double bearing models, assume 0.5 inch gap}
BEGIN {Slide Data}
   WITH Model[1] DO BEGIN
      Numbers := '400-B';
     WITH Slide_Dim DO BEGIN
       X :=  4.0;  Y := 2.206;  Z1 := 4.38;  Z2 := 3.47;
      END; {Slide_Dim}
     WITH Beam_Dim DO BEGIN
       X := 25.0;  Y := 1.235;  Z  := 2.485;
     END; {Beam_Dim}
     WITH Stiffness DO BEGIN
      Y :=  5E5;  Z := 2.5E5; Rx := 1.56E5; Ry := 3.6E5; Rz := 6.6E5;
      END; {Stiffness}
   END; {Model[1]}

   WITH Model[2] DO BEGIN
      Numbers := '400-B2';
     WITH Slide_Dim DO BEGIN
       X :=  (8.0 + GapLength);  Y := 2.206;  Z1 := 4.38;  Z2 := 3.47;
      END; {Slide_Dim}
     WITH Beam_Dim DO BEGIN
       X := (29.0 + GapLength);  Y := 1.235;  Z  := 2.485;
     END; {Beam_Dim}
     WITH Stiffness DO BEGIN
      Y :=  10E5;  Z := 5E5; Rx := 3.12E5;
        Ry := 2*Model[1].Stiffness.Rz
              + SQR(8.0 + GapLength)*Model[1].Stiffness.Y/2;
        Rz := 2*Model[1].Stiffness.Ry
              + SQR(8.0 + GapLength)*Model[1].Stiffness.Z/2;
      END; {Stiffness}
```

```
 END; {Model[2]}

WITH Model[3] DO BEGIN
   Numbers := '400-S';
 WITH Slide_Dim DO BEGIN
    X :=  4.0;  Y := 3.46;   Z1 := 4.38;  Z2 := 3.47;
  END; {Slide_Dim}
 WITH Beam_Dim DO BEGIN
    X := 25.0;  Y := 2.485;  Z  := 2.485;
  END; {Beam_Dim}
  WITH Stiffness DO BEGIN
   Y :=  5E5;  Z :=   5E5; Rx := 2.0E5; Ry := 6.6E5; Rz := 6.6E5;
   END; {Stiffness}
END; {Model[3]}

WITH Model[4] DO BEGIN
   Numbers := '400-S2';
 WITH Slide_Dim DO BEGIN
    X := (8.0 + GapLength);  Y := 3.46;   Z1 := 4.38;  Z2 := 3.47;
  END; {Slide_Dim}
 WITH Beam_Dim DO BEGIN
    X := (29.0 + GapLength);  Y := 2.485;  Z  := 2.485;
  END; {Beam_Dim}
  WITH Stiffness DO BEGIN
   Y := 10E5;  Z := 10E5;   Rx := 4.0E5;
     Ry := 2*Model[3].Stiffness.Rz
           + SQR(4.0 + GapLength)*Model[3].Stiffness.Y/2;
     Rz := 2*Model[3].Stiffness.Ry
           + SQR(4.0 + GapLength)*Model[3].Stiffness.Z/2;
  END; {Stiffness}
END; {Model[4]}

WITH Model[5] DO BEGIN
   Numbers := '400-S2M';
 WITH Slide_Dim DO BEGIN
    X :=  (8.0 + GapLength);  Y := 3.96;   Z1 := 4.38;  Z2 := 3.47;
  END; {Slide_Dim}
 WITH Beam_Dim DO BEGIN
    X := (29.0 + GapLength);  Y := 2.985;  Z  := 2.485;
  END; {Beam_Dim}
  WITH Stiffness DO BEGIN
   Y := 10E5;  Z :=   10E5; Rx := 4.0E5;
     Ry := 2*Model[3].Stiffness.Rz
```

```
            + SQR(4.0 + GapLength)*Model[3].Stiffness.Y/2;
        Rz := 2*Model[3].Stiffness.Ry
            + SQR(4.0 + GapLength)*Model[3].Stiffness.Z/2;
    END; {Stiffness}
END; {Model[5]}

WITH Model[6] DO BEGIN
    Numbers := '600-B';
   WITH Slide_Dim DO BEGIN
     X :=  6.0;  Y := 2.46;   Z1 := 4.38;  Z2 := 3.47;
    END; {Slide_Dim}
   WITH Beam_Dim DO BEGIN
     X := 27.0;  Y := 1.235;  Z  := 2.485;
    END; {Beam_Dim}
    WITH Stiffness DO BEGIN
     Y := 7.5E5; Z := 3.75E5; Rx := 2.26E5; Ry := 1.0E6; Rz := 15.4E5;
    END; {Stiffness}
END; {Model[6]}


WITH Model[7] DO BEGIN
    Numbers := '600-S';
   WITH Slide_Dim DO BEGIN
     X :=  6.0;  Y := 3.71;   Z1 := 4.38;  Z2 := 3.47;
    END; {Slide_Dim}
   WITH Beam_Dim DO BEGIN
     X := 27.0;  Y := 2.485;  Z  := 2.485;
    END; {Beam_Dim}
    WITH Stiffness DO BEGIN
     Y :=7.5E5;  Z := 7.5E5; Rx := 3.04E5; Ry :=15.4E5; Rz :=15.4E5;
    END; {Stiffness}
END; {Model[7]}

WITH Model[8] DO BEGIN
    Numbers := '600-S2';
   WITH Slide_Dim DO BEGIN
     X :=  (12.0 + GapLength);  Y := 3.71;   Z1 := 4.38;  Z2 := 3.47;
    END; {Slide_Dim}
   WITH Beam_Dim DO BEGIN
     X :=  (33.0 + GapLength);   Y := 2.485;  Z  := 2.485;
    END; {Beam_Dim}
    WITH Stiffness DO BEGIN
     Y :=15E5;  Z := 15E5; Rx := 6.08E5;
```

```
        Ry := 2*Model[7].Stiffness.Rz
              + SQR(6.0 + GapLength)*Model[7].Stiffness.Y/2;
        Rz := 2*Model[7].Stiffness.Ry
              + SQR(6.0 + GapLength)*Model[7].Stiffness.Z/2;
      END; {Stiffness}
    END; {Model[8]}

    WITH Model[9] DO BEGIN
      Numbers := '600-S2M';
     WITH Slide_Dim DO BEGIN
       X :=  (12.0 + GapLength);  Y := 4.21;   Z1 := 4.38;  Z2 := 3.47;
      END; {Slide_Dim}
     WITH Beam_Dim DO BEGIN
       X :=  (33.0 + GapLength);  Y := 2.985;  Z  := 2.485;
      END; {Beam_Dim}
      WITH Stiffness DO BEGIN
       Y :=15E5;  Z := 15E5; Rx := 6.08E5;
         Ry := 2*Model[7].Stiffness.Rz
              + SQR(6.0 + GapLength)*Model[7].Stiffness.Y/2;
         Rz := 2*Model[7].Stiffness.Ry
              + SQR(6.0 + GapLength)*Model[7].Stiffness.Z/2;
      END; {Stiffness}
    END; {Model[9]}

    WITH Model[10] DO BEGIN
      Numbers := '700-S';
     WITH Slide_Dim DO BEGIN
       X :=  7.0;  Y := 5.45;   Z1 := 7.0;  Z2 := 7.0;
      END; {Slide_Dim}
     WITH Beam_Dim DO BEGIN
       X := 28.0;  Y := 2.965;  Z  := 5.50;
      END; {Beam_Dim}
      WITH Stiffness DO BEGIN
       Y :=1.5E6;  Z := 8E5; Rx := 1.25E6; Ry :=2E6; Rz :=3.6E6;
      END; {Stiffness}
    END; {Model[10]}
END; {Slide Data}

PROCEDURE Calculate_Airbearing_Weight(Number:INTEGER);
BEGIN
WITH Model[Number] DO BEGIN
AirBearing_Weight  :=  0.1*(Slide_Dim.X*Slide_Dim.Y*Slide_Dim.Z2 +
                    (Slide_Dim.Z1-Slide_Dim.Z2)*Slide_Dim.X*
```

```
                    ((Slide_Dim.Y-Beam_Dim.Y)/2) -
                    Slide_Dim.X*Beam_Dim.Y*Beam_Dim.Z);
END;
END;

PROCEDURE  Calculate_Inertia_Without_Load(Number:integer);
VAR Ix,Iy,Iz : ARRAY[1..4] OF REAL;
BEGIN
   WITH Model[Number] DO BEGIN
          {**** X direction ****}
       WITH Slide_Dim DO BEGIN
            Ix[1] := Density_AL*X*Y*Z2/12*(SQR(Z2)+SQR(Y));
        END; {Slide_Dim}
          Ix[2] := -Density_AL*Slide_Dim.X*Beam_Dim.Z*Beam_Dim.Y/12*
            (SQR(Beam_Dim.Z)+SQR(Beam_Dim.Y));
          Ix[3] := 2*Density_AL*(Slide_Dim.Y-Beam_Dim.Y)*
                (Slide_Dim.Z1-Slide_Dim.Z2)*Slide_Dim.X/4*
               ((SQR(Slide_Dim.Z2-Slide_Dim.Z1)/4+
               SQR(Slide_Dim.Y-Beam_Dim.Y)/4)/12+
                SQR(Slide_Dim.Y/2-(Slide_dim.Y-Beam_Dim.Y)/4));
         Ix[4] :=  1.302 +2.5*(Slide_Dim.Y/2 + 0.75);
         Inertia.X := Ix[1] + Ix[2] + Ix[3] + Ix[4];
          {**** Y direction ****}
       WITH Slide_Dim DO BEGIN
            Iy[1] := Density_AL*X*Y*Z2/12*(SQR(Z2)+SQR(X));
        END; {Slide_Dim}
          Iy[2] := -Density_AL*Slide_Dim.X*Beam_Dim.Z*Beam_Dim.Y/12*
            (SQR(Slide_Dim.X)+SQR(Beam_Dim.Z));
         Iy[3] :=  2*Density_AL*(Slide_Dim.Y-Beam_Dim.Y)*
                (Slide_Dim.Z1-Slide_Dim.Z2)/4*Slide_Dim.X*
              ((SQR(Slide_Dim.X)+SQR(Slide_Dim.Z1-
Slide_Dim.Z2)/4)/12+
                SQR(Slide_Dim.Z1/4-Slide_Dim.Z2/4));
        Iy[4] :=  23.80;
         Inertia.Y := Iy[1] + Iy[2] + Iy[3] + Iy[4];
          {**** Z-direction ****}
       WITH Slide_Dim DO BEGIN
            Iz[1] := Density_AL*X*Y*Z2/12*(SQR(X)+SQR(Y));
        END; {Slide_Dim}
          Iz[2] := -Density_AL*Slide_Dim.X*Beam_Dim.Z*Beam_Dim.Y/12*
            (SQR(Slide_Dim.X)+SQR(Beam_Dim.Y));
          Iz[3] := 2*Density_AL*(Slide_Dim.Y-Beam_Dim.Y)*(Slide_Dim.Z1-
                Slide_Dim.Z2)*Slide_Dim.X/4*
```

```
                ((SQR(Slide_Dim.X)+SQR(Slide_Dim.Y-Beam_Dim.Y)/4)/12+
                SQR((Slide_Dim.Y-Beam_Dim.Y)/4+Beam_Dim.Y/2));
        Iz[4] :=  23.44 + 2.5*SQR(Slide_Dim.Y/2 + 0.75);
        Inertia.Z := Iz[1] + Iz[2] + Iz[3] + Iz[4];
{        WRITELN('  ',Numbers,Inertia.X:10:4,Inertia.Y:10:4,Inertia.Z:10:4);}
   END;
END;

PROCEDURE Calculate_Inertia_With_Varible_Load(Number:INTEGER;
Varible_Load:INTEGER);
VAR Load_Inertia,Mass,TMP: REAL;

BEGIN
WITH Model[Number] DO BEGIN
     Mass         := Varible_Load/Scale_Factor;
     TMP          := exp(0.3333*ln(Mass/Density_AL));
     Load_Inertia := Mass*SQR(TMP)/6;

     TotalInertia.X[Q]   := Inertia.X + Load_Inertia
                          + mass*sqr(tmp/2+Slide_Dim.Y/2);
     TotalInertia.Y[Q]   := Inertia.Y + Load_Inertia;
     TotalInertia.Z[Q]   := Inertia.Z + Load_Inertia
                          + mass*sqr(tmp/2+Slide_Dim.Y/2);
{     WRITELN('   ',Numbers,TotalInertia.X[Q]:10:4,TotalInertia.Y[Q]:10:4,
     TotalInertia.Z[Q]:10:4);}
END;
END;

PROCEDURE Calculate_Natural_Frequency(Number:INTEGER);
PROCEDURE Calculate_Slide_Natural_Frequency(VAR Omega:REAL;
Stiffness,Mass_or_Inertia:REAL);
BEGIN
     IF Mass_or_Inertia = 0.0 THEN Omega := 0.0 ELSE
       Omega := SQRT(Stiffness*386.4/ABS(Mass_or_Inertia));
END;
BEGIN
WITH Model[Number] DO BEGIN
Calculate_Slide_Natural_Frequency(Natural_Frequency.Y[Q],
Stiffness.Y,Load.Y[Q]);
Calculate_Slide_Natural_Frequency(Natural_Frequency.Z[Q],
Stiffness.Z,Load.Z[Q]);
Calculate_Slide_Natural_Frequency(Natural_Frequency.Rx[Q],
Stiffness.Rx,TotalInertia.X[Q]);
```

```
Calculate_Slide_Natural_Frequency(Natural_Frequency.Ry[Q],
Stiffness.Ry,TotalInertia.Y[Q]);
Calculate_Slide_Natural_Frequency(Natural_Frequency.Rz[Q],
Stiffness.Rz,TotalInertia.Z[Q]);
END;
END;

PROCEDURE Calculate_Composite_Natural_Frequency(Number:INTEGER);
VAR Massequ,Inertiaequ,Kbeam,K,leq :REAL;

PROCEDURE Calculate_Natural_Frequency(VAR Omega:REAL;
Stiffness1,Stiffness2,Mass_or_Inertia1,Mass_or_Inertia2:REAL);
VAR a,b,c,Omega1,Omega2,Tmp :REAL;
BEGIN
    a := Mass_or_Inertia1*Mass_or_Inertia2;
  b :=-
(Mass_or_Inertia2*(Stiffness1+Stiffness2)+Stiffness2*Mass_or_Inert
ia1);
    c := Stiffness1*Stiffness2;
    tmp := sqrt(b*b-4*a*c);
   IF (-b+tmp)>0.0 THEN Omega := SQRT((-b-tmp)/2/a)
   ELSE Omega := SQRT((-b+tmp)/2/a);

END;
BEGIN
WITH Model[Number] DO BEGIN
WITH Beam_Dim DO BEGIN
      Massequ := 5*Density_AL*X*Y*Z/8;
     Kbeam    := 4*E*Z*Y*Y*Y/(X*X*X);
END;
Calculate_Natural_Frequency(Composite_Natural_Frequency.Y[Q],
Kbeam,Stiffness.Y,Massequ,Load.Y[Q]);
WITH Beam_Dim DO BEGIN
       Inertiaequ  := Z/2*EXP(3*LN(Y/2))*(16/3-3.36*Y/Z*
                    (1-(EXP(4*LN(Y/2))/12/EXP(4*LN(Z/2)))));
    Kbeam      := 4*G*K/X;
END;
Calculate_Natural_Frequency(Composite_Natural_Frequency.Rx[Q],
Kbeam,Stiffness.Rx,Inertiaequ,TotalInertia.X[Q]);
WITH Beam_Dim DO BEGIN
          leq := X*0.42265;
       Inertiaequ  := Density_Al*Y*Z*leq*leq*leq/2;
    Kbeam      := E*Z*Y*Y*Y/X;
```

```
END;
Calculate_Natural_Frequency(Composite_Natural_Frequency.Rz[Q],
Kbeam,Stiffness.Rz,Inertiaequ,TotalInertia.Z[Q]);
END;
END;

PROCEDURE Calculate_Beam_Errors(Number:INTEGER);
PROCEDURE Calculate_Beam_Slope_And_Deflection(VAR
Beam_Deflection,
Beam_Rotation:REAL;B,H,A,X,L,Mo,W:REAL);

VAR I,Ra,Ma,Thetaa,Ya,Yc,Ym,Tc,Tm,Ys,Ts,Wa:REAL;

FUNCTION Singularity(x,a:REAL; Power:INTEGER):REAL;
BEGIN
IF (x-a) <= 0.0 THEN
Singularity := 0.0 ELSE
Singularity := EXP(power*LN(x-a));
END;

BEGIN
     I  := exp(3*ln(H))*(B)/12;
   {Concentrated_Loading;Simply supported,see Roark}
     Ra := w/L*(L-a);
   Ma := 0.0;
      Thetaa := -w*a*(2*L-a)*(L-a)/L;
    Ya := 0.0*E*I;
       Tc  := -(Thetaa/6+Ma*x+Ra*sqr(x)/2-w*Singularity(x,a,2)/2)/E/I;
      Yc  :=-(Ya+Thetaa*x/6+Ma*sqr(x)/2+Ra*x*sqr(x)/6-
w*Singularity(x,a,3)/6)/E/I;

   {Moment_Loading;Simply supported, see Roark}
    Ra := -Mo/L;
   Ma := 0.0;
      Thetaa := -Mo*(2*sqr(L)-6*a*I+3*sqr(a))/L;
   Ya := 0.0;
       Tm  :=-(Thetaa/6+Ma*x+Ra*sqr(x)/2+Mo*Singularity(x,a,1))/E/I;
   Ym :=-
(Ya+Thetaa*x/6+Ma*sqr(x)/2+Ra*x*sqr(x)/6+Mo*Singularity(x,a,2)/2)/
E/I;

   {Disturbited Loading;Simply supported, due to beam weight, see
Roark}
```

```
      Wa := H*B*Density_AL;
      Ra := Wa*L/2;
     Ma := 0.0;
      Thetaa := -Wa*SQR(L)*L/24;
     Ya := 0.0;
       Ts := (Thetaa+Ma*x+Ra*SQR(x)/2-Wa*SQR(x)*x/6)/E/I;
      Ys := (Ya+Thetaa*x+Ma*SQR(x)/2+Ra*SQR(x)*x/6-
Wa*SQR(x)*SQR(x)/24)/E/I;
     Beam_Deflection := Yc + Ym + Ys;
     Beam_Rotation   := Tc + Tm + Ts;
END;
BEGIN
WITH Model[Number] DO BEGIN
{VAR Beam_Deflection,Beam_Rotation:REAL;B,H,A,X,L,Mo,W:REAL}
Calculate_Beam_Slope_And_Deflection(Beam_Error.Y[Q],Beam_Error.Rz[
Q],
Beam_Dim.Z,Beam_Dim.Y,(Beam_Dim.X/2+Amplitude*Position),
(Beam_Dim.X/2+Amplitude*Position),Beam_Dim.X,Load.Rz[Q],Load.Y[Q]);
Calculate_Beam_Slope_And_Deflection(Beam_Error.Z[Q],Beam_Error.Ry[
Q],
Beam_Dim.Y,Beam_Dim.Z,(Beam_Dim.X/2+Amplitude*Position),
(Beam_Dim.X/2+Amplitude*Position),Beam_Dim.X,Load.Ry[Q],Load.Z[Q]);
END;
END;

PROCEDURE Calculate_Torsional_Bending_Error(Number:INTEGER);
VAR K:REAL;
BEGIN {see Roark for formula}
WITH Model[Number] DO BEGIN
K  :=  Beam_Dim.Z/2*EXP(3*LN(Beam_Dim.Y/2))*(16/3-
       3.36*Beam_Dim.Y/Beam_Dim.Z*(1-(
       EXP(4*LN(Beam_Dim.Y/2))/12/EXP(4*LN(Beam_Dim.Z/2)))));
Beam_Error.Rx[Q]  :=  Load.Rx[Q]*(Beam_Dim.X/2+Amplitude*Position)*
(Beam_Dim.X/2-Amplitude*Position)/G/K/Beam_Dim.X;
END;
END;

PROCEDURE Calculate_Slide_Errors(Number:INTEGER);
PROCEDURE Calculate_AirBearing_Slide_Errors(VAR Error:REAL;
Stiffness,
Load:REAL);
BEGIN
Error  :=  Load/Stiffness;
```

```
END;
BEGIN
WITH Model[Number] DO BEGIN
Slide_Error.X[Q] := 0.0;
Calculate_AirBearing_Slide_Errors(Slide_Error.Y[Q],Stiffness.Y,Load.Y[
Q]);
Calculate_AirBearing_Slide_Errors(Slide_Error.Z[Q],Stiffness.Z,Load.Z[
Q]);
Calculate_AirBearing_Slide_Errors(Slide_Error.Rx[Q],Stiffness.Rx,Load.
Rx[Q]);
Calculate_AirBearing_Slide_Errors(Slide_Error.Ry[Q],Stiffness.Ry,Load.
Ry[Q]);
Calculate_AirBearing_Slide_Errors(Slide_Error.Rz[Q],Stiffness.Rz,Load.
Rz[Q]);

END;
END;

PROCEDURE
Calculate_Accelerometer_Errors(Number:INTEGER;Varible_Load:REAL);
VAR Theta,A,L,R :REAL;

BEGIN
WITH Model[Number] DO BEGIN
Accelerometer_Errors.Rx[Q] := Beam_Error.Rx[Q] + Slide_Error.Rx[Q];
Accelerometer_Errors.Ry[Q] := Beam_Error.Ry[Q] + Slide_Error.Ry[Q];
Accelerometer_Errors.Rz[Q] := Beam_Error.Rz[Q] + Slide_Error.Rz[Q];

A := EXP(LN(Varible_Load/Scale_Factor/Density_AL)/3);
L := Model[Number].Slide_Dim.Y/2 + A/2;
R := SQRT(SQR(A/2)+SQR(L));
Theta := ARCTAN(A/L/2);
 Beam_Error.X[Q] := 0.0;
Slide_Error.X[Q] := 0.0;
WITH Accelerometer_Errors DO BEGIN
    X[Q]  := Beam_Error.X[Q] + Slide_Error.X[Q] +
             -R*(SIN(Rz[Q]+Theta)-SIN(Theta)) -
                0.1875*Amplitude*SQR(2*PI*Frequency)*Position/386.4
              /A/2*(1/E+1.2/G); {note that 0.1875 is 2 accel masses}
    Y[Q]  := Beam_Error.Y[Q] + Slide_Error.Y[Q] +
             R*(COS(Rz[Q]+Theta)-COS(Theta));
    Z[Q]  := Beam_Error.Z[Q] + Slide_Error.Z[Q] +
             L*Rx[Q] +A*Ry[Q];
```

```
System_Error[Q] := SQRT(SQR(X[Q])+SQR(Y[Q])+SQR(Z[Q]));
END;
END;
END;


PROCEDURE BOUNDARY(VAR VAL:REAL);
VAR ICOUNT,IFLAG :INTEGER;
   TMP:REAL;
   CH : CHAR;
BEGIN
  ICOUNT := 0;
  IFLAG  := 1;
  TMP := ABS(VAL);
  IF(VAL < 0.0) THEN IFLAG := -1;
IF (ABS(VAL) < 1.0) AND (ABS(VAL) > 0.0) THEN
  BEGIN
     REPEAT
           TMP := 10*TMP;
         ICOUNT := ICOUNT + 1;
      UNTIL (INT(TMP) <> 0.0);
     IF(FRAC(TMP) <> 0.0) THEN
       BEGIN
       IF(FRAC(TMP)<=0.5) THEN TMP :=INT(TMP)+1
        ELSE TMP := ROUND(TMP);
       END;
      VAL := IFLAG*TMP*EXP(-ICOUNT*LN(10));
  END ELSE
  BEGIN
     REPEAT
           TMP := TMP/10;
         ICOUNT := ICOUNT + 1;
      UNTIL (INT(TMP) = 0.0);
     IF (ICOUNT = 1) THEN
       BEGIN
        TMP := TMP*10;
     IF(FRAC(TMP) <> 0.0) THEN
       BEGIN
       IF(FRAC(TMP)<=0.5) THEN TMP :=INT(TMP)+1
        ELSE TMP := ROUND(TMP);
       END;
        VAL := IFLAG*TMP;
```

```
      END ELSE BEGIN
        TMP := TMP*EXP((ICOUNT-1)*LN(10));
       IF(FRAC(TMP) <> 0.0) THEN
         BEGIN
         IF(FRAC(TMP)<=0.5) THEN TMP :=INT(TMP)+1
          ELSE TMP := ROUND(TMP);
         END;
        VAL := IFLAG*TMP*10;
      END;
  END;
END;

PROCEDURE Plot_Data(a:Plotarray;n,g:INTEGER);
CONST MaxCurves = 5;

var   Temp,UnitIncr :REAL;
    k,TRANS      :INTEGER;

BEGIN
{    initgraphic;}
  ClearScreen;
   UnitIncr    :=  2.95*(YmaxGlb+1)*6/5/(YmaxGlb-49);
   DefineWindow(1,0,17,(XmaxGlb-10),YmaxGlb);
  DefineWindow(2,(XmaxGlb-8),49,XmaxGlb,YmaxGlb); {SET TO 49 FOR
HGC}
  DefineWorld(2,0,0,10,30);                          {set to 29 for ibm}
   FindWorld(1,a,(g*n),1,1.125);
 With World[1] DO BEGIN
     Temp  := Y1;
     Y1    := Y2;
     Y2    := Temp;
    BOUNDARY(Y1);
    BOUNDARY(Y2);
    BOUNDARY(X1);
    BOUNDARY(X2);
 End;
  SelectWindow(2);
  DrawBorder;
  SelectWorld(1);
  SelectWindow(1);
  SetBackground(0);
 GOTOXY(1,1);
 WRITELN(TITLE);
```

```
    DrawAxis(5,5,0,0,0,0,0,0,false);

   {The display of several functions by repeated calls of DrawPolygon}
  FOR K := 0 TO (g-1) DO BEGIN
   {The Plot Points}
    SelectWorld(1);
    SelectWindow(1);
    ResetAxis;
    DrawBorder;
    SetLinestyle(k);
    DrawPolygon(a,(k*n+1),((k+1)*n),0,0,0);
    SelectWorld(2);
    SelectWindow(2);
    DrawLine(1,((MaxCurves-K+1)*UnitIncr),9,((MaxCurves-
K+1)*UnitIncr));
  GOTOXY(74,(7+K*3));
   WRITELN(COPY(Axis_Labels,(k*6+1),6));
  END;

  GOTOXY(74,20);
  WRITELN('F=',Frequency:3:0);
  GOTOXY(74,21);
   WRITELN('A=',Amplitude:3:2);
  GOTOXY(74,22);
   WRITELN('G=',Acceleration:3:2);
  GOTOXY(74,23);
   WRITELN('L=',(Q/Scale_Factor):2:1);
  GOTOXY(70,24);
   WRITELN('X=',Cross_Axis_Motion_Range:8:5,'%');

    SetLinestyle(0);
  GOTOXY(73,2);
   WRITELN('Print');
  GOTOXY(73,3);
   WRITELN('0 or 1?');
  GOTOXY(80,3);
  READ(KBD,CH);
  IF (CH = #49) THEN
  BEGIN
   WRITELN(LST,#27,#64);
  HARDCOPY(False,6);
  WRITE(LST,'HARDCOPY AT: ');
  {TIME; IBM ONLY}
```

```
  WRITELN(LST);
  WITH Model[J] DO BEGIN
  WRITELN(LST,'BEARING MODEL ',Numbers);
  WRITELN(LST);
  WRITELN(LST,'DIMENSIONS-BEAM:');
  WRITELN(LST,'  X  = ',Beam_Dim.X:5:2,'    Y  = ',Beam_Dim.Y:5:2,
  '    Z  = ',Beam_Dim.Z:5:2,'    IN');
  WRITELN(LST);
  WRITELN(LST,'DIMENSIONS-SLIDE:');
  WRITELN(LST,'  X = ',Slide_Dim.X:5:2,'    Ry = ',Slide_Dim.Y:5:2,
  '    Z = ',Slide_Dim.Z1:5:2,'    IN');
  WRITELN(LST);
  WRITELN(LST,'SLIDE-STIFFNESS:');
  WRITELN(LST,'  Y = ',STiffness.Y:9,'    Z = ',Stiffness.Z:9,' LB/IN');
  WRITELN(LST,'  Rx = ',Stiffness.Rx:9,'    Ry = ',Stiffness.Ry:9
  ,'    Rz = ',Stiffness.Ry:9,'    IN-LB/RAD');
  WRITELN(LST);
  WRITELN(LST,'FREQUENCY-AMPLITUDE-ACCELERATION');
  WRITELN(LST,'F = ',Frequency:4:1,'  A = ',Amplitude:7:6,'  Accel = ',
              Acceleration:4:3);
  WRITELN(LST);
   WRITELN(LST,'Air bearing Weight = ',Airbearing_Weight:6:3);
  WRITELN(LST);
   WRITELN(LST,'Maximum Acceleration =
',(25.5/(3.7+AirBearing_Weight)):4:3);
  WRITELN(LST);
  WRITELN(LST,'CROSS AXIS MOTION = ',
   Cross_Axis_Motion_Range:8:5,'%');
  WRITELN(LST);
  WRITELN(LST,^L);
  END;
  END;
   {leavegraphic;}
END;

PROCEDURE Calculate_Loading_Vector(Number,Varible_Load:INTEGER);
BEGIN
WITH Model[Number] DO BEGIN
Load.Y[Q]   := -Varible_Load/Scale_Factor - 2*Retroreflector_Weight
            - Motor_Weight - Airbearing_Weight;
Load.X[Q]   := -ABS((1+Percent_Wire)*Load.Y[Q])*Amplitude*
            SQR(2*PI*Frequency)*Position/386.4;
Load.Z[Q]   := Percent_Side*Varible_Load/Scale_Factor;
```

```
Load.Rx[Q] := Load.Z[Q]*Slide_Dim.Y/2;
Load.Ry[Q] := Load.Z[Q]*Slide_Dim.X/2+Load.X[Q]*Percent_Wire/
              (1+Percent_Wire)*Slide_Dim.Z1/2;
Load.Rz[Q] := Load.X[Q]*(1.125+Slide_Dim.Y/2);{1.25 est. of motor
moment arm}
WITH LOAD DO BEGIN
{WRITELN(X[Q],Y[Q],Z[Q],Rx[Q],Ry[Q],Rz[Q])};
END;
END;
END;

PROCEDURE INTERACTIVE;
BEGIN
CLRSCR;
GapLength := 0.0;
Bearing_Data;
FOR Inc := 1 TO Number_of_Bearings DO BEGIN
GOTOXY(30,(2+Inc));
WRITELN(Inc:4,' - ',Model[Inc].Numbers);
END;
GOTOXY(30,14);
WRITE('Enter Bearing Number ==> ');
READ(J);
GOTOXY(30,15);
WRITE('Enter Bearing Gap Length ==> ');
READ(GapLength);
Bearing_Data;
{Find the initial static errors}
Amplitude := 0.0;
Frequency := 0.0;
Position  := 0.0;
Acceleration := 0.0;

GOTOXY(30,17);
WRITELN('   1 - Amplitude := 8.0      Frequency := 1.0');
GOTOXY(30,18);
WRITELN('   2 - Amplitude := 0.0008   Frequency := 100.0');
GOTOXY(30,19);
WRITELN('   3 - Amplitude := Maximum Frequency := 100.0');
GOTOXY(30,20);
WRITELN('   4 - Amplitude := 0.00294 Frequency := 50.0');
GOTOXY(30,22);
WRITE('Enter case number ==> ');
```

```
READ(W);

CASE W OF
   1: BEGIN
        Amplitude := 8.0;
       Frequency := 1.0;
          Acceleration := Amplitude*SQR(2*PI*Frequency)/386.4;
      END;
   2: BEGIN
        Amplitude := 0.0008;
       Frequency := 100.0;
          Acceleration := Amplitude*SQR(2*PI*Frequency)/386.4;
      END;
   3: BEGIN
          Acceleration := (25.5/(3.7+Model[J].AirBearing_Weight));
       Frequency := 100.0;
          Amplitude := Acceleration/SQR(2*PI*Frequency)*386.4;
      END;
   4: BEGIN
        Amplitude := 0.00319;
       Frequency := 50.0;
          Acceleration := Amplitude*SQR(2*PI*Frequency)/386.4;
      END;
END;
GOTOXY(30,25);
WRITE('Time Out .....');
Cross_Axis_Motion_min := 1E10;
Cross_Axis_Motion_max :=-1E10;
FOR C := 1 TO 21 DO BEGIN
    Position  := (C-11)/10;
     Calculate_Inertia_Without_Load(J);
     Calculate_Airbearing_Weight(J);

  FOR Q := 1 TO Number_of_Points  DO BEGIN
       Calculate_Loading_Vector(J,Q);
     If C = 1 THEN BEGIN
     WITH Model[J] DO BEGIN
      Starting_Load.X[Q] := Load.X[Q];
      Starting_Load.Y[Q] := Load.Y[Q];
      Starting_Load.Z[Q] := Load.Z[Q];
      Starting_Load.Rx[Q] := Load.Rx[Q];
      Starting_Load.Ry[Q] := Load.Ry[Q];
      Starting_Load.Rz[Q] := Load.Rz[Q];
```

```
      END;
      END;
          Calculate_Inertia_With_Varible_Load(J,Q);
         Calculate_Natural_Frequency(J);
        Calculate_Beam_Errors(J);
         Calculate_Torsional_Bending_Error(J);
         Calculate_Slide_Errors(J);
         Calculate_Accelerometer_Errors(J,Q);
      WITH Model[J] DO BEGIN
        Cross_Axis_Motion[C] := SQRT(SQR(Accelerometer_Errors.Y[Q])+
                                SQR(Accelerometer_Errors.Z[Q]))
                               /AMPLITUDE*100/2;
    END;{MODEL}
    END;{END Q}
    IF Cross_Axis_Motion[C] < Cross_Axis_Motion_min
      THEN Cross_Axis_Motion_min := Cross_Axis_Motion[C];
    IF Cross_Axis_Motion[C] > Cross_Axis_Motion_max
      THEN Cross_Axis_Motion_max := Cross_Axis_Motion[C];

N := 21;
WITH Model[J] DO BEGIN
{Store Accelerometer data in array DA for plotting}
DA[C,1]        := Amplitude*Position;
DA[C,2]         := Accelerometer_Errors.X[1]*Multiplier;
DA[(N+C),1]    := Amplitude*Position;
DA[(N+C),2]     := Accelerometer_Errors.Y[1]*Multiplier;
DA[(2*N+C),1]  := Amplitude*Position;
DA[(2*N+C),2]  := Accelerometer_Errors.Z[1]*Multiplier;
DA[(3*N+C),1]  := Amplitude*Position;
DA[(3*N+C),2]  := System_Error[1]*Multiplier;

{Store Accelerometer data in array DT for plotting}
DT[C,1]        := Amplitude*Position;
DT[C,2]         := Accelerometer_Errors.RX[1]*Multiplier;
DT[(N+C),1]    := Amplitude*Position;
DT[(N+C),2]     := Accelerometer_Errors.RY[1]*Multiplier;
DT[(2*N+C),1]  := Amplitude*Position;
DT[(2*N+C),2]  := Accelerometer_Errors.RZ[1]*Multiplier;
DT[(3*N+C),1]  := Amplitude*Position;
DT[(3*N+C),2]  := System_Error[1]*Multiplier;

{Store Beam data in array DB for plotting}
DB[C,1]        := Amplitude*Position;
```

```
DB[C,2]        := Beam_Error.X[1]*Multiplier;
DB[(N+C),1]    := Amplitude*Position;
DB[(N+C),2]    := Beam_Error.Y[1]*Multiplier;
DB[(2*N+C),1]  := Amplitude*Position;
DB[(2*N+C),2]  := Beam_Error.Z[1]*Multiplier;

{Store Beam data in array DR for plotting}
DR[C,1]        := Amplitude*Position;
DR[C,2]        := Beam_Error.RX[1]*Multiplier;
DR[(N+C),1]    := Amplitude*Position;
DR[(N+C),2]    := Beam_Error.RY[1]*Multiplier;
DR[(2*N+C),1]  := Amplitude*Position;
DR[(2*N+C),2]  := Beam_Error.RZ[1]*Multiplier;

{Store Slide data in array DD for plotting}
DD[C,1]        := Amplitude*Position;
DD[C,2]        := Slide_Error.X[1]*Multiplier;
DD[(N+C),1]    := Amplitude*Position;
DD[(N+C),2]    := Slide_Error.Y[1]*Multiplier;
DD[(2*N+C),1]  := Amplitude*Position;
DD[(2*N+C),2]  := Slide_Error.Z[1]*Multiplier;

{Store Slide data in array DS for plotting}
DS[C,1]        := Amplitude*Position;
DS[C,2]        := Slide_Error.RX[1]*Multiplier;
DS[(N+C),1]    := Amplitude*Position;
DS[(N+C),2]    := Slide_Error.RY[1]*Multiplier;
DS[(2*N+C),1]  := Amplitude*Position;
DS[(2*N+C),2]  := Slide_Error.RZ[1]*Multiplier;
END;{MODEL}
END;
Cross_Axis_Motion_range := Cross_Axis_Motion_max -
                           Cross_Axis_Motion_min;

Initgraphic;
Title := 'Accelerometer Errors: Error(uin) VS Position(in) for '+
Model[J].Numbers +
       ' Dover Air Bearing';
                    {'1-----2-----3-----4-----5-----'}
Axis_Labels := 'X    Y    Z    ';
Plot_Data(DA,n,3);
```

```
Title := 'Accelerometer Errors: Rotation(urad) VS Position(in) for '+
Model[J].Numbers +
        ' Dover Air Bearing';
                        {'1-----2-----3-----4-----5-----'}
Axis_Labels := 'RX   RY   RZ   ';
Plot_Data(DT,n,3);

Title := 'Beam Errors: Error(uin) VS Position(in) for '+ Model[J].Numbers
+
        ' Dover Air Bearing';
                        {'1-----2-----3-----4-----5-----'}
Axis_Labels := 'X    Y    Z    ';
Plot_Data(DB,n,3);

Title := 'Beam Errors: Rotation(urad) VS Position(in) for '+
Model[J].Numbers +
        ' Dover Air Bearing';
                        {'1-----2-----3-----4-----5-----'}
Axis_Labels := 'RX   RY   RZ   ';
Plot_Data(DR,n,3);

Title := 'Slide Errors: Error(uin) VS Position(in) for '+ Model[J].Numbers
+
        ' Dover Air Bearing';
                        {'1-----2-----3-----4-----5-----'}
Axis_Labels := 'X    Y    Z    ';
Plot_Data(DD,n,3);

Title := 'Slide Errors: Rotation(urad) VS Position(in) for '+
Model[J].Numbers +
        ' Dover Air Bearing';
                        {'1-----2-----3-----4-----5-----'}
Axis_Labels := 'RX   RY   RZ   ';
Plot_Data(DS,n,3);
LeaveGraphic;
END;

PROCEDURE SETA;
BEGIN
clrscr;
GapLength := 0.0;
{Bearing  Number}
FOR J := 1 TO Number_of_Bearings DO BEGIN
```

```
{Enter Bearing Gap Length}
GapLength := 0.5;
Bearing_Data;
Amplitude := 0.0;
Frequency := 0.0;
Position  := 0.0;
Acceleration := 0.0;

Calculate_Airbearing_Weight(J);

W:=1;

CASE W OF
   1: BEGIN
        Amplitude := 8.0;
       Frequency := 1.0;
          Acceleration := Amplitude*SQR(2*PI*Frequency)/386.4;
     END;
   2: BEGIN
        Amplitude := 0.0008;
       Frequency := 100.0;
          Acceleration := Amplitude*SQR(2*PI*Frequency)/386.4;
      END;
   3: BEGIN
          Acceleration := (25.5/(3.7+Model[J].AirBearing_Weight));
       Frequency := 100.0;
          Amplitude := Acceleration/SQR(2*PI*Frequency)*386.4;
     END;
   4: BEGIN
        Amplitude := 0.00319;
       Frequency := 50.0;
          Acceleration := Amplitude*SQR(2*PI*Frequency)/386.4;
     END;
END;
     Calculate_Inertia_Without_Load(J);
     Calculate_Airbearing_Weight(J);

FOR C := 1 TO 21 DO BEGIN
    Position  := (C-11)/10;
  FOR Q := 1 TO Number_of_Points  DO BEGIN
       Calculate_Loading_Vector(J,Q);
        Calculate_Inertia_With_Varible_Load(J,Q);
       Calculate_Natural_Frequency(J);
```

```
          Calculate_Beam_Errors(J);
           Calculate_Torsional_Bending_Error(J);
          Calculate_Slide_Errors(J);
           Calculate_Accelerometer_Errors(J,Q);
   END;

N := 21;
WITH Model[J] DO BEGIN
{Store Accelerometer data in array AD for FILE}
AD[C,1] := Amplitude*Position;
AD[C,2] := System_error[1]*Multiplier;
AD[C,3] := Accelerometer_Errors.X[1]*Multiplier;
AD[C,4] := Accelerometer_Errors.Y[1]*Multiplier;
AD[C,5] := Accelerometer_Errors.Z[1]*Multiplier;
AD[C,6] := Accelerometer_Errors.Rx[1]*Multiplier;
AD[C,7] := Accelerometer_Errors.Ry[1]*Multiplier;
AD[C,8] := Accelerometer_Errors.Rz[1]*Multiplier;

{Store Beam data in array BD for FILE}
BD[C,1] := Amplitude*Position;
BD[C,2] := SQRT(SQR(Beam_Error.X[1])+SQR(Beam_Error.Y[1])
          +SQR(Beam_Error.Z[1]))*Multiplier;
BD[C,3] := Beam_Error.X[1]*Multiplier;
BD[C,4] := Beam_Error.Y[1]*Multiplier;
BD[C,5] := Beam_Error.Z[1]*Multiplier;
BD[C,6] := Beam_Error.Rx[1]*Multiplier;
BD[C,7] := Beam_Error.Ry[1]*Multiplier;
BD[C,8] := Beam_Error.Rz[1]*Multiplier;

{Store Slide data in array SD for FILE}
SD[C,1] := Amplitude*Position;
SD[C,2] := SQRT(SQR(Slide_Error.X[1])+SQR(Slide_Error.Y[1])
          +SQR(Slide_Error.Z[1]))*Multiplier;
SD[C,3] := Slide_Error.X[1]*Multiplier;
SD[C,4] := Slide_Error.Y[1]*Multiplier;
SD[C,5] := Slide_Error.Z[1]*Multiplier;
SD[C,6] := Slide_Error.Rx[1]*Multiplier;
SD[C,7] := Slide_Error.Ry[1]*Multiplier;
SD[C,8] := Slide_Error.Rz[1]*Multiplier;

END;{with model[j]}
END;{postion loop}
END;
```

```
{***** Output Data *****}
FileIndexData;
FOR Increment := 1 TO 21 DO BEGIN
FileName := 'graph' + Fileindex[Increment] + '.dat';
ASSIGN(OUTFILE,FileName);
REWRITE(OUTFILE);
WRITELN(OUTFILE,'*');
WRITE(OUTFILE,'Position (in)',#9);
FOR U := 1 TO Number_of_Bearings DO BEGIN
WRITE(OUTFILE,Model[U].Numbers,#9);
END;
WRITELN(OUTFILE);

FOR C := 1 TO 21 DO BEGIN
WRITE(OUTFILE,Model[1].AD[c,1]:7:4,#9);
FOR J := 1 TO Number_of_Bearings DO BEGIN
  WITH Model[J] DO BEGIN
      CASE Increment of
       1..7:    WRITE(OUTFILE,ad[c,(Increment+1)]:7:2,#9);
       8..14:   WRITE(OUTFILE,bd[c,(increment-6)]:7:2,#9);
       15..21:  WRITE(OUTFILE,sd[c,(increment-13)]:7:2,#9);
     END;{case}
  END;
END;{end bearings}
WRITELN(OUTFILE);
END;{end 21 pt loop}
CLOSE(OUTFILE);
END;{end fileindex}
END;{seta}

PROCEDURE SETB;
BEGIN
GapLength := 0.0;
Bearing_Data;
ASSIGN(OUTFILE,'GAP.DAT');
REWRITE(OUTFILE);
WRITELN(OUTFILE,'*');
WRITE(OUTFILE,'Gap Length (in)',#9);
FOR Ua := 1 TO Number_of_Bearings DO BEGIN
FOR Uc := 1 TO 3 DO BEGIN
  WRITE(OUTFILE,Model[Ua].Numbers,#9);
END;END;
```

```
WRITELN(OUTFILE);
clrscr;
{Set Bearing Gap Length}
FOR U := 0 TO 20 DO BEGIN
     GapLength := U/10;
WRITE(OUTFILE,GapLength:10:6,#9);
{Set Bearing Number}
FOR J := 1 TO Number_of_Bearings DO BEGIN

Bearing_Data;

Amplitude := 0.0;
Frequency := 0.0;
Position  := 0.0;
Acceleration := 0.0;

Calculate_Airbearing_Weight(J);

{Set case number}
   W := 1;

CASE W OF
   1: BEGIN
        Amplitude := 8.0;
       Frequency := 1.0;
          Acceleration := Amplitude*SQR(2*PI*Frequency)/386.4;
     END;
   2: BEGIN
        Amplitude := 0.0008;
       Frequency := 100.0;
          Acceleration := Amplitude*SQR(2*PI*Frequency)/386.4;
      END;
   3: BEGIN
          Acceleration := (25.5/(3.7+Model[J].AirBearing_Weight));
       Frequency := 100.0;
          Amplitude := Acceleration/SQR(2*PI*Frequency)*386.4;
     END;
   4: BEGIN
        Amplitude := 0.00319;
       Frequency := 50.0;
          Acceleration := Amplitude*SQR(2*PI*Frequency)/386.4;
     END;
END;
```

```
      Calculate_Inertia_Without_Load(J);
      Calculate_Airbearing_Weight(J);
        Cross_Axis_Motion_min := 1E10;
        Cross_Axis_Motion_max :=-1E10;
FOR C := 1 TO 21 DO BEGIN
    Position   := (C-11)/10;
  FOR Q := 1 TO Number_of_Points  DO BEGIN
        Calculate_Loading_Vector(J,Q);
         Calculate_Inertia_With_Varible_Load(J,Q);
        Calculate_Natural_Frequency(J);
         Calculate_Composite_Natural_Frequency(J);
        Calculate_Beam_Errors(J);
         Calculate_Torsional_Bending_Error(J);
        Calculate_Slide_Errors(J);
         Calculate_Accelerometer_Errors(J,Q);
     WITH Model[J] DO BEGIN
       Cross_Axis_Motion[C] := SQRT(SQR(Accelerometer_Errors.Y[Q])+
                               SQR(Accelerometer_Errors.Z[Q]))
                              /AMPLITUDE*100/2;
    END;END;
    IF Cross_Axis_Motion[C] < Cross_Axis_Motion_min
      THEN Cross_Axis_Motion_min := Cross_Axis_Motion[C];
    IF Cross_Axis_Motion[C] > Cross_Axis_Motion_max
      THEN Cross_Axis_Motion_max := Cross_Axis_Motion[C];
     END;{postion loop}
       Cross_Axis_Motion_range := Cross_Axis_Motion_max -
                                  Cross_Axis_Motion_min;

WITH Model[J] DO BEGIN
     WRITE(OUTFILE,Composite_Natural_Frequency.Y[1]:6:1,#9,
      Composite_Natural_Frequency.Rz[1]:6:1,#9,
      Cross_Axis_Motion_range:8:5,#9);
END;{with  model[j]}
END;{model number}
WRITELN(OUTFILE);
END;{gaplength}
CLOSE(OUTFILE);
END;{setb}
BEGIN
{INTERACTIVE;}
SETA;
SETB;
END.
```

Appendix B

Equipment Cost

Zenith PC AT Computer	$1900.00
Data Translation DT2817 32 Bit Digital I/0	200.00
Data Translation DT2823 16 Bit Analog I/O	2700.00
ATLab Software Drivers for DT2823	450.00
HP 3522A Function Generator	5000.00
Anorad Brushless Linear DC Motor model LP2	1500.00
Baldor Brushless Servo Amplifier	1200.00
Machine Shop Cost and Materials	3000.00
Zygo Axiom 2/20 Laser Transducer Single axis, with linear interferometer	18,000.00
Dover Instruments linear Air Bearing model 850-S with 20 inch travel	5000.00
Miscellaneous Costs	1200.00
Microsoft C compiler	350.00
Microsoft Assembler	100.00
Graphics software	350.00
Total	$40,950.00